The Nonlinear Dynamics of Cyclone Waves

By
T. J. Simons

Department of Atmospheric Science
Colorado State University
Fort Collins, Colorado

Department of
Atmospheric Science

Paper No. 162

THE NONLINEAR DYNAMICS OF CYCLONE WAVES

by

T. J. Simons

Technical Report to
The National Science Foundation
Grant No. GA-11637
Program Supervisor, F. Baer

Department of Atmospheric Science
Colorado State University
Fort Collins, Colorado

June 1970

Atmospheric Science Paper No. 162

This report was a dissertation submitted
by the author in partial fulfillment of
the requirements for the degree of Doctor
of Philosophy at Colorado State University.

The Nonlinear Dynamics of Cyclone Waves

by

T. J. Simons

Colorado State University

ABSTRACT

The development of atmospheric cyclones is studied from the viewpoint of the instability of large-scale wave perturbations superimposed on a zonal current. The stability properties of the observed mean January flow are investigated and the linear results are extended to include the effects of nonlinear processes on the growth of a cyclone-scale wave. The initial-value aspect of the problem receives special attention. An hemispheric model is employed in this investigation and solutions are obtained by spectral techniques.

It is found that the observed atmospheric zonal current is highly unstable in a hydrodynamic sense. The instability is of a baroclinic character with barotropic stabilizing effects. The nonlinear computations show that the growth of the most unstable waves is brought to a halt when the perturbation kinetic energy reaches a level consistent with atmospheric observation. The barotropic energy exchanges are found to play a major role in this process by feeding a large amount of kinetic energy into the zonal flow when the baroclinic energy conversions reach a maximum. The damping effect of the nonlinear processes on the growth of the unstable wave is found to be slightly reduced when the horizontal resolution of the model is increased in either zonal or latitudinal direction. On the other hand, the growth

rate of the cyclone-scale wave is reduced under influence of the self-interaction of a long quasi-permanent wave, the wave number of which is one half that of the cyclone wave.

The effects of the initial configuration of a wave are found to be comparable to the effects of the scale of the perturbation with regard to the subsequent growth of the wave. The baroclinic development of a perturbation is found to exhibit a maximum when the initial disturbance is centered around the 600-mb level.

ACKNOWLEDGEMENTS

The author is indebted to Dr. F. Baer, his thesis supervisor, for the advice and guidance given throughout the course of this study. In addition, the author wishes to thank Drs. J. E. Cermak, B. Haurwitz, and H. Riehl for serving as members of his thesis committee and for offering their valuable criticism of this paper.

Special thanks are extended to Dr. D. B. Rao for stimulating and enlightening discussions on the subject of dynamic instability. With regard to the computational aspect of the present study, the author has greatly benefited from the expertise of his colleagues, Messrs. F. N. Alyea and R. L. King.

This research was supported by the National Science Foundation, Grant NSF GA-11637.

TABLE OF CONTENTS

LIST OF FIGURES

I. INTRODUCTION

A. Historical Background

The theory of atmospheric development can be traced back to investigations of the stability of hydrodynamic flow by Thomson, Rayleigh, and Helmholtz. Thus the growth of cyclone-scale disturbances in the atmosphere is visualized in terms of the stability properties of zonal currents. The instabilities arising from the general shearing motions in the free atmosphere are naturally divided into two classes, since the main cause of the instability may be either the vertical shear or the latitudinal variation of the zonal wind. The physical processes responsible for the growth of the large-scale perturbations on the basic flow are accordingly of two types. In the case of a zonal flow without lateral shear the only source of energy for the atmospheric eddies is the potential and internal energy of the zonal current available for conversion into perturbation energy. This energy is known as the "available potential energy" and may be related to the vertical shear of the zonal wind. Development of this type is referred to as baroclinic instability. On the other hand, if the perturbations grow due to the latitudinal variations of the basic flow, the source of energy is the kinetic energy of this flow and the instability is of a barotropic nature.

Most of our knowledge concerning the stability properties of the atmosphere is the result of theoretical investigations of zonal currents possessing either vertical or lateral shear. Charney (1947) and Eady (1949) presented the first mathematical treatments of cyclone waves in terms of the baroclinic character of the general shearing motions in the free atmosphere. Previous studies had focused attention on

perturbations at the interface between two air masses of different density and velocity. Subsequent investigations of the baroclinic stability problem by Kuo (1952), Burger (1962), and Miles (1964), were concerned principally with elaborations of Charney's model. Under normal atmospheric conditions a maximum of instability has been shown to exist for wavelengths corresponding to the scale of cyclone perturbations. Kuo (1953) found that the shorter unstable baroclinic waves are shallow while the longer ones have maximum amplitudes in the upper atmosphere.

The barotropic instability problem was considered by Kuo (1949), who applied Rayleigh's theory of the stability of parallel flows to zonal currents in the atmosphere. The barotropic basic current was shown to be stable if the meridional gradient of absolute vorticity has the same sign everywhere. Kuo's work was extended by Howard and Drazin (1964) and by Lipps (1962, 1965). Lipps (1963) also made an analysis of the barotropic stability for a two-layer incompressible fluid and Jacobs and Wiin-Nielsen (1966) discussed the stability of the barotropic zonal current in a stratified atmosphere. An important theorem concerning the stability of a general barotropic-baroclinic zonal current was derived by Charney and Stern (1962). By using integral techniques, they showed that a necessary condition for instability of an internal jet is that the meridional profile of the "potential vorticity" has an extremum at some place in the basic flow. The potential vorticity is a quantity incorporating both the effects of the absolute vorticity and the vertical shear and will be defined in the following. Pedlosky (1963, 1964a) and Blumen (1968) generalized the stability theorem above.

Pedlosky (1964b) also made a detailed investigation of unstable perturbations in a two-layer barotropic-baroclinic model.

Along with these analytical investigations of the atmospheric instability problem, numerous studies have taken a numerical approach to the problem. Green (1960) considered the baroclinic problem as defined by Charney and Eady and his work has been extended by Hirota (1968). The computational aspect of the problem was the subject of studies by Wiin-Nielsen (1962) and Rosenthal (1964). Numerical methods were applied to obtain the stability characteristics of barotropic flows by Eliasen (1954), Wiin-Nielsen (1961), Haltiner and Song (1962), and recently by Yanai and Nitta (1968). Haltiner (1963) and Gary (1965) proceeded to numerical investigations of basic currents containing both vertical and lateral shears. The most comprehensive study of the general barotropic-baroclinic problem was recently completed by Brown (1969a, 1969b). A numerical model of high horizontal and vertical resolution was used to obtain instability results for zonal basic flows possessing both vertical and lateral shears. These results were compared with those of the purely baroclinic and purely barotropic atmospheres in order to obtain estimates of the effects of one type of instability upon the other. The following is a summary of Brown's results.

Consider meridionally symmetric, jet-type westerly currents which have vertical profiles representative of atmospheric winds at middle latitudes. The basic wind profiles either have absolute vorticity extrema within each layer (cosine jets), or they do not have such extrema (parabolic jets). For the cosine jet two distinct wavelengths of maximum instability are evident in most cases. By obtaining the

energy conversions it is determined that the relatively short waves amplify due to a dominating baroclinic effect. These waves are simultaneously subject to a barotropic stabilizing influence and thus strengthen the zonal kinetic energy of the basic current. For the relatively long unstable waves both the basic flow kinetic and available potential energies act as sources of perturbation energy. On the other hand, the parabolic jet does not satisfy the criteria for barotropic instability and consequently all unstable waves are characterized by a dominating baroclinic effect with a tendency for barotropic damping.

A basic assumption underlying all the investigations above is that the large-scale motions of the atmosphere are described to a satisfactory degree by the so-called quasi-geostrophic system of equations. A detailed discussion of this approximation has been presented by Phillips (1963). The main purpose of the quasi-geostrophic approximation is to filter out the gravitational modes of oscillation while retaining the rotational modes of oscillation in the atmosphere. Supposedly the latter are responsible for the development of atmospheric cyclones while the former are meteorologically insignificant. More recently the effects of departures from quasi-geostrophic balance on the stability properties of the atmosphere have been subjected to a critical evaluation. The non-geostrophic baroclinic problem was studied by Arnason (1963) and Derome and Wiin-Nielsen (1966), and for the two-layer model by Wiin-Nielsen (1963) and Magata (1964). Phillips (1964) suggested that the most important non-geostrophic effects in baroclinic stability studies might be related to the lateral variations of the perturbations. Stone (1966) and Sela and Jacobs (1968) tried to incorporate these effects by assuming wave solutions periodic in the lateral direction

normal to the basic current. Simons (1970) evaluated the instability of non-geostrophic baroclinic perturbations in a channel with two vertical walls. The computations were performed on a particular two-layer model which incorporates all the effects of the north-south dependence present in more sophisticated models. The results of all these studies indicate that the major baroclinic instability of cyclone-scale perturbations is not significantly altered by non-geostrophic effects. Nevertheless it should be realized that the quasi-geostrophic approximation does eliminate any instability which could be induced by non-rotational modes of oscillation. Simons and Rao (1970) showed that the internal gravity modes may combine with the rotational modes in a two-fluid model to produce instability of perturbations having the dimensions of a few thousand kilometers. The same mechanism had been shown to be responsible for instability in a frontal model by Rao and Simons (1969). Again, however, such instabilities were found to exist outside the region of the major quasi-geostrophic instability without significantly modifying the latter.

B. Outline of Present Study

The present investigation is concerned with the interaction of finite wave perturbations with a barotropic-baroclinic basic current as observed in the atmosphere. This study does not consider the problem of atmospheric instability for its own sake, but rather is directed toward an interpretation of such instability in terms of the actual development of atmospheric cyclones. The atmosphere is always unstable in a hydrodynamic sense. This might of course be inferred from the cyclone perturbations which are seen to develop persistently in the earth's

atmosphere. However, there is also ample evidence that any zonal current, obtained in some fashion from atmospheric data, is unstable with respect to small wave perturbations superimposed on such a current in a numerical model. Furthermore the atmosphere displays at any moment an abundance of large-scale eddies, and new perturbations are created continuously by thermal processes and the effects of the earth's topography. The problem at hand is then to study the development of these disturbances under such conditions and to determine why certain eddies grow while others do not. Clearly the cause of such growth is not necessarily the unstable character of the zonal current but may also lie in the interactions among various perturbations. In the second place it seems unrealistic that the growth of an eddy would for a given basic state be determined only by its scale as predicted by stability theory. Obviously the configurations of some of the perturbations present in the atmosphere at any given time are more favorable for development than others.

There are many ways to approach the above problem. The approach taken in the present investigation is to start from the theory of atmospheric instability and extend such studies to include the effects of nonlinear interactions between the zonal flow and the eddies and the effects of the initial eddy structure. The purpose is not to reproduce the actual behavior of the atmosphere but only to simulate certain large-scale processes in the atmosphere. Thus the model incorporates no effects of dissipation or diabatic heating which would in the present context only obscure the interpretation of the results. Furthermore the model is quasi-geostrophic since we will restrict ourselves to scales of motion corresponding to perturbations of major instability.

The spherical geometry of the earth is incorporated in order to include the effects of this geometry on the flow and to deal with natural lateral boundaries.

The field of atmospheric motions may be represented by a complete spectrum of planetary waves. The basic assumption underlying the study of dynamic instability of the atmosphere is that one individual wave can be studied independently from its interaction with the remaining part of the spectrum. This procedure can be justified mathematically by disturbing a basic zonal flow by a perturbation which is sufficiently small for terms of second and higher order to be negligible. In a nonlinear model the interactions of the various planetary waves cannot be ignored and consequently the complete spectrum of waves should be considered. It is however possible to consider a particular initial state which renders the problem considerably more tractable. This initial state consists of a zonal flow and one individual planetary wave. The nonlinear effects will indeed modify the zonal flow and also introduce new waves, but all these waves will be higher harmonics of the original wave. This may be considered to constitute the first step of the nonlinear extension of the study of atmospheric instability and may shed some light on the development of a mature cyclone.

The nonlinear aspects of the baroclinic instability problem have received some attention in the past. Phillips (1954) computed the second-order changes in the basic current resulting from an unstable wave superimposed on this current in a two-layer model. Baer (1968) presented an exact solution for the nonlinear interaction between the zonal flow and a finite-amplitude wave in a two-layer purely baroclinic system. This solution is periodic for all values of the basic state

parameters and for all wavelengths. Thus the growth of the perturbation will be reduced and finally halted when the wave amplitude becomes sufficiently large. But the solution also implies that the amplitude of the wave will subsequently decrease and become at least as small as its initial value. Precisely the same conclusions were reached recently by Pedlosky (1970) who adopted the same physical model but a different mathematical approach. It may be anticipated that the second half of the nonlinear cycle will be drastically altered if the barotropic energy exchange processes are allowed to come into play. These effects and the effects of the higher harmonic of the primary wave perturbation constitute a major subject of the present investigation.

One of the most significant aspects of a nonlinear study is the initial-value problem. In a study of the present type one might solve this problem by invoking the results of linear instability theory. If the amplitude of the wave is sufficiently small for nonlinear effects to be negligible the perturbation will grow toward the structure of the most unstable normal mode. This particular configuration can therefore be adopted for the initial perturbation in the nonlinear extension of the instability problem. Clearly then, the implicit assumption is that the time-scale of the quasi-linear development is such that the perturbation has an opportunity to adjust to the normal mode structure. In case of atmospheric development, however, we are dealing with finite initial disturbances which might cause the nonlinear effects to become active very rapidly. In such case the initial configuration might be more important than the character of the linear growth of the wave. This brings out the need for adequate information concerning the effects of the initial structure of a perturbation on its subsequent growth.

Aside from this, the latter problem might also have some bearing on the preference of certain types of perturbations with respect to atmospheric development. Other important aspects of the initial value problem in the theory of hydrodynamic instability have been stressed by Case (1960, 1962) and Pedlosky (1964c). This initial-value problem is therefore another major subject of this investigation.

The following presentation consists of three parts in addition to a description of the mathematical model. The first part consists of a study of the linear stability properties of the basic flow to be used in the nonlinear study. This basic flow is the climatological-mean zonal current for January. The same chapter also includes a brief description of the stability properties of the mean January flow as a function of longitude. The latter is of interest since the development of atmospheric cyclones is doubtless determined more by local conditions than by the zonally-averaged character of the mean flow. The next chapter is concerned with the nonlinear aspects of the stability problem. First we consider the development of the most unstable waves under influence of the nonlinear interactions with the zonal flow. Subsequently we allow for the higher harmonic of the primary wave and finally we consider the interaction of a highly-unstable cyclone wave with a quasi-permanent long wave. The final part of this paper is devoted to the initial-value problem. A general solution of this problem has not been attempted. Instead we have followed the course outlined by linear instability studies and considered first the baroclinic aspects of the problem. The barotropic nonlinear initial-value problem has been considered to some extent by Baer (1968) and King (1970).

Due to the complexity of the flow patterns the solutions are obtained by numerical methods. There are two numerical techniques available by which our equations can be integrated. The most widely used is the gridpoint method whereby the vertical and lateral derivatives are replaced by finite differences. A draw-back of this method as applied to nonlinear equations is the occurrence of nonlinear computational instabilities (Phillips, 1959) which can be only suppressed by certain smoothing or damping operations or by simulating the effects of diffusion. Since it is the purpose of the present study to obtain a solution to the given initial value problem which is not effected by such artificial means, we have turned to the other alternative, known as the spectral method. In this case the atmospheric flow field is represented in terms of a series of orthogonal polynomials. It is clearly advantageous if such polynomials are chosen to be characteristic functions of certain operators which occur in the dynamical equations. Useful horizontal representations of this type have been introduced in numerical meteorology by Silberman (1954) and later by Lorenz (1960) and Platzman (1960). Their polynomials are characteristic functions of the horizontal Laplace operator occurring in the quasi-geostrophic relationship between vorticity and height field. In the present problem one of the two horizontal coordinates will be eliminated from the outset (Section IIB) and the appropriate orthogonal functions are simply the associated Legendre functions of the first kind.

The vertical representation of the atmosphere in terms of analytical functions is by no means original either. In the early years of numerical forecasting, Eady (1952) and Eliassen (1952) introduced the two-parameter models in which the vertical layered structure of the

atmosphere was rejected in favor of a representation in terms of given functions of the vertical coordinate. A few attempts have been made to extend this representation to more parameters but a general solution has not yet been proposed. However, for a model with standard static stability such as the one dealt with in the following, the present author has suggested an expansion in terms of orthogonal polynomials which are eigenfunctions of a vertical operator occurring in the quasi-geostrophic potential vorticity (Simons, 1968). This method has been applied in the last part of this study for reasons of the special nature of the problem. In the first part, which includes the linear studies, we have adopted the usual atmospheric modeling in terms of layers.

II. MATHEMATICAL MODEL

A. The Quasi-Geostrophic System of Equations

It is most important that any simplified system of equations meets certain integral requirements which are satisfied by the complete equations (Hollmann, 1956; Wiin-Nielsen, 1959; Lorenz, 1960). In the absence of friction and diabatic heating, the equations governing the motions in the atmosphere conserve the total vorticity and the total energy of the earth's atmosphere. The following quasi-geostrophic equations are consistent in this respect. This simplified system of equations has been treated in detail by Phillips (1963) and therefore we will restrict ourselves to a brief review of the relevant equations.

The horizontal wind can be written as the sum of a nondivergent and an irrotational component $\mathbf{V} = \mathbf{k} \times \nabla\psi + \nabla\chi$ where ψ is the stream-function, χ is the velocity potential, $\mathbf{k}$ is the vertical unit vector and ∇ is the horizontal gradient operator. If ζ and δ denote the vertical component of vorticity and the horizontal divergence, respectively, then clearly $\zeta = \nabla^2\psi$ and $\delta = \nabla^2\chi$. The horizontal equations of motion may be transformed into the vorticity equation and the divergence equation. When pressure is used as the vertical coordinate the quasi-geostrophic simplified form of the divergence equation is

$$f_o\nabla^2\psi - \nabla^2\Phi = 0 \qquad (1)$$

where Φ is the geopotential and f_o is a constant value of the Coriolis parameter $f = 2\Omega\sin\phi$. If now the vorticity equation is truncated to the form

$$\frac{\partial}{\partial t}\nabla^2\psi + J(\psi,\nabla^2\psi + f) + f_o\nabla^2\chi = 0 \qquad (2)$$

where J denotes the Jacobian operator, then these equations satisfy the consistency requirements mentioned above.

The atmosphere is assumed to be in quasi-hydrostatic balance. Under this condition the continuity equation in pressure coordinates becomes

$$\nabla^2\chi + \frac{\partial\omega}{\partial p} = 0 \tag{3}$$

where p is pressure and $\omega \equiv dp/dt$ is a measure of the vertical component of velocity. The vertical equation of motion reduces then to the hydrostatic equation which may be combined with the equation of state to give

$$\frac{\partial\Phi}{\partial p} + R\frac{T}{p} = 0 \tag{4}$$

where T is temperature and R is the specific gas constant.

The thermodynamic equation for adiabatic motion is used in the following form

$$\frac{\partial T}{\partial t} + J(\psi,T) + \left(\frac{\partial T}{\partial p} - \frac{T}{p}\frac{R}{c_p}\right)\omega = 0 \tag{5}$$

where the term in the parentheses is a measure of the static stability of the atmosphere. The second term of (5) results from the assumption that the temperature is advected by the nondivergent part of the windfield similar to the advection of vorticity in (2). Now the static stability must be replaced by a standard value depending on pressure alone if the system of equations is to conserve the sum of kinetic energy and available potential energy (Lorenz, 1960).

All the terms of (5) involve the temperature T and therefore are related to the height field by (4) and to the stream field by (1).

Since however the static stability is not allowed to vary in time or in the horizontal, the streamfunction and the static stability must be uncoupled. It is therefore useful to define the streamfunction as a deviation of the geopotential height from its standard value, i.e., $f_o\psi = \Phi - \bar{\Phi}(p)$ which satisfies (1). From (4) the temperature is then related to the streamfunction as follows

$$T = \bar{T}(p) - \frac{pf_o}{R}\frac{\partial \psi}{\partial p} \tag{6}$$

where $\bar{T} = -(p/R)\, d\bar{\Phi}/dp$. Now the second term on the right of (6) should be neglected in computing the static stability. The static stability parameter used in the following is defined

$$\sigma(p) = -\frac{R}{p}\left(\frac{d\bar{T}}{dp} - \frac{\bar{T}}{p}\frac{R}{c_p}\right) \tag{7}$$

The basic equations for the present model are now obtained by substituting (3) into (2) and (6) into (5). The resulting equations are

$$\frac{\partial}{\partial t}\nabla^2\psi + J(\psi, \nabla^2\psi + f) - f_o\frac{\partial \omega}{\partial p} = 0 \tag{8}$$

$$\frac{\partial}{\partial t}\frac{\partial \psi}{\partial p} + J\left(\psi, \frac{\partial \psi}{\partial p}\right) + \frac{\sigma}{f_o}\omega = 0 \tag{9}$$

where it is understood that σ is only a function of pressure as given by (7). For the actual prediction of the streamfield we eliminate ω by differentiating (9) with respect to pressure and adding the resulting equation to (8). We then obtain the following

$$\frac{\partial}{\partial t}\left(\nabla^2\psi + f_o^2 \frac{\partial}{\partial p}\left(\frac{1}{\sigma}\frac{\partial \psi}{\partial p}\right)\right) + J\left(\psi, \nabla^2\psi + f + f_o^2 \frac{\partial}{\partial p}\left(\frac{1}{\sigma}\frac{\partial \psi}{\partial p}\right)\right) = 0 \qquad (10)$$

This is the quasi-geostrophic potential vorticity equation.

The spherical geometry of the earth is taken into account in the present model, together with the lateral boundary conditions imposed on the flow by nature. It is convenient to choose our basic units accordingly and to normalize the depth and width of the model. The earth's radius is chosen as the unit of length and the reciprocal of the earth's angular rotation speed as the unit of time. The lateral coordinate is defined $\mu \equiv \sin\phi$ where ϕ is latitude and therefore μ ranges from 0 at the equator to 1 at the North Pole. A new vertical coordinate is introduced which increases upward from the surface of the earth.

$$z \equiv \frac{p_o - p}{p_o - p_1}$$

where p_o is the lower pressure surface of the model and p_1 is its upper pressure level. Again z ranges from 0 at the surface to 1 at the top of the model atmosphere. The longitude is denoted by λ.

The Coriolis parameter becomes simply $f \equiv 2\Omega \sin\phi = 2\mu$ and the Laplace operator and the Jacobian operator become respectively

$$\nabla^2 = \frac{\partial}{\partial \mu}\left((1-\mu^2)\frac{\partial}{\partial \mu}\right) + \frac{1}{1-\mu^2}\frac{\partial^2}{\partial \lambda^2} \qquad (12)$$

$$J(a,b) = \frac{\partial a}{\partial \lambda}\frac{\partial b}{\partial \mu} - \frac{\partial a}{\partial \mu}\frac{\partial b}{\partial \lambda} \qquad (13)$$

The basic equations (8) and (9) may then be written in the following form

$$\frac{\partial}{\partial t} \nabla^2\psi + 2 \frac{\partial \psi}{\partial \lambda} + J\ (\psi, \nabla^2\psi) + \frac{\partial w}{\partial z} = 0 \qquad (14)$$

$$\frac{\partial}{\partial t} \frac{\partial \psi}{\partial z} + J\ \left(\psi, \frac{\partial \psi}{\partial z}\right) - s\ w = 0 \qquad (15)$$

where we have defined a new measure for the vertical velocity component

$$w \equiv \omega\ f_o/(p_o - p_1) \qquad (16)$$

and a new measure for the gravitational stability of the atmosphere

$$s \equiv \sigma\ (p_o - p_1)^2/f_o^2 \qquad (17)$$

which is again a function of pressure only according to (7). For completeness we will also write down the expression for the temperature deviation from its standard value which is denoted by $\tau = T - \overline{T}(p)$ and which by (6) and (11) becomes

$$\tau = \frac{f_o}{R} \left(\frac{p_o}{p_o - p_1} - z \right) \frac{\partial \psi}{\partial z} \qquad (18)$$

The boundary conditions which are consistent with the quasi-geostrophic equations and a flat surface (Phillips, 1963) are that $\omega = 0$ at the top and bottom of the model atmosphere. In the lateral direction we impose the condition of symmetry of the flow field with respect to the equator. Since in the quasi-geostrophic model the zonal velocity $u = -\cos\phi\ \partial\psi/\partial\mu$ and the meridonal velocity component $v = (1/\cos\phi)\ \partial\psi/\partial\lambda$, it follows that ψ is an odd function of the lateral coordinate μ and consequently $\psi = 0$ at the equator, if the pressure-dependent integration constant is incorporated in the first term on the right of (6). The global atmospheric model is herewith reduced to an hemispheric model ($0 < \mu < 1$) with boundary conditions

$$w(\lambda,\mu,z,t) = w_o(\mu,z,t) + 2Re\left(w_1(\mu,z,t)e^{i\ell\lambda} + w_2(\mu,z,t)e^{2i\ell\lambda}\right)$$

$$\tau(\lambda,\mu,z,t) = \tau_o(\mu,z,t) + 2Re\left(\tau_1(\mu,z,t)e^{i\ell\lambda} + \tau_2(\mu,z,t)e^{2i\ell\lambda}\right) \tag{25}$$

Substituting now (21), (22) and (25) into (14) we obtain an equation of the form $C_o + C_1 \exp(i\ell\lambda) + C_1' \exp(-i\ell\lambda) + C_2 \exp(2i\ell\lambda) + \ldots = 0$, which can be satisfied only if the coefficients $C_j(\mu,z,t)$ are individually equal to zero. The three coefficients C_o, C_1, and C_2 give the equations

$$\frac{\partial \Lambda_j}{\partial t} + 2i\ell_j\psi_j + G_j + H_j + \frac{\partial w_j}{\partial z} = 0 \qquad j = 0,1,2 \tag{26}$$

where G_j and H_j resulting from the Jacobian term in (14) are given below. The coefficients C_1' and C_2' produce two equations which are the complex conjugates of the equations for C_1 and C_2 and therefore can be dispensed with. The equations resulting from $C_j = 0$ for $j>2$ must be discarded since these equations tend to generate the waves of wave numbers 3ℓ and 4ℓ which are precluded by equation (21). A similar procedure applied to (15) results into the set of equations

$$\frac{\partial^2 \psi_j}{\partial t \partial z} + s\,(P_j + Q_j - w_j) = 0 \qquad j = 0,1,2, \tag{27}$$

Finally, the potential vorticity equation (20) becomes

$$\frac{\partial \Lambda_j}{\partial t} + \frac{\partial}{\partial z}\left(\frac{1}{s}\frac{\partial^2 \psi_j}{\partial z \partial t}\right) + 2i\ell_j\psi_j + G_j + H_j + \frac{\partial P_j}{\partial z} + \frac{\partial Q_j}{\partial z} = 0 \tag{28}$$

It should be noted that the new set of prediction equations (26), (27) and (28) do not involve the longitudinal coordinate λ. All of the

dependent variables are functions of only μ,z, and t, and the nonlinear functions G_j and H_j may be easily found from (14)

$$G_1 = i\ell\left(\psi_1 \frac{\partial \Lambda_o}{\partial \mu} - \frac{\partial \psi_o}{\partial \mu} \Lambda_1\right)$$

$$G_o = -2\ell \, \mathrm{Im}\left(\psi_1 \frac{\partial \Lambda_1^*}{\partial \mu} - \frac{\partial \psi_1^*}{\partial \mu} \Lambda_1\right) \qquad G_2 = 2i\ell\left(\psi_2 \frac{\partial \Lambda_o}{\partial \mu} - \frac{\partial \psi_o}{\partial \mu} \Lambda_2\right)$$

$$H_o = -4\ell \, \mathrm{Im}\left(\psi_2 \frac{\partial \Lambda_2^*}{\partial \mu} - \frac{\partial \psi_2^*}{\partial \mu} \Lambda_2\right) \qquad H_2 = i\ell\left(\psi_1 \frac{\partial \Lambda_1}{\partial \mu} - \frac{\partial \psi_1}{\partial \mu} \Lambda_1\right) \tag{29}$$

$$H_1 = i\ell\left(2\psi_2 \frac{\partial \Lambda_1^*}{\partial \mu} + \frac{\partial \psi_2}{\partial \mu} \Lambda_1^* - 2 \frac{\partial \psi_1^*}{\partial \mu} \Lambda_2 - \psi_1^* \frac{\partial \Lambda_2}{\partial \mu}\right)$$

where Im denotes the imaginary part of a complex number and the asterisk indicates the complex conjugate. The nonlinear function P_j is obtained from G_j and Q_j is obtained from H_j by simply replacing Λ_j by $(1/s)\partial\psi_j/\partial z$.

The significance of the nonlinear terms G_j, H_j, P_j, and Q_j is evident from an inspection of (28) and (29). Starting from a small perturbation of wave number ℓ superimposed on the zonal flow, the terms G_1 and P_1 represent the effect of the basic zonal flow ψ_o on the developing wave ψ_1. Only these two terms are therefore retained in the linear study discussed in the next chapter. The nonlinear effects of the developing wave upon the zonal flow are represented by G_o and P_o, and this problem will be considered in Section IVB. Finally, if the primary wave has become sufficiently large, the nonlinear functions H_2 and Q_2 will generate the secondary wave of wave number 2ℓ, which will then interact with the zonal flow by virtue of the functions G_2 and P_2, and with the primary wave through H_1 and Q_1, while its nonlinear effects on the zonal flow are represented by H_o and Q_o (section IVC).

In order to extrapolate the streamfunctions in time we apply two well-known numerical techniques. Spectral expansions are used in the horizontal and either layered or spectral representations are employed in the vertical. The horizontal-spectral representation is discussed in Appendix A, the vertical-spectral representation in Appendix B, and the layered model equations are derived in Appendix C.

C. Energy and Energy Conversions

The development of unstable perturbations on a zonal current is studied most easily by determining the generation of the kinetic energy of the perturbations and the exchange of energy between the zonal flow and the eddies. The first quantity we are concerned with is the kinetic energy per unit mass which is defined

$$KE = \tfrac{1}{2}(u^2+v^2) = \tfrac{1}{2}\left[(1-\mu^2)(\partial\psi/\partial\mu)^2 + (\partial\psi/\partial\lambda)^2/(1-\mu^2)\right] \tag{31}$$

For the present purposes it is sufficient to consider the mean energy quantities for the hemisphere. Thus averaging (31) with respect to longitude and latitude, substituting (21), and integrating by parts using the lateral boundary condition (19), we obtain

$$K \equiv \frac{1}{2\pi}\int_0^{2\pi}\int_0^1 (KE)\, d\lambda d\mu = K_o + K_1 + K_2$$

$$K_o \equiv -\int_0^1 \tfrac{1}{2}\,\psi_o\Lambda_o\, d\mu \qquad K_j \equiv -\int_0^1 \psi_j^*\Lambda_j\, d\mu,\ j = 1,2 \tag{32}$$

where the asterisk denotes the complex conjugate, Λ_j is defined by (23), and K_o, K_1, and K_2 can be easily shown to be real quantities. Clearly

then K_o, K_1, and K_2, represent the area-mean kinetic energy per unit mass in the zonal flow, the first wave, and the second wave, respectively.

Another energy quantity which has been shown by Lorenz (1960) to be very useful for a study of the present type is inversely proportional to the atmospheric Richardson number. This quantity is known as the "available potential energy" and represents in our model the only source of kinetic energy. Following Lorenz, recalling the definition for the static stability (7), and using (6), (11), and (17), we may write this available energy as

$$AE = \frac{1}{2\sigma}\left(\frac{R}{p}(T-\bar{T})\right)^2 = \frac{f_o^2}{2\sigma}\left(\frac{\partial\psi}{\partial p}\right)^2 = \frac{1}{2s}\left(\frac{\partial\psi}{\partial z}\right)^2 \tag{33}$$

Again averaging over the hemisphere and substituting (21), we arrive at

$$A = \frac{1}{2\pi}\int_0^{2\pi}\int_0^1 (AE)\, d\lambda d\mu = A_o + A_1 + A_2$$

$$A_o \equiv \int_0^1 \frac{1}{2s}\left(\frac{\partial\psi_o}{\partial z}\right)^2 d\mu; \quad A_j \equiv \int_0^1 \frac{1}{s}\frac{\partial\psi_j}{\partial z}\frac{\partial\psi_j^*}{\partial z}\, d\mu, \quad j = 1,2 \tag{34}$$

The main advantage of this available potential energy lies in the fact that the vertical average of the sum $\bar{K}+\bar{A}$ is conserved by the present system of equations as we shall see in the sequel.

The time rate of change of the area-mean kinetic energy is obtained by differentiating (31) with respect to time, averaging over the hemisphere, and integrating by parts. The results are

$$\frac{\partial K_o}{\partial t} = -\int_0^1 \psi_o \frac{\partial\Lambda_o}{\partial t}\, d\mu; \quad \frac{\partial K_j}{\partial t} = -2\mathrm{Re}\int_0^1 \psi_j^* \frac{\partial\Lambda_j}{\partial t}\, d\mu, \quad j = 1,2 \tag{35}$$

and similarly for the available energy

$$\frac{\partial A_o}{\partial t} = \int_0^1 \frac{1}{s}\frac{\partial \psi_o}{\partial z}\frac{\partial^2 \psi_o}{\partial t \partial z}\,d\mu; \quad \frac{\partial A_j}{\partial t} = 2Re \int_0^1 \frac{1}{s}\frac{\partial \psi_j^*}{\partial z}\frac{\partial^2 \psi_j}{\partial t \partial z}\,d\mu, \quad j=1,2 \tag{36}$$

The energy conversions are then obtained by substituting the vorticity equation (26) into (35) and by using the thermodynamic equation (27) in (36). Let us denote the exchange of kinetic energy between wave j and wave k by CK_{jk}, their exchange of available energy by CA_{jk}, and the conversion of potential to kinetic energy by CAK. The energy equations may then be written

$$\begin{aligned}
\frac{\partial K_o}{\partial t} &= CK_{10} + CK_{20} + CAK_o & \frac{\partial A_o}{\partial t} &= CA_{10} + CA_{20} + CKA_o \\
\frac{\partial K_1}{\partial t} &= CK_{01} + CK_{21} + CAK_1 & \frac{\partial A_1}{\partial t} &= CA_{01} + CA_{21} + CKA_1 \\
\frac{\partial K_2}{\partial t} &= CK_{02} + CK_{12} + CAK_2 & \frac{\partial A_2}{\partial t} &= CA_{02} + CA_{12} + CKA_2
\end{aligned} \tag{37}$$

where from (26), (27), (35), and (36) we obtain readily

$$\begin{aligned}
CK_{10} &= \int_0^1 \psi_o G_o\,d\mu & CK_{01} &= 2Re \int_0^1 \psi_1^* G_1\,d\mu \\
CK_{20} &= \int_0^1 \psi_o H_o\,d\mu & CK_{02} &= 2Re \int_0^1 \psi_2^* G_2\,d\mu \\
CK_{21} &= 2Re \int_0^1 \psi_1^* H_1\,d\mu & CK_{12} &= 2Re \int_0^1 \psi_2^* H_2\,d\mu
\end{aligned} \tag{38}$$

$$\begin{aligned}
CA_{10} &= -\int_0^1 \frac{\partial \psi_o}{\partial z} P_o\,d\mu & CA_{01} &= -2Re \int_0^1 \frac{\partial \psi_1^*}{\partial z} P_1\,d\mu \\
CA_{20} &= -\int_0^1 \frac{\partial \psi_o}{\partial z} Q_o\,d\mu & CA_{02} &= -2Re \int_0^1 \frac{\partial \psi_2^*}{\partial z} P_2\,d\mu \\
CA_{21} &= -2Re \int_0^1 \frac{\partial \psi_1^*}{\partial z} Q_1\,d\mu & CA_{12} &= -2Re \int_0^1 \frac{\partial \psi_2^*}{\partial z} Q_2\,d\mu
\end{aligned} \tag{39}$$

$$CAK_o = \int_0^1 \psi_o \frac{\partial w_o}{\partial z}\, d\mu \qquad CKA_o = \int_0^1 \frac{\partial \psi_o}{\partial z} w_o d\mu$$

$$CAK_1 = 2Re \int_0^1 \psi_1^* \frac{\partial w_1}{\partial z}\, d\mu \qquad CKA_1 = 2Re \int_0^1 \frac{\partial \psi_1^*}{\partial z} w_1 d\mu \qquad (40)$$

$$CAK_2 = 2Re \int_0^1 \psi_2^* \frac{\partial w_2}{\partial z}\, d\mu \qquad CKA_2 = 2Re \int_0^1 \frac{\partial \psi_2^*}{\partial z} w_2 d\mu$$

By using the expressions for the nonlinear functions (29) it can be shown easily that $CK_{10} = - CK_{01}$, $CK_{20} = - CK_{02}$, $CK_{21} = - CK_{12}$, and similarly for CA. This is true at each level in the vertical since no vertical integration has yet been performed. After vertical integration we find also by virtue of the vertical boundary condition (19) that $CAK_j = - CKA_j$ for $j = 1,2,3$. This is used as a check on the numerical computations. Furthermore it follows then immediately that $d\overline{A}/dt + d\overline{K}/dt = 0$ if the bar denotes a vertical average. Thus $\overline{A}+\overline{K}$ is a conservative quantity for the present model, which may be computed at regular time intervals as a check on the time extrapolation by finite difference methods.

The meaning of the various energy conversion terms follows immediately from an inspection of (37) and (38). A common way of representing such energy processes is shown below

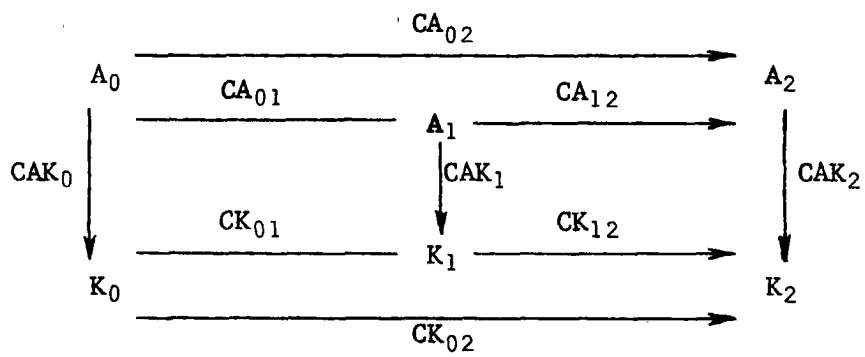

It should be recalled that the kinetic energy and the potential energy are defined per unit mass, and hence the same is true for the energy conversions. The energies will be expressed in units of m^2/sec^2 and the energy conversions in units of m^2/sec^2 per day. The actual energy in a vertical atmospheric column is related in a simple manner to our energy quantities. Using the definition (11) we obtain for instance for the kinetic energy in a vertical column

$$\frac{1}{g}\int_0^{p_o} K\,dp = \frac{p_o-p_1}{g}\int_0^1 K dz = \frac{p_o-p_1}{g}\overline{K}$$

Taking $p_o = 10^3$ mb, $p_1 = 0$, and $g = 10\ m^2/sec^2$, we have $(p_o-p_1)/g = 10^4\ kg/m^2$. Thus if we multiply the vertical-mean energy per unit mass by 10^4 we obtain the energy per unit of surface area in units of joules/m^2.

III. LINEAR ANALYSIS

A. Computational Technique

The linear study is concerned with a small periodic disturbance superimposed on a zonal flow which is constant in time. The total streamfunction is

$$\psi(\lambda,\mu,z,t) = \psi_o(\mu,z) + 2\mathrm{Re}\left(\psi_1(\mu,z,t)e^{i\ell\lambda}\right) \tag{41}$$

where it has been assumed that the perturbation consists of a single planetary wave of wave number ℓ, and clearly ψ_1 is a complex quantity. The development of the wave in time is described by (28) for j=1, where the nonlinear terms H_1 and Q_1 are to be discarded since they represent interactions with the wave of wave number 2ℓ which is ignored in the linear model. Owing to the time-independent character of the zonal flow ψ_o, the functions G_1 and P_1 become linear in the time-dependent variables and (28) reduces to an equation with time-independent coefficients. From (23), (28), and (29) we have

$$\frac{\partial \Lambda_1}{\partial t} + \frac{\partial}{\partial z}\left(\frac{1}{s}\frac{\partial^2 \psi_1}{\partial z \partial t}\right) + 2i\ell\,\psi_1 + G_1 + \frac{\partial P_1}{\partial z} = 0 \tag{42}$$

$$G_1 \equiv i\ell\left(\frac{\partial \Lambda_o}{\partial \mu}\psi_1 - \frac{\partial \psi_o}{\partial \mu}\Lambda_1\right); \qquad P_1 \equiv \frac{i\ell}{s}\left(\frac{\partial^2 \psi_o}{\partial \mu \partial z}\psi_1 - \frac{\partial \psi_o}{\partial \mu}\frac{\partial \psi_1}{\partial z}\right) \tag{43}$$

$$\Lambda_1 \equiv \frac{\partial}{\partial \mu}(1-\mu^2)\frac{\partial \psi_1}{\partial \mu} - \frac{\ell^2 \psi_1}{1-\mu^2}; \qquad \Lambda_o \equiv \frac{\partial}{\partial \mu}(1-\mu^2)\frac{\partial \psi_o}{\partial \mu} \tag{44}$$

Since the coefficients of (42) are arbitrary functions of the lateral and vertical coordinates we must have recourse to numerical techniques in order to obtain the solution.

For the present computations we have combined a spectral technique in the horizontal direction (Appendix A) with a layered representation

in the vertical (Appendix C). The details of this procedure are given in Appendix E, and we will here restrict ourselves to an outline of the numerical method, which may clarify the subsequent discussion. Thus the perturbation streamfunction ψ_1 is represented by a series of polynomials which are functions of μ only

$$\psi_1 = \sum_{\beta} \psi_\beta(z,t)\ Y_\beta\ (\mu) \tag{45}$$

The polynomials $Y_\beta\ (\mu)$ are the associated Legendre functions whose properties are discussed in Appendix A. The coefficients of the expansion (45) are clearly functions of z and t, and we refer to these coefficients as "horizontal-spectral components". Each of these components is now defined at regular intervals in the vertical, which means that each component is itself represented by a number of "parameters" which are functions of time only. If the horizontal expansion is truncated after N terms, and the atmosphere is divided vertically into M layers, then we are dealing effectively with L≡N x M time-dependent wave parameters, which are complex quantities since ψ_1 is complex.

The governing equation (42) for the wave perturbation ψ_1 is now replaced by a system of L ordinary differential equations with time as the only independent variable. The latter equations are obtained by substituting (45) into (42) to (44), using the orthogonality of the polynomials Y_β, and applying the resulting horizontal-spectral equations at the midpoints of the layers. This procedure involves an integration with respect to the lateral coordinate μ, which requires a knowledge of the variation of the basic state streamfunction ψ_o with μ. Given this function ψ_o, the integrations may be either carried out numerically,

or the streamfunction ψ_o may be first expanded in a series similar to (45) but with time-independent coefficients. The latter method has been used here in view of the subsequent nonlinear study. The relevant equations are derived in Appendix E, where it is shown that the resulting system of equations may be written as

$$\frac{d}{dt}\vec{\Psi}_1 + i\,\mathbb{D}\,\vec{\Psi}_1 = 0 \tag{46}$$

Where $\vec{\Psi}_1$ is the array of the L time-dependent wave parameters discussed before, and $\mathbb{D}$ is the coefficient matrix of order L made up of basic state constants such as static stability and zonal flow parameters.

The linear system of equations above allows for solutions of the form exp (-iνt) and thus the linear problem reduces to an eigenvalue problem where ν is the eigenvalue. It follows from (41) that if

$$\psi_1 \sim \exp(-i\nu t) \tag{47}$$

then the eastward angular propagation speed of the wave perturbation equals

$$\omega = \nu/\ell \tag{48}$$

and consequently the eigenvalue is directly related to the wave speed. At the same time it is seen that if the eigenvalue is complex, $\nu = \nu_r + i\nu_i$, then the perturbation grows in time with "growth rate" ν_i. Such perturbations with exponentially increasing amplitude are called unstable.

Since (46) represents a system of L coupled equations, there will be L eigenvalues. Most of these eigenvalues are real numbers and do not correspond to unstable wave solutions. In general however we will find a number of complex eigenvalues. Owing to the character

of the coefficient matrix, the complex eigenvalues can only be found as complex conjugate pairs. In this case a growing and a decaying mode will exist simultaneously, and we are, of course, mainly concerned with the growing wave. The total solution for the wave perturbation ψ_1 is a linear combination of the normal mode solutions and it follows that the most unstable mode will eventually take over and determine the structure of the wave. The horizontal and vertical structure of the unstable wave will therefore be given by the eigenvector associated with the eigenvalue which has the largest imaginary part.

B. Basic State Parameters

It follows from (28) and (29) that the basic state is completely determined by the parameters s(z) and $\psi_0(\mu,z)$, that is, by the (standard) static stability and the zonal flow. The reciprocal of the standard static stability adopted for most of the present calculations is shown in Fig. 1. This inverse static stability is obtained by averaging the values for summer and winter presented by Gates (1961). In the same figure we have included Gates' static stability profile for the winter months which will be used later to study the quantitative effects of variations of static stability.

The basic zonal streamfunction ψ_0 is obtained from climatological mean zonal wind data for January. In order to contribute to an easier interpretation of the subsequent results, we will describe the character of the zonal flow by presenting the horizontal wind profiles at vertical intervals of 100 mb. and the vertical profiles at horizontal intervals of 10 degrees of latitude. Fig. 2 thus shows the climatological-mean zonal component of the wind for January averaged zonally around the earth.

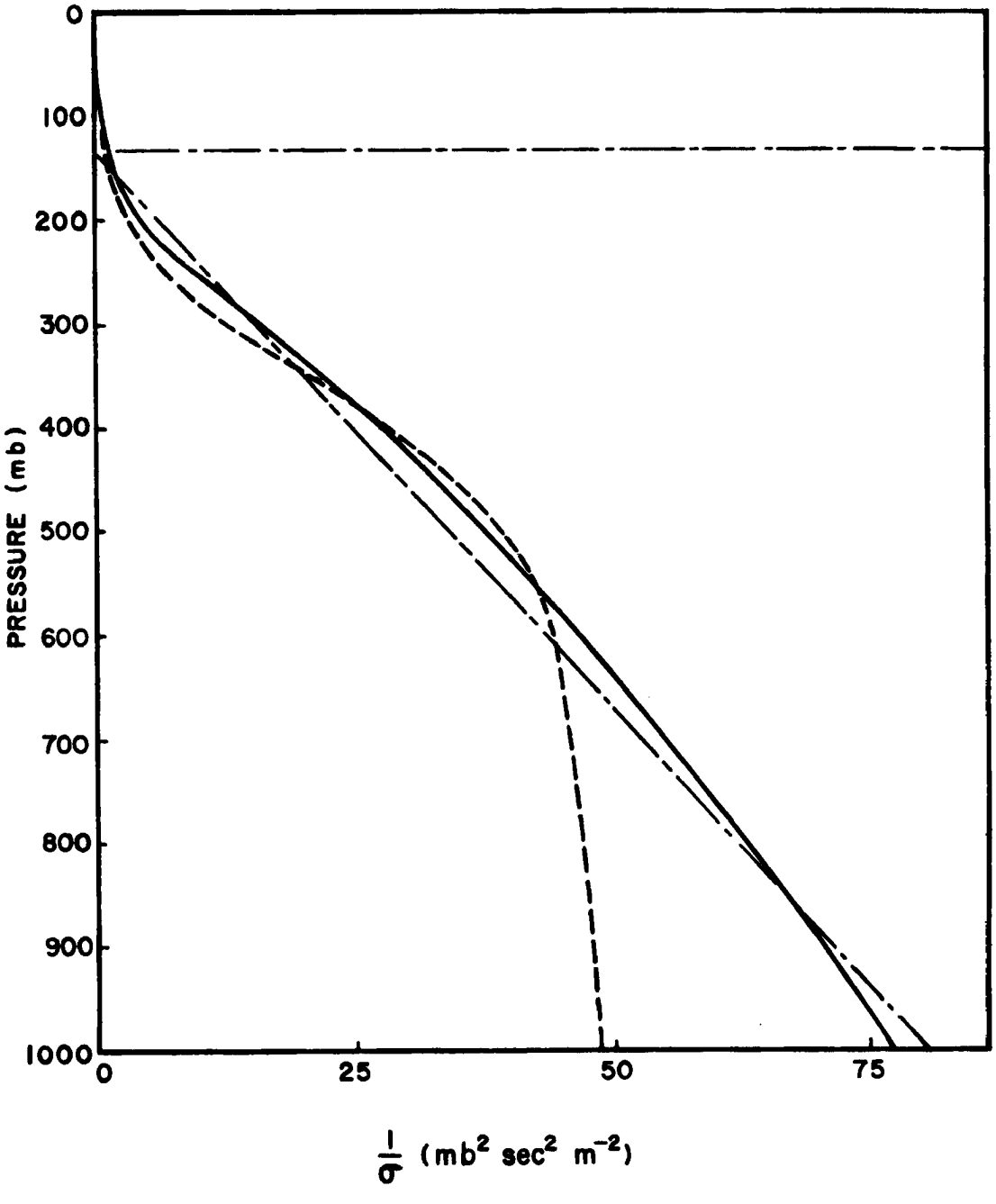

Fig. 1

Inverse of standard static stability employed in the following. Solid line: mean static stability for year; dashed line: winter static stability. Dash-dot lines to be discussed in Chapter V.

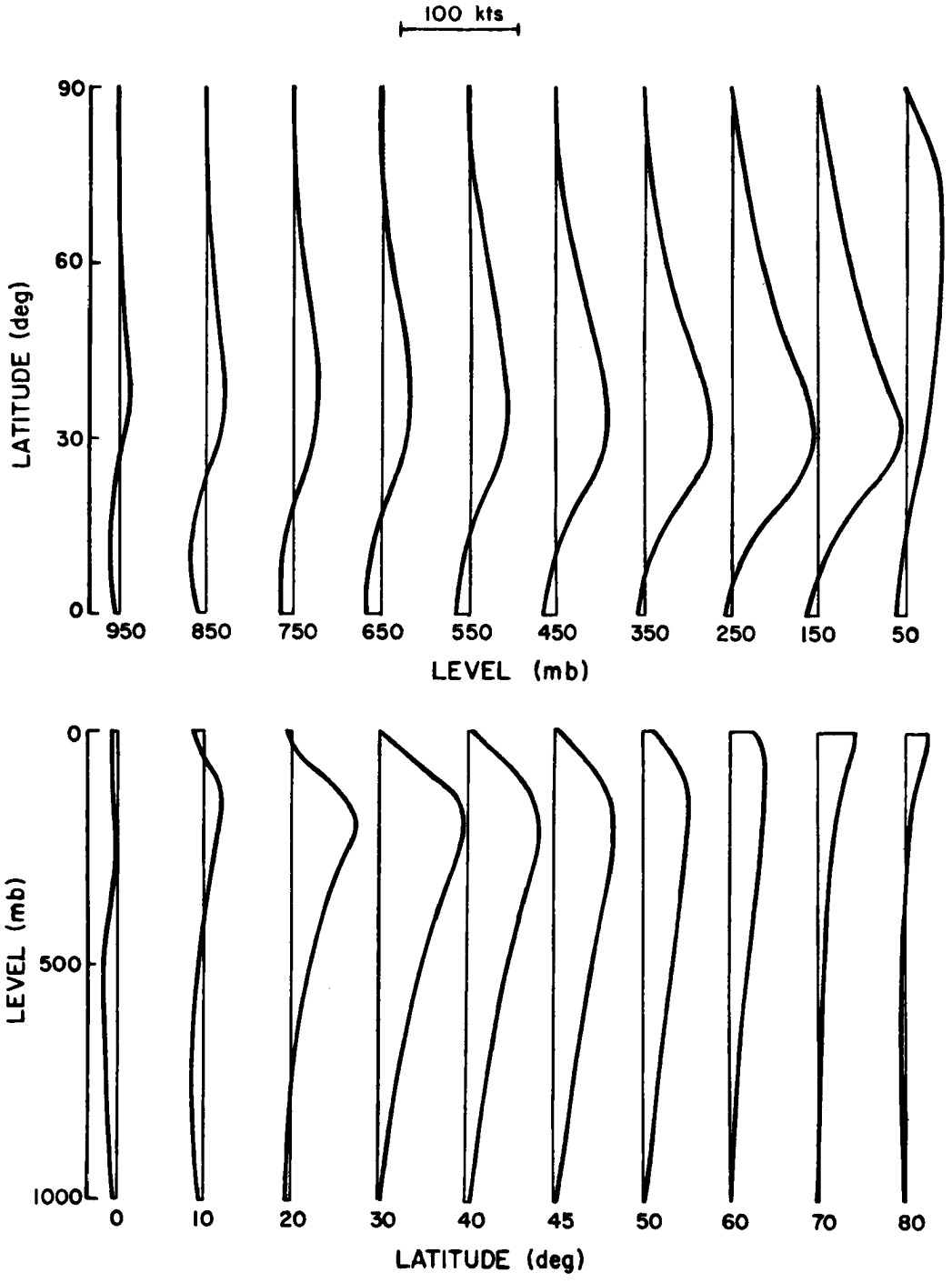

Fig. 2

Horizontal and vertical profiles of climatological mean zonal wind for January. West winds to the right of the vertical coordinate.

The zonal average of the windfield smooths out significant local patterns of the flow. In particular it is noticed that the profiles of the time-averaged zonal wind component over the Pacific are distinctly different from those over the Atlantic. If it is assumed that a developing cyclone is largely affected by the local "basic flow" pattern, then it seems worthwhile to investigate the stability character of such flows. We have therefore averaged the climatological-mean zonal component of the wind over 60 degrees of longitude, thus obtaining January mean zonal wind profiles representative for Europe, Asia, the West-Pacific, East-Pacific, North America, and the Atlantic, respectively. These profiles of course do not represent a basic zonal flow in the sense defined in Chapter II, i.e., a flow averaged zonally around the world, but they will in the following be treated as such. This may be an acceptable procedure for waves of cyclone scale and shorter waves. The 60-degree average zonal wind profiles are shown in Fig. 3. Of particular interest as compared with Fig. 2 are the averages for 120-180E (extremely strong jet at low latitudes) and for 0-60W (double jet over the Atlantic).

The zonal wind component does not figure directly in our perturbation equation (42) but rather the basic state streamfunction $\psi_o(\mu,z)$ does. The latter follows directly from the mean zonal wind by virtue of the relationship $u_o = - \partial\psi_o/\partial y$ where y is the south-to-north coordinate. The arbitrary constant of integration must be chosen such that $\psi_o = 0$ at the equator, in view of the boundary condition (19).

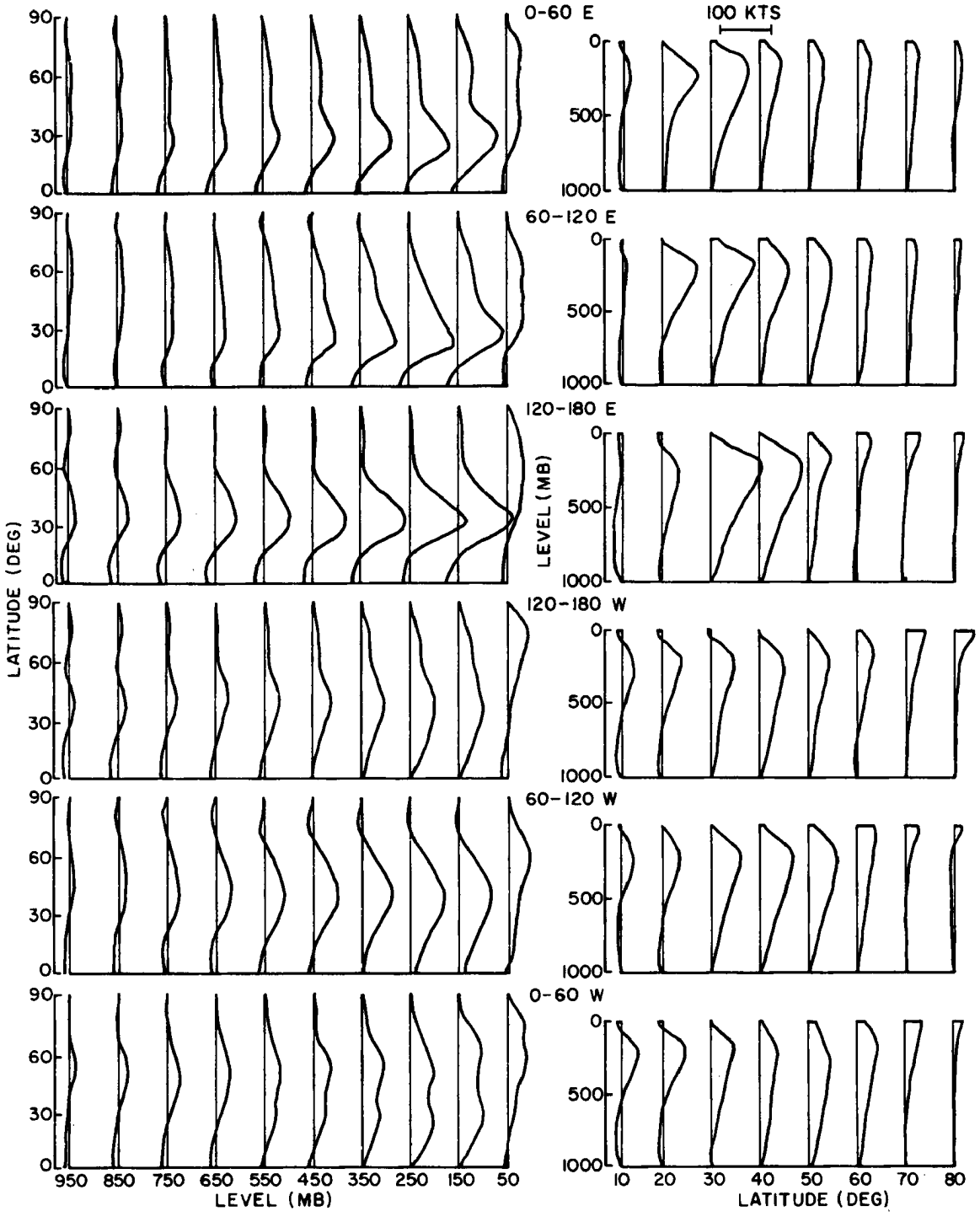

Fig. 3

Horizontal and vertical profiles of zonal wind component for January averaged over 60 degrees of longitude.

C. Results of Linear Analysis

In this section we present the normal mode instability associated with the climatological-mean zonal wind for January which is shown in Fig. 2. The basic static stability is the average for the year shown by the solid curve of Fig. 1. The effect of the winter static stability represented by the dashed curve will be discussed in IIID, but this stability profile has been obtained over the American continent and may be too stable for our global model.

The resolution of the numerical model is comparable for the horizontal and the vertical. Unless stated otherwise, the horizontal-spectral expansion includes 8 components (N=8) and the number of layers in the vertical is M = 10. The coefficient matrix (46) is therefore of order 80. The vertical resolution has been studied frequently in connection with the baroclinic stability problem. Most recently this problem has been considered by Gary (1965), Brown (1968), and Simons (1969). A resolution of 10 layers seems to be satisfactory, at least for determining the most unstable normal mode of cyclone-scale perturbations. The horizontal truncation is justified presently by evaluating the convergence of the most unstable roots as a function of an increasing number of terms in expansion (45).

Fig. 4 shows all the unstable modes for wave numbers ℓ=3,6,8, and 16, and for horizontal truncations N=6,7, and 8. The unstable roots are presented in terms of the growth rates per day and the angular wave speed in degrees of longitude per day. It is seen that in general we find about 10 complex eigenvalues out of a total number of 60 to 80 eigenvalues (for N = 6 to 8, respectively). The tail end of the

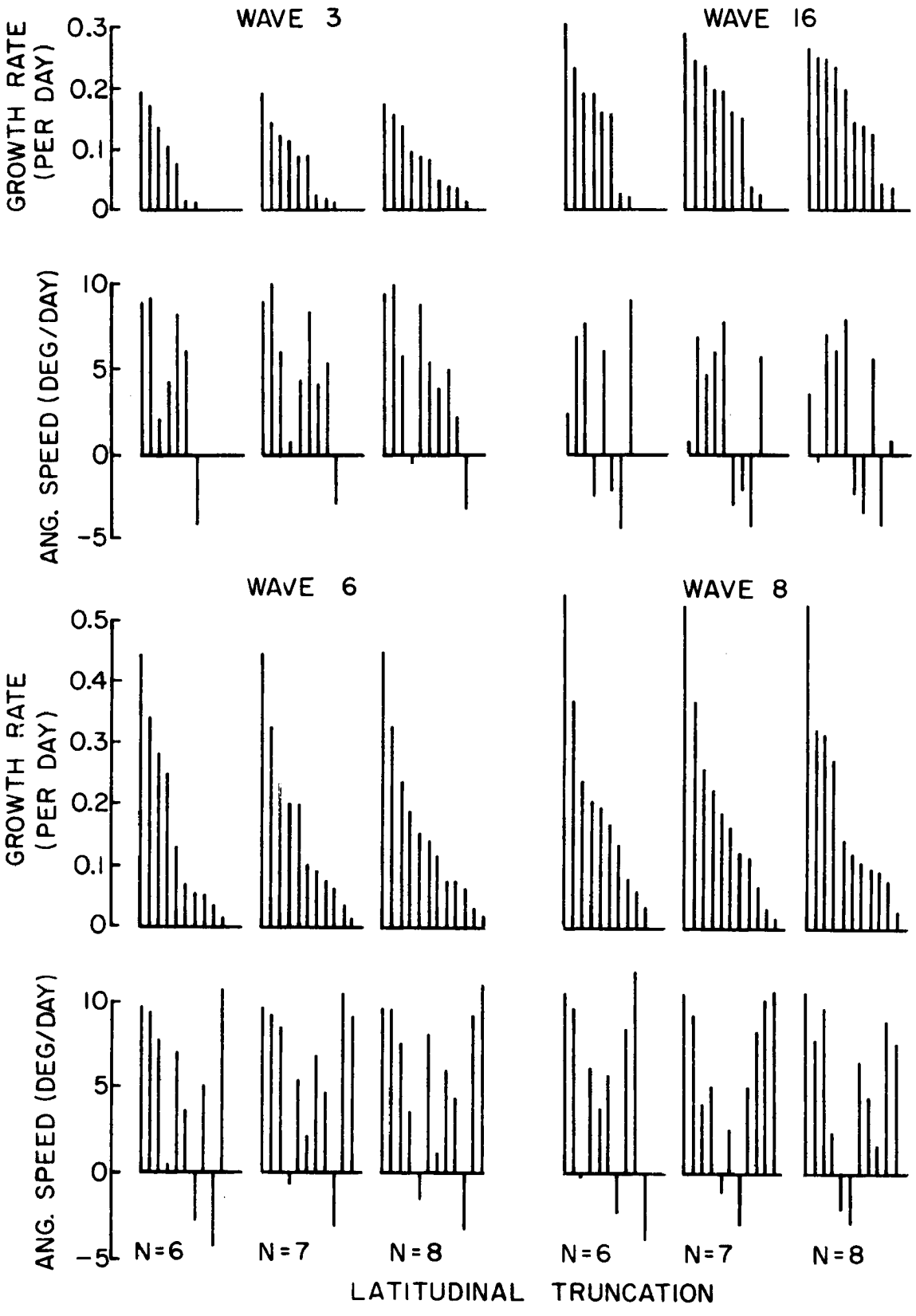

Fig. 4

Convergence of unstable normal modes for basic current of Fig. 2

eigenvalue spectrum is modified considerably as the resolution increases. This is particularly obvious for the wave speeds since the roots have been arranged according to the growth rate and therefore may switch positions. However, the convergence of the most unstable modes is very satisfactory except for the very short waves. The latter waves show also a poor convergence with respect to the vertical resotion and, of course, the quasi-geostrophic approximation is not well justified for such waves either. The results for the very short waves should therefore be viewed with a critical eye.

The instability of the January mean zonal wind has been determined for planetary wave numbers 1 through 16. The computations were made for a horizontal truncation N=8 and a vertical truncation M=10. All unstable modes are shown in Fig. 5 in terms of growth rates per day and eastward angular wave speeds in degrees per day. The growth rate is defined as the imaginary part of the eigenvalue ν_i, thus according to (47) the amplitudes of our most unstable waves will grow in one day by a factor of about $\sqrt{e} = 1.65$. The waves of maximum instability show one mode which is distinctly more unstable than the other growing modes. For these waves it seems therefore plausible that the most unstable modes will eventually take over and will determine the structure of the waves. For the longer waves and certainly for the short waves such governing unstable modes do not exist, at least not in the present model. The angular wave speeds of the most unstable modes are of the order of 10 degrees of longitude per day. This is important in the light of our later discussion of basic state flows obtained by averaging the zonal wind component over 60 degrees of longitude. The assumption there is that the wave is effected mainly by the local character of the basic

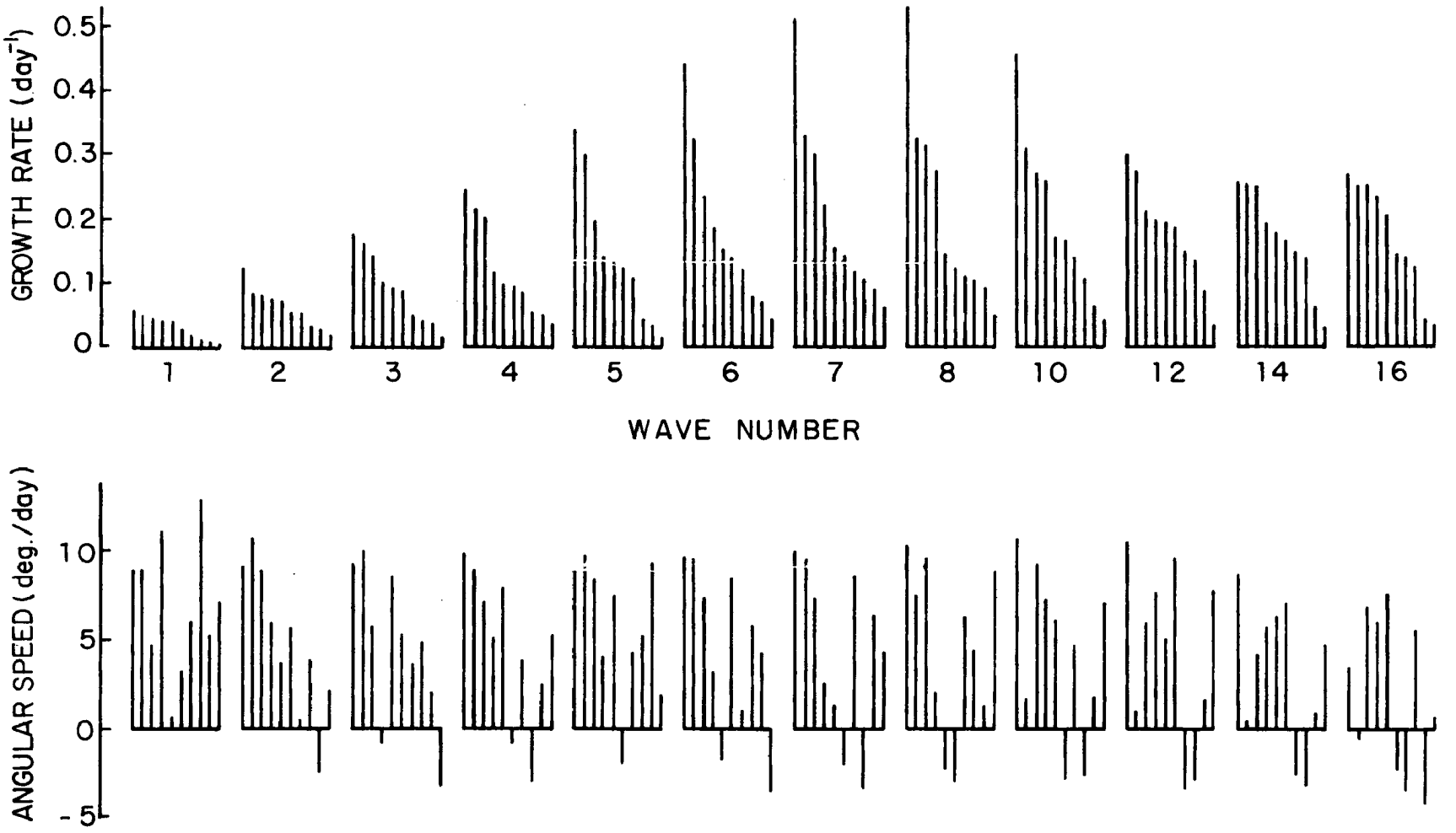

Fig. 5

Unstable modes for climatological-mean January zonal wind shown in Fig. 2.

flow, and a prerequisite of such a study is clearly that the wave stays for some days in a given sector.

The instabilities presented in Fig. 5 give, of course, no information about the nature of the instability of our observed mean wind. Thus the instability may be due partly to the vertical shear and partly to the horizontal shear of the zonal flow, i.e., we may be dealing with both baroclinic and barotropic instability. To establish the character of the instability we consider the energy conversion processes which are responsible for the growth of the waves. The baroclinic instability is characterized by a conversion of available potential energy into perturbation kinetic energy. On the other hand, in a barotropic atmosphere a perturbation can only amplify as a result of a transfer of basic flow kinetic energy to the wave. Considering the energy-cycle discussed in Chapter IIC we notice that, in the absence of the second wave, the sources of wave kinetic energy are given by the terms CAK and CK_{01}. Obviously the first term represents the baroclinic process, while the second term is a measure of barotropic instability.

In order to determine the energy processes we must first establish the horizontal and vertical structure of the wave perturbation. The energy cycle associated with a given unstable mode may be studied by determining the structure of this particular mode, i.e., by computing the eigenvector associated with this unstable root. The initial amplitude of the perturbation in a linear model is arbitrary in the sense that a change of amplitude without a change of structure results into a multiplication of all energies and their conversions by the same constant factor for all times. It is therefore convenient to divide all energy quantities by one basic parameter such as the wave kinetic energy,

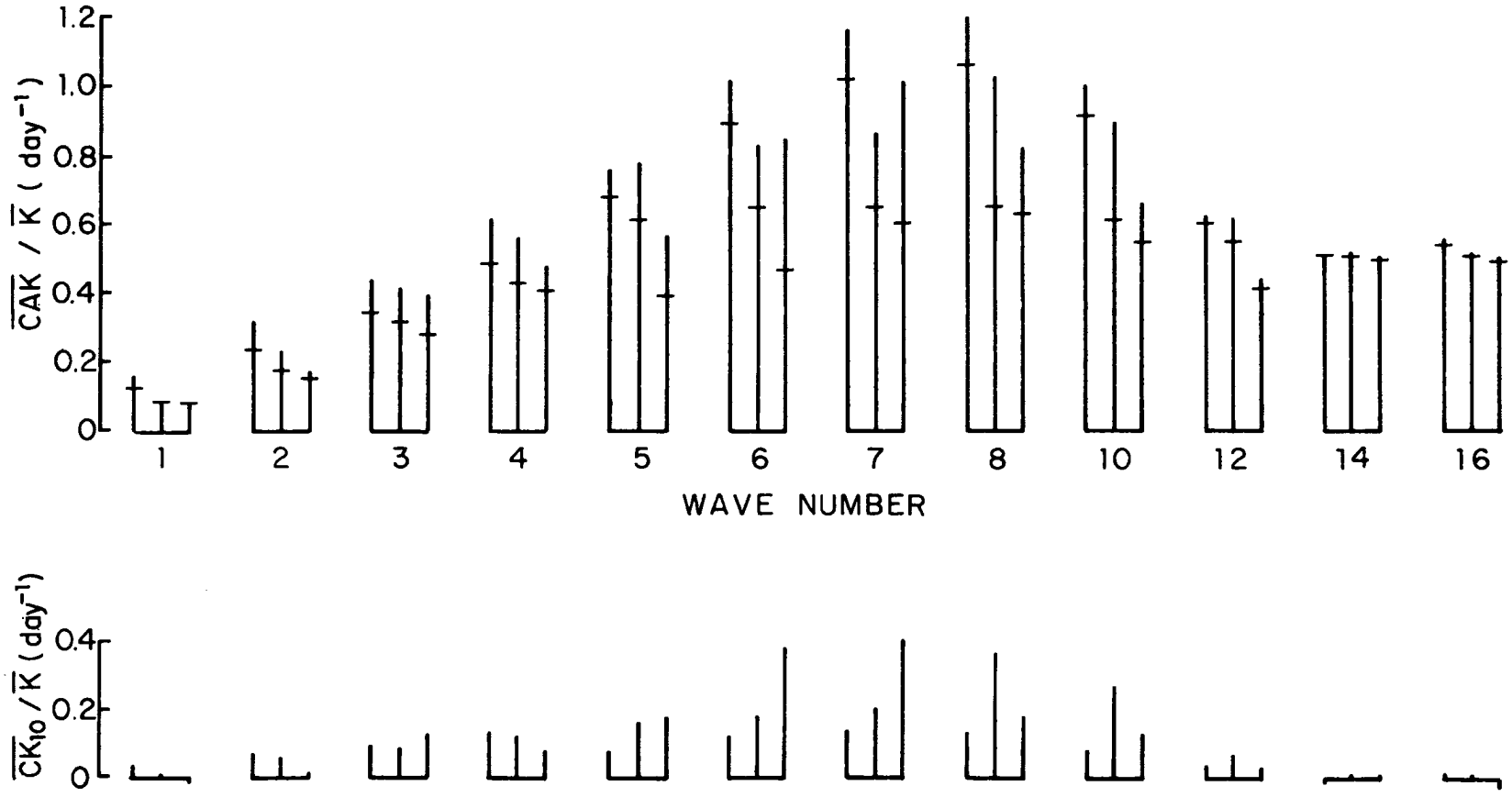

Fig. 6

Energy conversions of three most unstable modes for waves shown in Fig. 5. Conversion of potential to kinetic energy (above) and release of kinetic energy from the wave to the zonal flow (below).

cycle may be represented as follows, if the arrows are made to point into the direction of the flow of energy

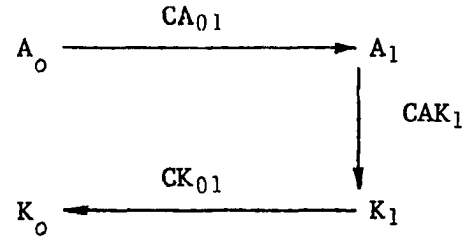

The cycle is of course interrupted on the left since the zonal flow is not allowed to change in the linear model.

The vertical distributions of the various energy conversions in the unstable wave are presented in Fig. 7. The unit of energy is the vertical-mean wave kinetic energy. Two waves are shown: wave 6 and wave 12. The first is typical for all long and cyclone-scale waves in our model. This means that we do not have any waves with the typical structure found for the very long waves in other studies (e.g. Gary, 1965; Brown, 1968; Simons, 1969). In all other respects, the vertical profiles are typical for baroclinic unstable waves. The wave kinetic energy and its time rate of change have two maxima, one at the surface and one at the jetstream level, the first of which increases with wave number while the second one decreases. It is of interest to note that the generation of kinetic energy (CAK) has two maxima while the loss of potential energy (-CKA) shows one maximum at the level of zero divergence. Integrated in the vertical the two must cancel and the implication is that the source of kinetic energy is basically located in the mid-troposphere, from where the energy is transported upward and downward such that it becomes available for the growth of the perturbation at these levels. It may be recalled here that the term CKA is related

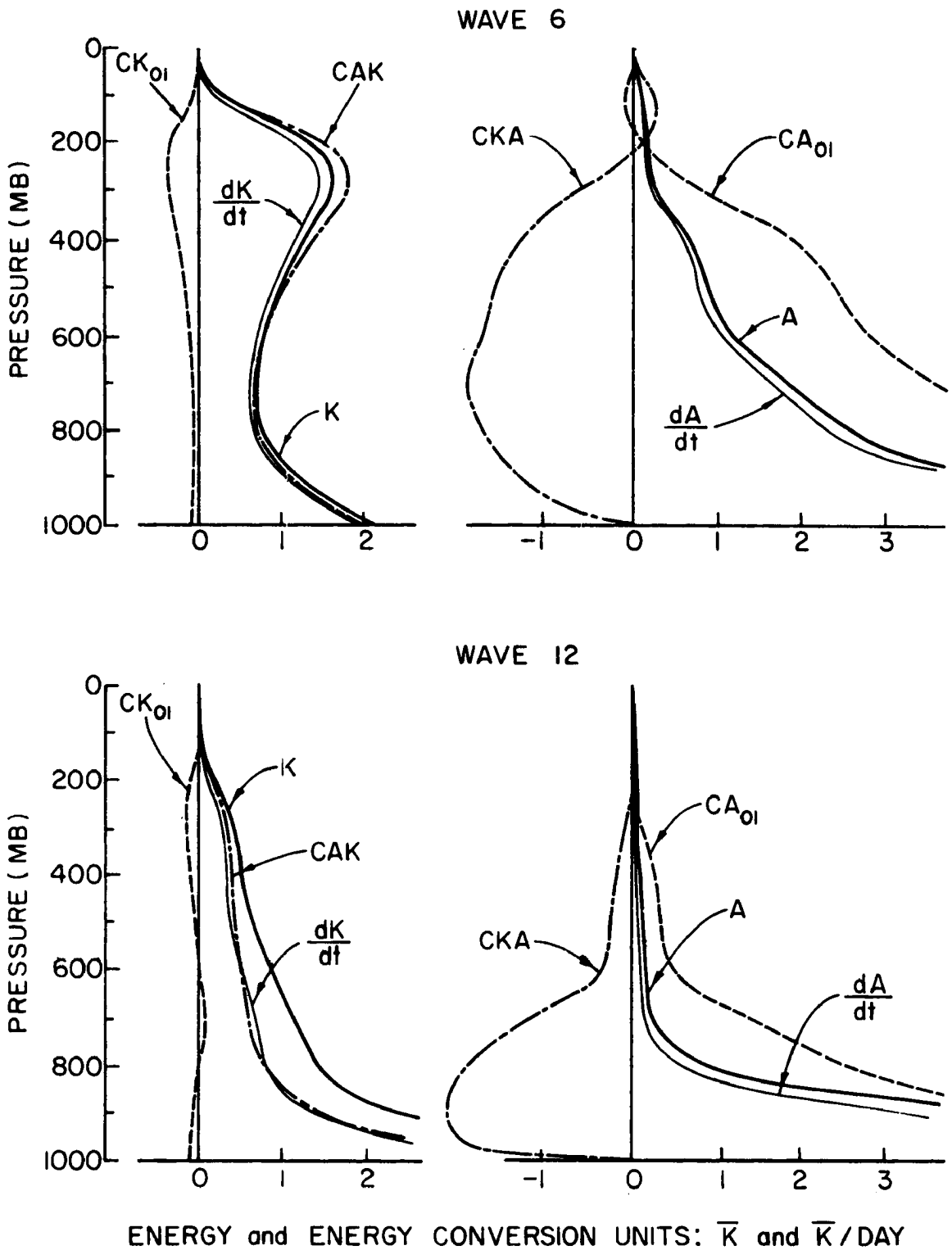

Fig. 7

Vertical profiles of energy and energy conversions for most unstable normal modes of waves 6 and 12.

of the mean wind for a 60-degree sector. The variations of instability from one sector to the next are as large as expected from Fig. 3. Sectors of pronounced cyclone-scale instability are the North-American continent, Asia and the West-Pacific. Over the East-Pacific, and especially over the Atlantic, we find a shift of instability towards the shorter waves and the cyclone-scale instability is reduced considerably. In fact, the one pronounced mode of maximum instability disappears completely over the Atlantic Ocean.

Another basic flow parameter which certainly varies horizontally in the actual atmosphere is the static stability. However its effect is rather straight-forward in the sense that a larger static stability tends to reduce the instability of the basic flow. As an example we have computed the instability corresponding to the winter static stability shown by the dashed line in Fig. 1. The results are shown in the upper part of Fig. 9. For easy comparison we have reproduced our previous results of Fig. 5 on the same scale and included them in Fig. 9. Indeed the more stable winter atmosphere shows smaller growth rates and possibly a shift of maximum instability towards longer wavelengths. However, the general characteristics are quite similar.

The remainder of Fig. 9 is concerned with quasi-baroclinic calculations, the results of which have been included in the same figure for easy comparison with our previous result. A purely baroclinic model is characterized by the absence of horizontal shears in the basic flow. The present spherical model becomes purely baroclinic if the basic state streamfunction ψ_0 is a linear function of the lateral coordinate μ. It follows from (43) that in this case the coefficients of the perturbation equation become independent of the lateral coordinate. The mathematical

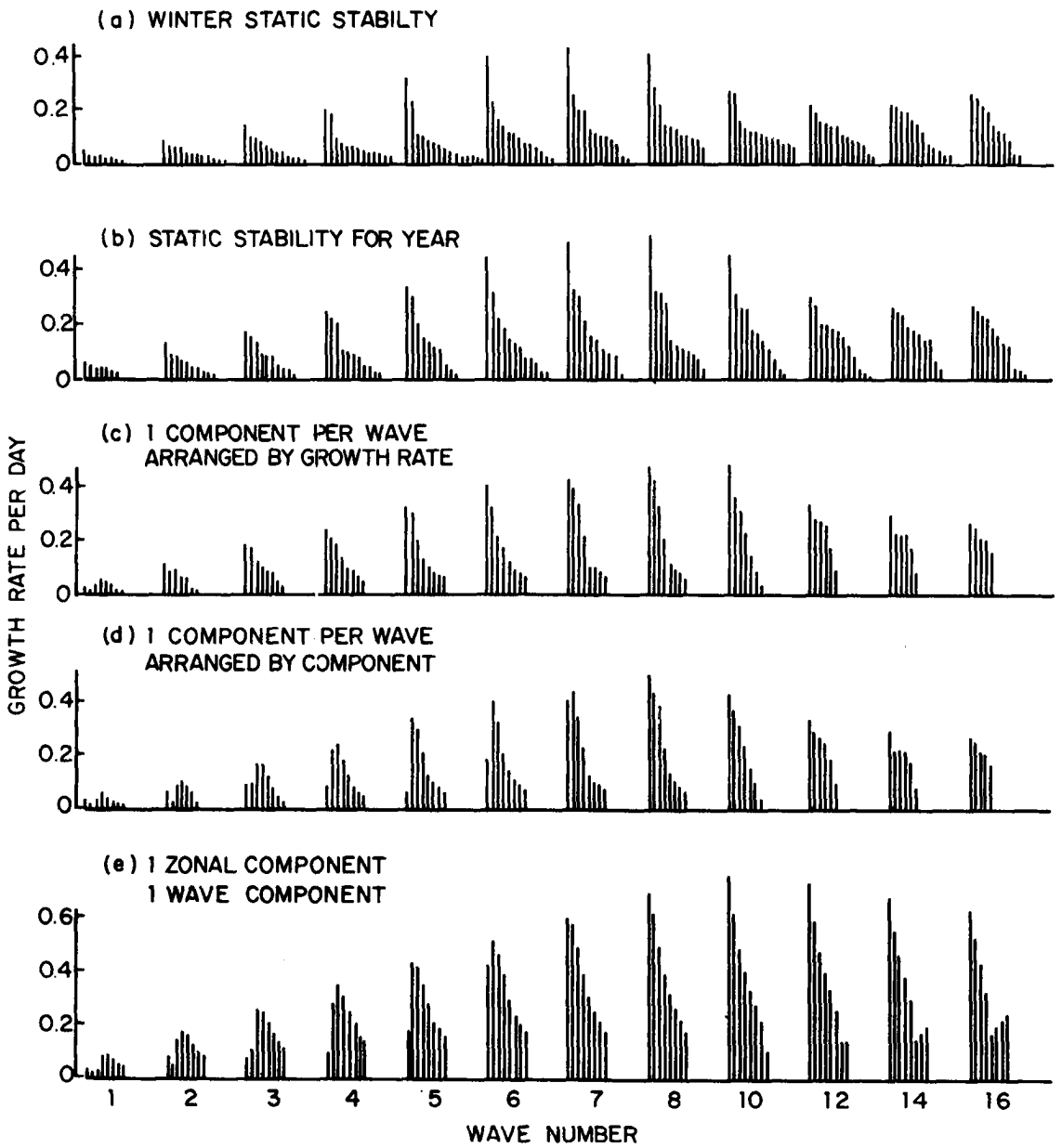

Fig. 9

Instability properties of January mean zonal wind shown in Fig. 2 for two profiles of static stability and for various quasi-baroclinic models.

implication is that the equations for the spectral components defined by (45) become uncoupled, that is, the coefficient matrix appearing in (46) reduces to N matrices of order M each. In other words if the initial perturbation has a latitudinal structure corresponding to a single associated Legendre polynomial, the perturbation will preserve such a structure, and no spectral components other than the initial one will be generated.

Let us now consider the baroclinic equivalent of our previous model. A linear variation with μ of the basic state streamfunction implies a mean zonal wind of constant angular velocity. This is clearly quite different from our observed latitudinal profiles. However, as a matter of interest we will adopt a rather common procedure and consider the zonal wind profile at 45 degrees North. The basic state streamfunction is now chosen such that its derivative with respect to μ is a constant corresponding to the zonal wind at 45° N. The instability of this wind is now determined with respect to each of the spectral components for a given wave. The results are given at the bottom of Fig. 9 arranged according to the order of the components in the spectral expansion (45). It is seen that the lowest components, that is, the largest latitudinal scales, are the most unstable ones except for the very long waves. This is an agreement with similar studies for a β-plane.

A comparison of the baroclinic results of Fig. 9e with our previous results shown in Fig. 9b is not encouraging. This is due largely to the fact that a constant angular velocity wind profile overestimates the basic flow velocity at low latitudes if it is made to represent the flow at high and middle latitudes. We may of course reduce the

baroclinic instabilities by reducing the basic flow velocity arbitrarily, but this still does not remove the relatively high instabilities of the shorter waves. Instead we have devised another type of quasi-baroclinic model. In this model we simply preclude the barotropic energy exchange between the zonal flow and the wave by considering one single term of the wave expansion (45). The zonal flow is completely arbitrary which implies that each spectral component of the wave perturbation "sees" a different vertical zonal wind profile. In a mathematical sense this quasi-baroclinic model is inconsistent since the initial latitudinal structure of the wave cannot be conserved owing to the lateral variation of the basic flow. However, we will find in this manner whether the coupling between the various baroclinically unstable modes in one wave is so important as to change the overall instability of the wave. The results of these quasi-baroclinic calculations are shown in Figs. 9c and 9d, arranged, respectively, according to the growth rates and by the order of the spectral components within one wave. Comparison of 9b and 9c indicates that the coupling of the baroclinic modes in our general model is not so strong as to obscure the purely baroclinic instabilities. The major coupling effect seems to be the growth of the most unstable mode in a given wave. In general, however, this particular quasi-baroclinic model seems to give a good indication of the major instabilities, and consequently we will use this method for the baroclinic calculations of Chapter V.

In conclusion of this section we have reproduced a figure from an earlier study by the author (Simons, 1969). Fig. 10 shows the baroclinic instability of the mean January zonal wind at 45°N as computed

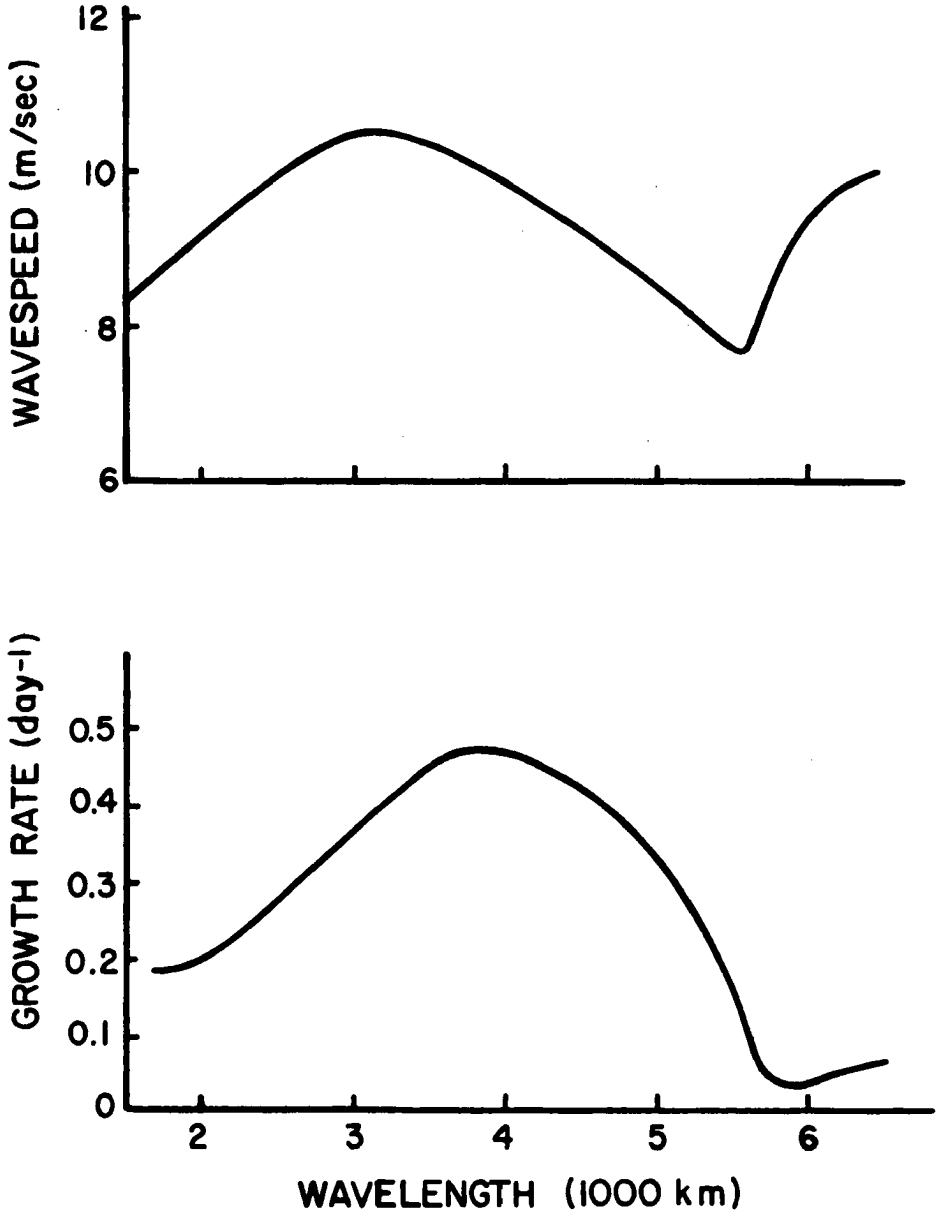

Fig. 10

Baroclinic instability of January mean zonal wind at 45°N with respect to wave perturbations without lateral variations on the beta-plane (Simons, 1969).

with a β-plane model without lateral variations of the perturbations. Considering these approximations, the agreement with our results of Fig. 5, both with respect to growth rates and wave speeds, is striking.

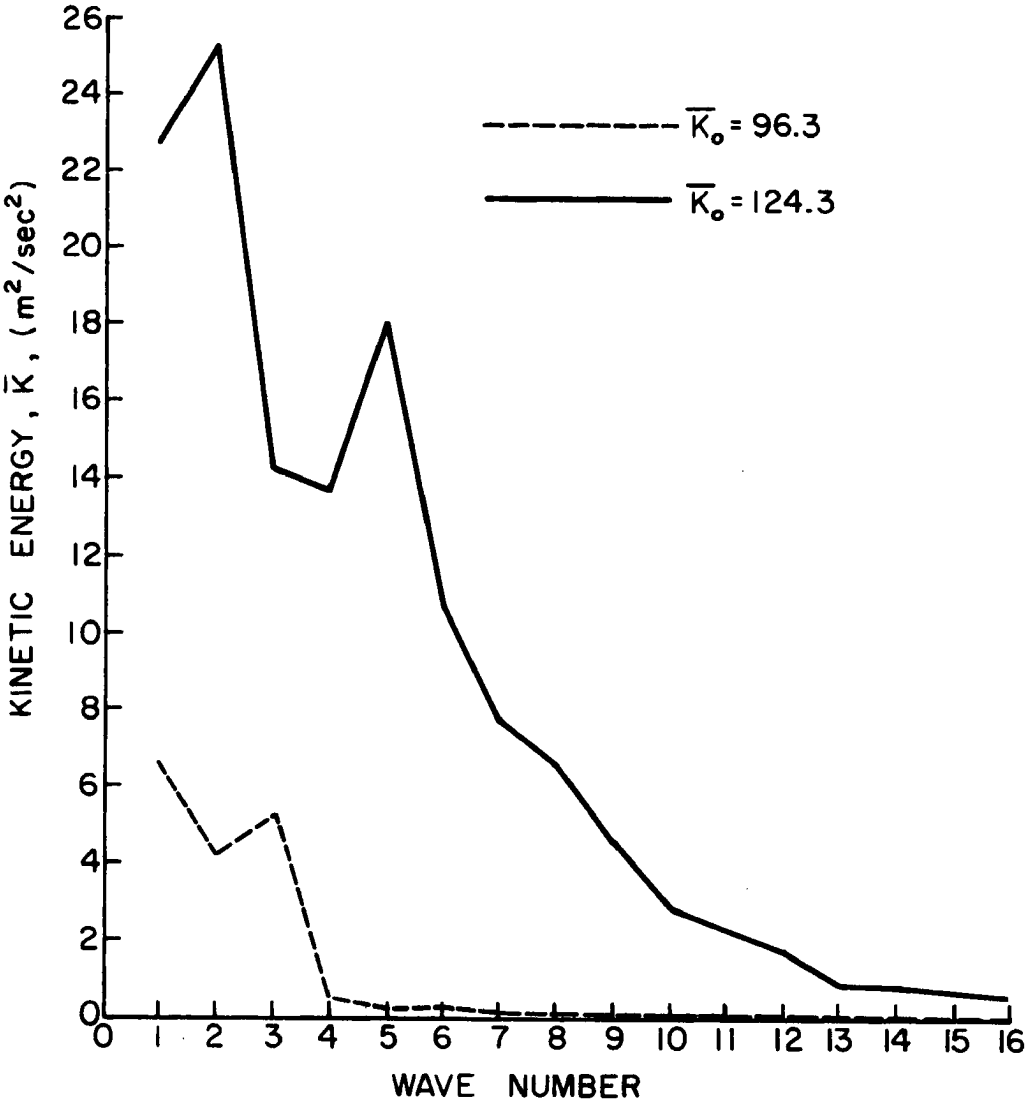

Fig. 11

Spectral distribution of mean kinetic energy per unit mass for the northern hemisphere. Dashed line: energy of climatological-mean January flow; solid line: average of daily energy for January 1-10, 1969.

is of the order of magnitude observed in the atmosphere. At that point the wave amplitude decreases and the wave starts returning the available potential energy which it extracted before from the unstable zonal flow.

The second half of this nonlinear cycle is a necessary consequence of the prescribed latitudinal profile of the wave perturbation. Thus, as mentioned at the end of Chapter III, the stability problem is of a purely baroclinic nature if the series expansion for the wave (45) is truncated after one term, independent of the latitudinal profile of the zonal wind. This implies that no barotropic exchange of kinetic energy can take place in the baroclinic low-order system described above. We may extend this system by allowing a more complete spectrum of expansion coefficients in the wave, and integrate the resulting equations by numerical time extrapolation starting from the same one-component initial perturbation. We observe then that when the growth of this component slows down due to nonlinear processes, it tends to feed its energy to the higher-order components in the wave. This in turn will cause a barotropic energy exchange between the zonal flow and the eddy which drastically alters the behavior of the mature perturbation, as we will see in the following more general study. However, the actual conversion process of available potential energy into wave kinetic energy appears to be quite well described by the baroclinic low-order system for the period during which this conversion is growing to its maximum.

Let us now turn to wave perturbations superimposed on the basic zonal flow described by the cross-sections in Fig. 2. In particular we are interested in the nonlinear effects on the growth rates of the most unstable cyclone-scale waves. The normal mode instabilities for our

zonal wind were shown in Fig. 5 and the energy conversion associated with the most unstable modes have been presented in Fig. 6. Since Fig. 5 shows that each of the most unstable wave numbers is characterized by one dominating unstable mode, we will concentrate on the latter. Thus we have determined the structure of the perturbation corresponding to the most unstable normal mode, and set the perturbation energy initially equal to the energy level represented by the dashed line of Fig. 11. The subsequent development of the perturbation and the zonal flow is then described by the equations derived in Chapter II, where all terms relating to the interaction with the second wave are discarded for the calculations of the present section. As in the previous chapter we have used a spectral representation in the horizontal (Appendix A) and a layered representation in the vertical (Appendix C). For the time extrapolation we employed a centered-differencing scheme, starting with a forward time step and one centered time step using one half of the regular time interval.

The computations described in the present section were carried out for the wave numbers 6,7, and 8. No significant differences were found from one wave to the next. Therefore the discussion will be restricted to one wave. In connection with subsequent discussions in Section IVC we have chosen the perturbation of wave number 6. Fig. 4 shows that the most unstable mode of wave 6 has converged quite well for the horizontal truncation N = 8, which we consider first. The vertical profiles of the energy distributions have been presented in the upper part of Fig. 7, from which it is clear that the instability is of a baroclinic character, with stabilizing barotropic effects. Fig. 12 illustrates the development of the wave with time. The curves show the vertical-mean of the

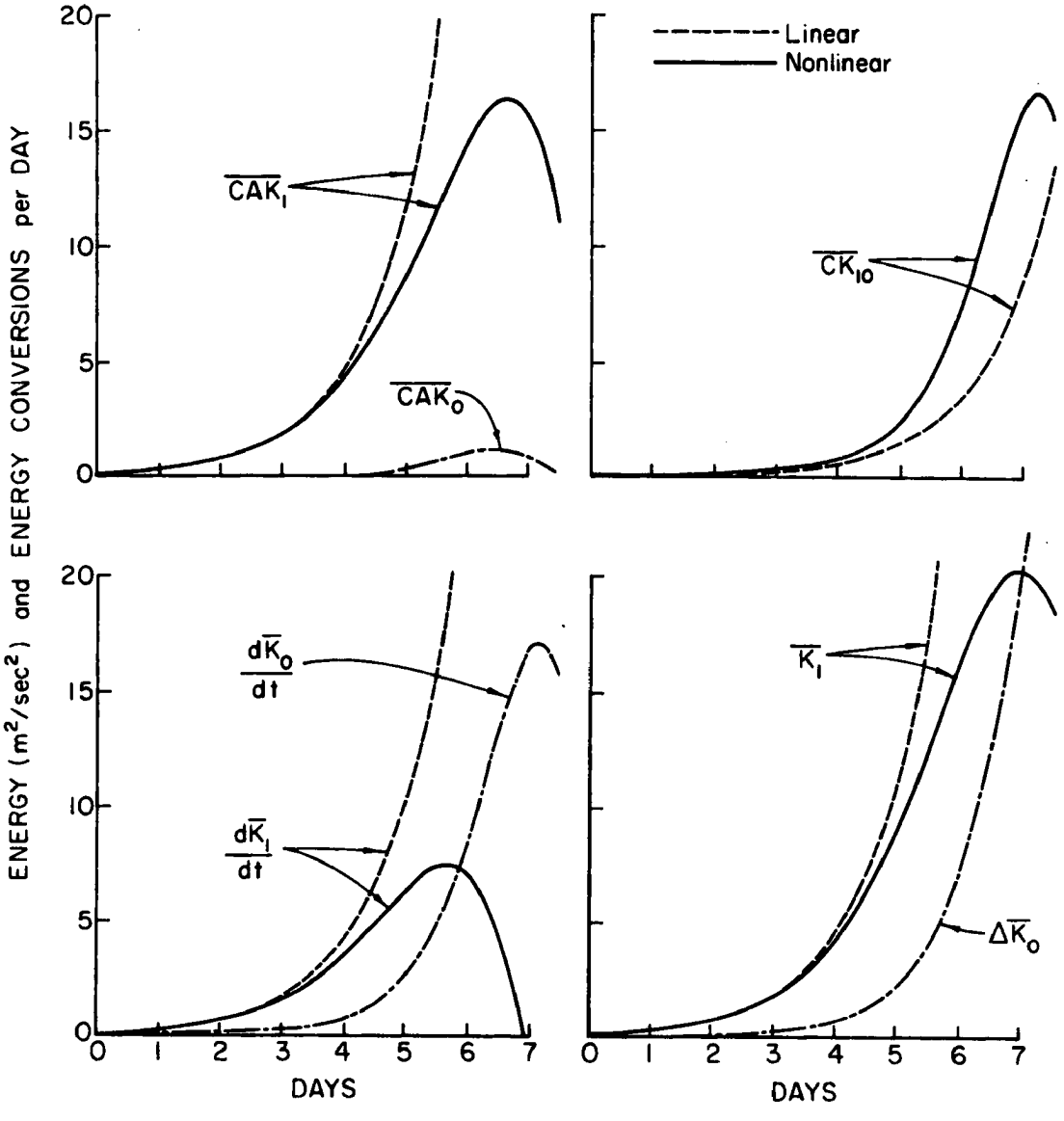

Fig. 12

Kinetic energy and energy conversions for system of zonal (subscript o) and wave 6 (subscript 1). Horizontal truncation N = 8.

kinetic energy per unit mass and the conversions of such energy per day. Note that all energy parameters are always averaged horizontally as shown in Section IIC. The dashed lines represent the linear development without changes of the zonal wind. The solid curves represent the nonlinear behavior of the wave and the dash-dot lines show the nonlinear variations of the zonal flow. The notation is defined in Section IIC.

Consider first the wave kinetic energy (bottom right). Owing to the small initial amplitude ($\overline{K}_1$ = .13 m^2/sec^2) the wave behaves quasi-linear for 3-4 days. From that time on, the growth of the wave is reduced by the nonlinear effects and it stops growing after three more days. The perturbation kinetic energy is then about 20 m^2/sec^2 which exceeds the energy shown by the solid curve of Fig. 11, but which is of the same order of magnitude and which is found on individual days although not in the 10-day average. The processes by which the wave growth comes to a halt are illustrated by the other curves of Fig. 12. The conversion of potential energy to eddy kinetic energy, CAK_1, is reduced by the nonlinear interactions as indicated by the nonlinear baroclinic solutions discussed at the beginning of this section. Most interesting, however, is the increase of the stabilizing barotropic energy release from the wave to the zonal flow, CK_{10}, beyond the linear values. Thus while Fig. 6 shows that in the linear model the conversion CK_{10} is only about .125 K_1 as compared to CAK_1 = 1.02 K_1, it is apparent that the barotropic energy transfer becomes comparable to the baroclinic conversion in the nonlinear model. It is this combination of nonlinear effects which results in the drastic reduction of the net energy conversion dK_1/dt shown at the bottom left of Fig. 12. At the same time the increased release of kinetic energy to the zonal flow is a

tremendous source of energy for the latter, as shown by the curve labeled ΔK_0 which represents the change of zonal kinetic energy. This increase of zonal kinetic energy becomes of the order of 20 m^2/sec^2 which may be compared with the initial zonal energy $\overline{K}_0 = 96.3\ m^2/sec^2$ (see Fig. 11).

The energetics are presented as a function of height in Fig. 13 for day 6 and day 7. By comparison with Fig. 7 it is seen that the vertical profiles of the wave energy and its conversions are quite well preserved. The barotropic transfer CK_{10} shows two maxima corresponding to the maxima of the baroclinic conversion CAK_1. Note however that the rate of change of zonal kinetic energy does not show the maximum at the jet-stream level. The only source of zonal kinetic energy in addition to CK_{10} is its own baroclinic conversion CAK_0. The remarkable fact is that this conversion is negative at upper levels and positive at lower levels, therefore transporting the kinetic energy received from the wave to the surface layers. Recalling from Section IIC that the conversion CAK is directly related to the cross-isobaric flow $-\mathbb{W}.\nabla\Phi$, the above implies that the zonal wind tends to deviate from the geostrophic wind toward higher pressure at upper levels and toward lower pressure at lower levels. This particular process is not indicative of any symmetric overturning of the zonal flow which is in this model represented by the loss of potential energy-CKA and which is related to the correlation of vertical motion and temperature. To show this we have entered the conversion CKA_0 into Fig. 13, from which it follows that the contribution from this term is small.

It is suggested that our model describes the development of atmospheric perturbations from a linearly unstable wave to a mature cyclone in considerable detail. The break-down of the growing perturbation is

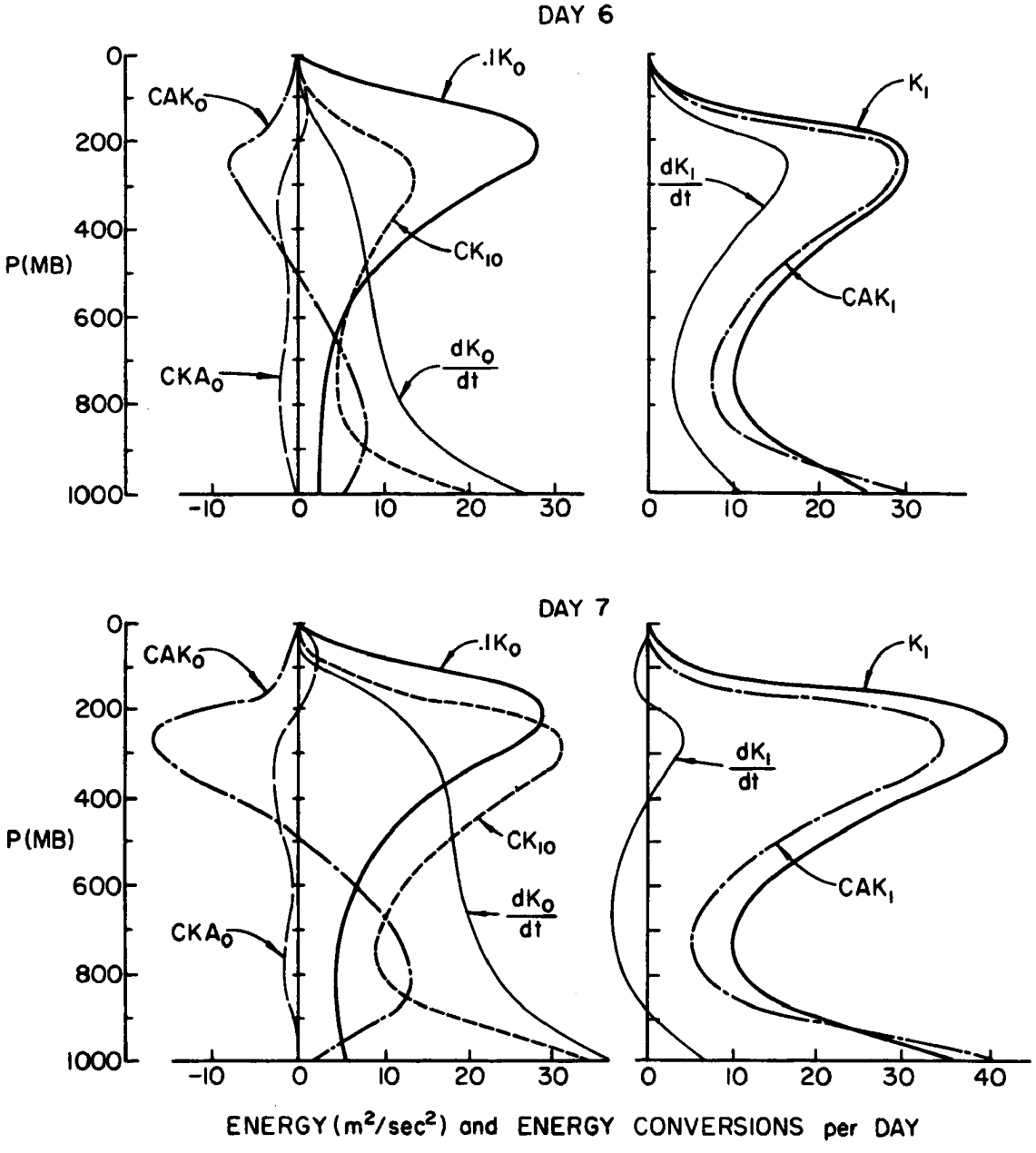

Fig. 13

Vertical profiles of kinetic energy and energy conversions shown in Fig. 12 after 6 and 7 days respectively.

accomplished at a reasonable value of the amplitude without invoking the effects of frictional dissipation. The mature perturbation is found to release a very large amount of kinetic energy to the zonal flow, thus bringing its own growth to a halt but at the same time maintaining the zonal flow against frictional losses. The zonal flow is of much assistance in this process by transporting the kinetic energy downwards. This support of the zonal flow by barotropic energy exchange was discussed by Kuo (1951) and has since been verified by many computations on the energetics of the mid-latitudes. Recent calculations by Kung (1970) also show that the actual energy conversions calculated from the cross-isobaric flow $\mathbf{V}.\nabla\Phi$ are relatively small at higher levels in the belt of atmospheric Westerlies. According to Fig. 13 the present model produces a similar result due to the cancellation of the positive wave conversion CAK_1 by the negative zonal conversion CAK_0 at these levels.

The results discussed so far were obtained by integration of a numerical model which necessarily incorporates the errors introduced by truncation in space and time. Considering first the time-truncation we integrated the equations for time steps varying from .5 to 1.5 hours and compared the solutions. The total wave energy and the zonal energy shown in Fig. 12 are found to be practically the same. However, as pointed out by Baer and Simons (1968), the errors in the energy of the individual spectral components have a tendency to cancel one another, and we should also take a close look at these energies. Owing to the small time interval we find in the present case that the component energies vary by less than 1 per cent after 7 days if the time step varies from .5 to 1.5 hours. Further we may also recall that for all

integrations the total energy (available + kinetic) should be conserved which is verified at all times. Here the error does not exceed one hundredth of one per cent.

A far more serious problem is the space truncation. Actually it is the space truncation which forces us to break off the present calculations after 7 days when the wave stops growing. As mentioned before, the results shown in Fig. 12 and Fig. 13 were obtained for a horizontal-spectral truncation of 8 terms in the series (45), that is for N = 8. The linear calculations shown in Fig. 4 indicated a perfect convergence of the most unstable mode for this truncation. We have found however (Simons, 1969) in testing the convergence of solutions as a function of vertical truncation, that an arbitrary perturbation does not converge at the same rate as the normal mode solution. We have therefore extended the present spectral truncation up to N = 11 to investigate this problem. The results are shown in Fig. 14. It is apparent that the convergence becomes extremely poor as the wave approaches its maximum amplitude. In effect there are indications that the rate of change of wave kinetic energy dK_1/dt does not become negative but merely very small, to increase again at a later time. For this reason we cannot put any confidence into the present calculations beyond the time period shown in Figs. 12-14. In spite of this, however, we do observe that the basic processes described before in connection with the breakdown of the growth of the wave are found for all truncations. Further we have also found exactly the same energy patterns for the waves of wave number 7 and 8 for which the present calculations were performed.

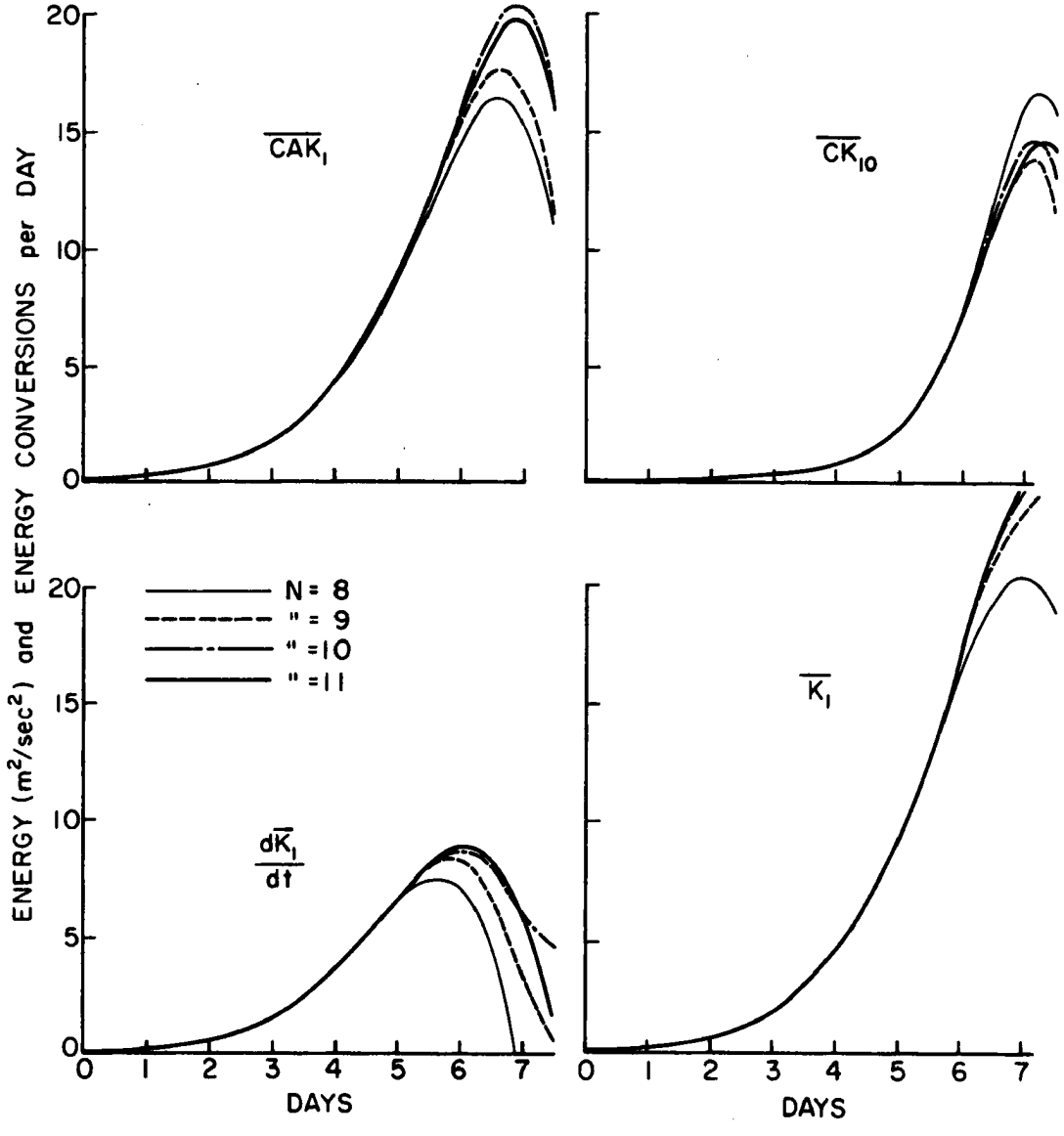

Fig. 14

Wave kinetic energy and energy conversions for system of zonal and wave 6 as a function of horizontal-spectral truncation.

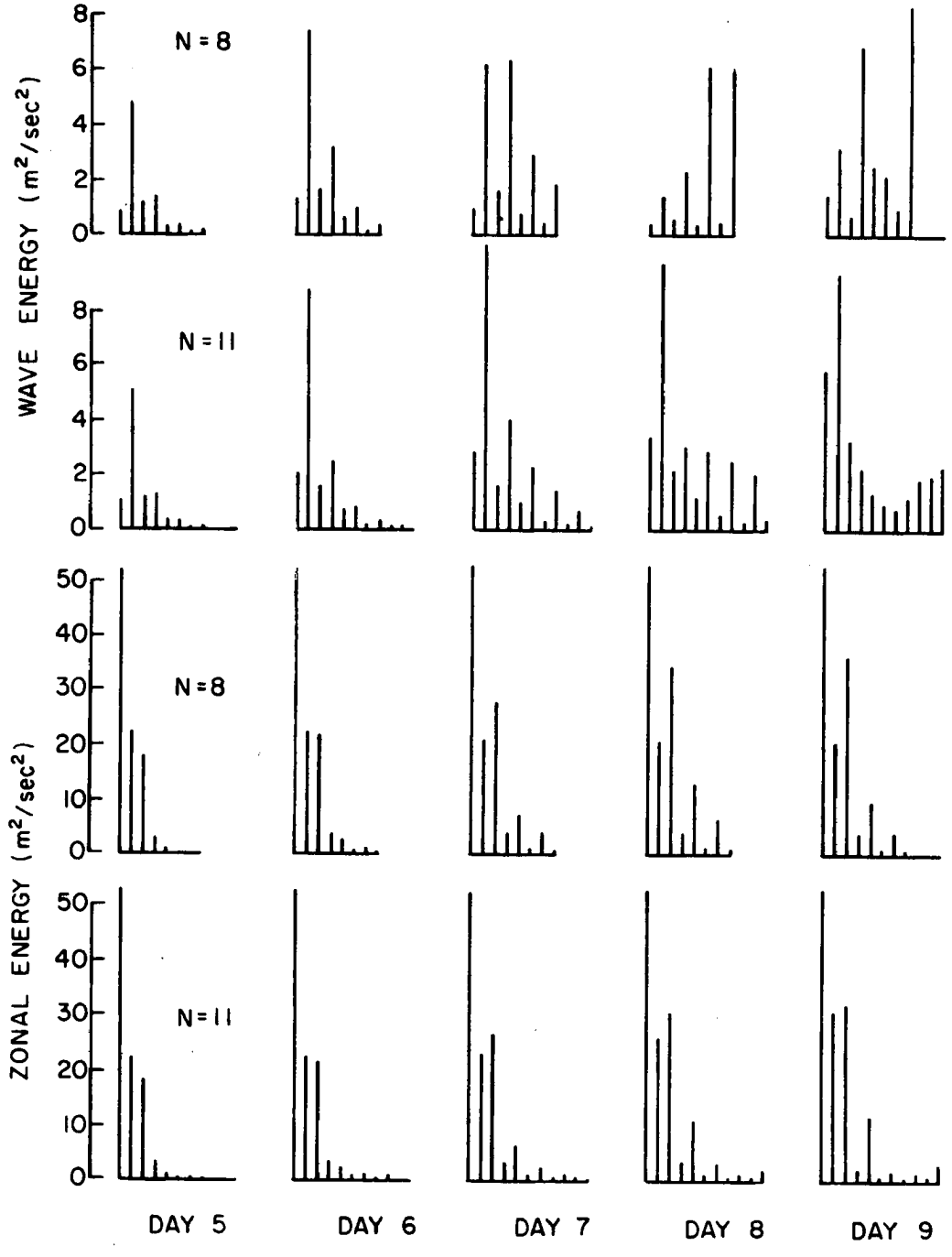

Fig. 15

Vertical-mean kinetic energy in each of the horizontal-spectral components of wave (above) and zonal flow (below) for system of zonal and wave 6.

The spectral truncation problem is investigated in some more detail in Fig. 15. Here we present the distribution of the kinetic energy over all horizontal-spectral components starting with day 5 and continuing through day 9. The initial perturbation is the one described in the previous pages, but the upper row of Fig. 15 is for a truncation N = 8 while the second row if for N = 11. The components have been arranged within the wave according to their order in the series (45) from left to right. Consider first the truncation N = 8. After 5 days the energy distribution over the spectral wave components is still very similar to the normal mode distribution from which we started. Thus most of the energy is concentrated in the second component which is the most unstable one in a baroclinic sense according to Fig. 9. After day 6 the second wave component starts to decline and, since the actual conversion of potential to kinetic energy, CAK_1, reaches a maximum according to Fig. 12, it is indicated that the remaining wave components are mainly growing by transfer of kinetic energy. It is apparent that the latter process is impeded by the severe truncation. On the other hand we notice that the truncation N = 11 allows us to extend the integration at least to day 7 before the flow of energy appears to be obstructed by the truncation. Further computations indicate that the required horizontal resolution is proportional to the vertical resolution, which is consistent with the damping of the smaller scales of motion in, for instance, a two-level model.

C. The Interaction of Two Planetary Waves with the Zonal Flow

It has been shown in Chapter II that a perturbation of wave number ℓ superimposed on a basic zonal current may eventually generate a higher

harmonic of wave number 2ℓ which can no longer be neglected. In the present section we consider the effects of this nonlinear process on the growth of a cyclone-scale perturbation. The system of equations which describes the behavior of two waves of wave numbers ℓ and 2ℓ, respectively, superimposed on a zonal flow, has been derived in Chapter II. The same system of equations may also be used to study the interaction of a long wave of quasi-permanent character with a cyclone-scale wave. This problem will be considered briefly at the end of this chapter. The numerical results were obtained from the model described in Appendix C, i.e., a spectral representation in the horizontal given by (45) is combined with a vertically-layered representation. The calculations were performed for the three waves of wave numbers $\ell = 6$, 7, and 8, including in each case the wave of wave number 2ℓ, i.e., waves 12, 14, and 16, respectively. The initial structure of the primary wave corresponds to the most unstable normal mode and its amplitude is taken from the dashed curve of Fig. 11 which assures an initially linear growth of the perturbation. The secondary wave of wave number 2ℓ is initially set equal to sero and must therefore be generated by nonlinear processes.

The effects of the waves of wave number 2ℓ on the primary waves was found to be quite consistent for the three cyclone-waves here considered. Again, we will therefore restrict the discussion to the wave of wave number 6. The effects of the presence of wave 12 on the energy conversions in wave 6 and between the zonal and wave 6 are indicated in Fig. 16. These results have been taken from a numerical model with a horizontal-spectral truncation of $N = 11$, which has been shown in Fig. 15 to possess a sufficiently convergent solution for the time

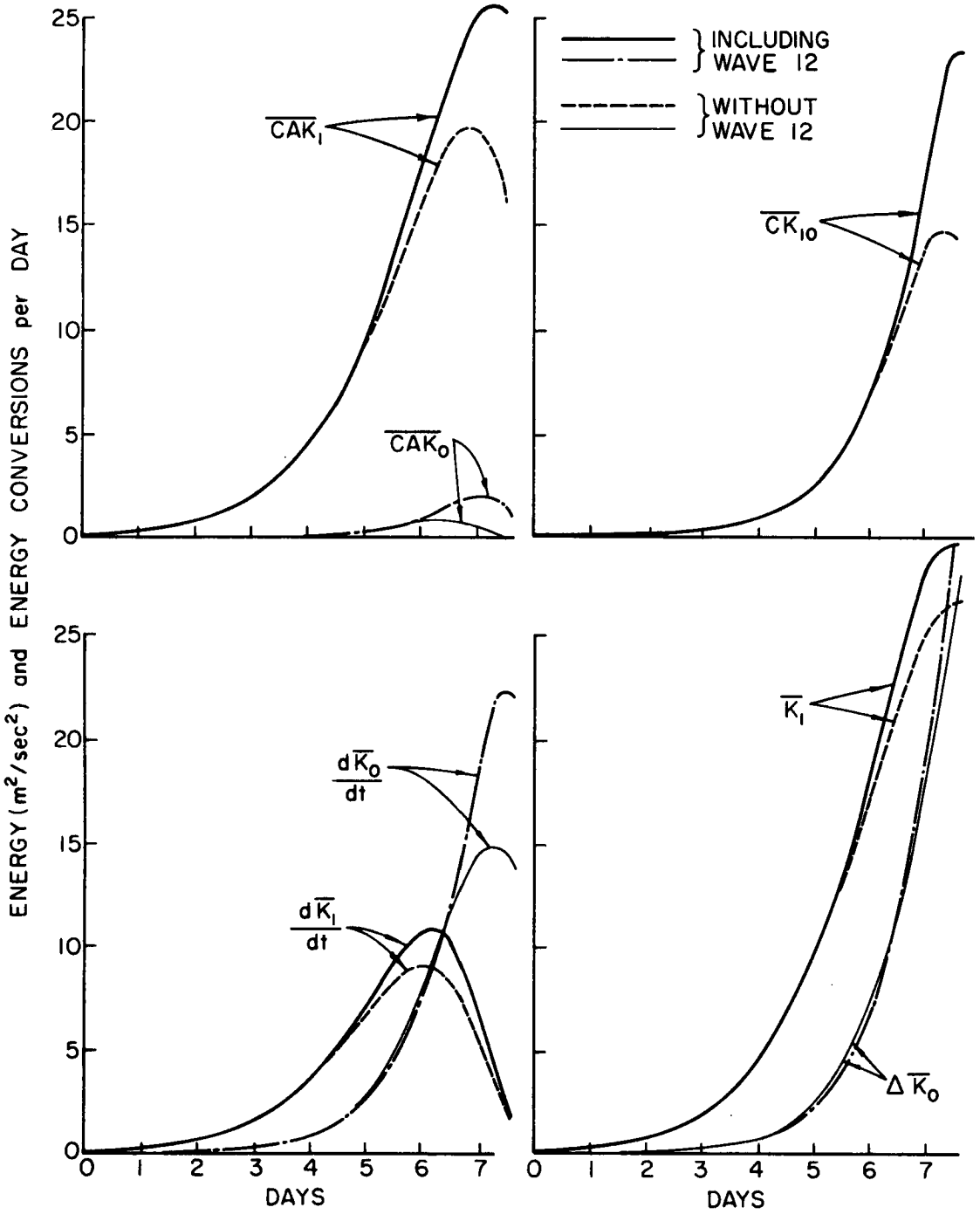

Fig. 16

Kinetic energy and energy conversions for system of zonal (subscript o) and wave 6 (subscript 1) with or without wave 12. Horizontal-spectral truncation N = 11.

period shown in Fig. 16. The rate of convergence was also tested after including wave 12 and was found to be quite comparable to the convergence without wave 12. For comparison with the case discussed in the previous section, Fig. 16 shows the energy conversions for the system including wave 12 and the system without wave 12. All energy conversions in both the zonal flow and wave 6, and the energy exchange between the zonal flow and wave 6, show a considerable increase in magnitude owing to the presence of wave 12. Generally speaking, this is consistent with the effect of higher horizontal resolution within the primary wave as presented in Fig. 14. From both Fig. 14 and Fig. 16, however, it is apparent that the general character of the solution is preserved. Since this solution has been discussed in considerable detail in connection with Fig. 12, there is no need to repeat the discussion here.

The complete solution of the present system includes of course a number of additional energy conversions which have not been included in Fig. 16. These are the conversion of potential to kinetic energy by wave 12, the exchange of energy between the zonal and wave 12, and the exchange between wave 6 and wave 12. Fig. 17 presents a few of these energy conversions and the kinetic energy in wave 12. The rate of convergence of these quantities as a function of the horizontal resolution is not as good as the convergence of the corresponding quantities for the zonal and the primary wave. This is in particular true for the baroclinic energy conversion CAK_2, as was also observed in the normal mode study (Fig. 4). However, this particular conversion does not seem to exert much influence on the zonal flow and the primary wave as indicated by the much better convergence of CK_{02} and CK_{12}.

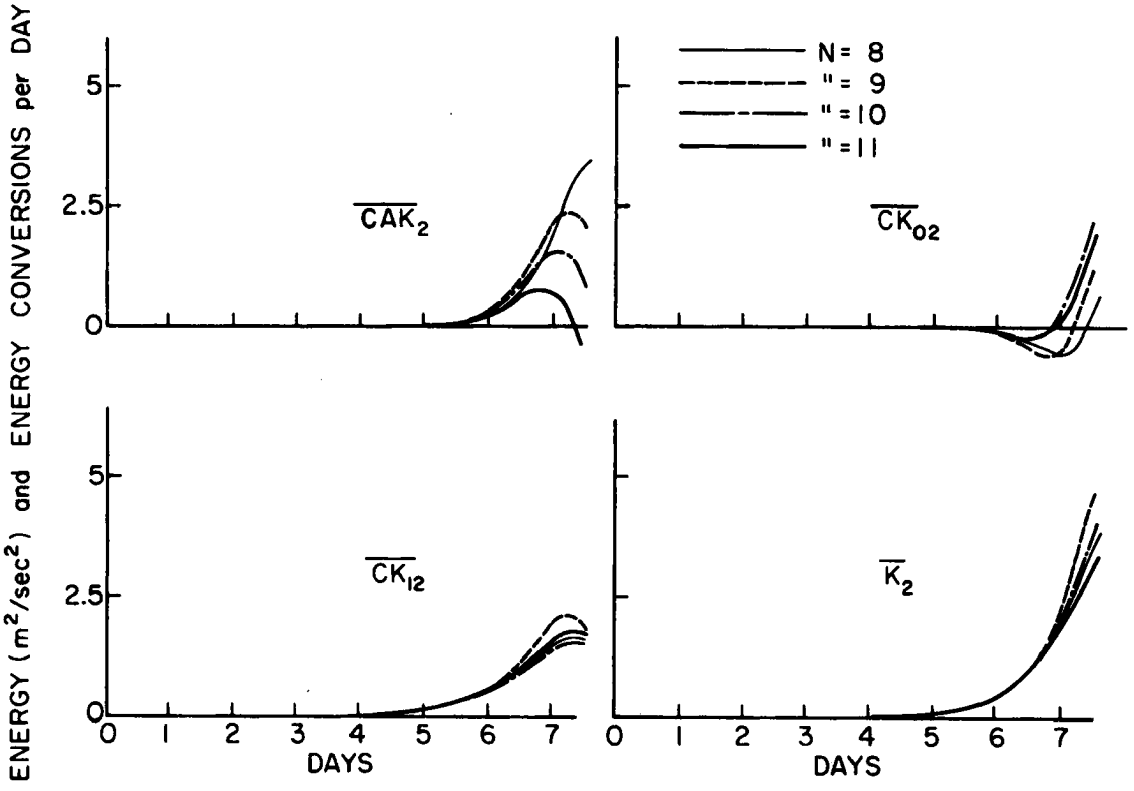

Fig. 17

Kinetic energy and energy conversions for wave 12 as part of system of zonal, wave 6, and wave 12, and for various horizontal-spectral truncations.

The conversions of energy related to wave 12 are an order of magnitude smaller than those shown in Fig. 16. The conversion of potential to kinetic energy by wave 12 appears to be positive at least till the primary wave reaches its maximum rate of growth. The transfer of kinetic energy from the primary wave to the secondary wave is positive, and the exchange of kinetic energy between the zonal flow and wave 12 is initially in the direction of the zonal flow but is later reversed. It is clear from Fig. 17 that most of the kinetic energy of wave 12 results from the release of kinetic energy from the zonal flow and wave 6. An inspection of Fig. 16 and Fig. 17 shows further that the net result of the barotropic exchange of kinetic energy is that the zonal kinetic energy and the energy of the secondary wave increase at the expense of the primary wave, such that the flow of energy to the zonal flow is larger than that to the secondary wave (compare Fjørtoft, 1953).

The preceding results shown in Figs. 12-17 indicate the decrease of the rate of growth of an unstable wave-perturbation as a result of the nonlinear interactions between the zonal flow and the wave. It would then be convenient to have a certain parameter by which such nonlinear effects could be measured and compared. Let us therefore consider the rate of change of wave kinetic energy expressed in terms of the actual wave kinetic energy. If we divide this quantity by two, then it follows from (49) that the result is equal to the growth rate of a linearly unstable perturbation. It is thus suggested to define the growth rate of any perturbation, linear or nonlinear, as follows

$$\text{growth rate} \equiv \frac{1}{2K}\frac{dK}{dt} \tag{50}$$

As pointed out before, the quantity above is independent of the initial amplitude of the perturbation in a linear model, and the growth rate is constant with respect to time if we are dealing with one single unstable normal mode solution. In the nonlinear case, however, the growth rate will be a function of time and it will depend upon the initial energy of the wave. In addition, of course, the growth rate is a function of the basic state parameters and the wave length as in the linear case.

Fig. 18 presents the growth rates of the wave of wave number 6 for the various models discussed in this and the previous sections. The horizontal line represents the growth of the most unstable normal mode of wave 6 as shown in Fig. 5. Since the initial configuration of wave 6 in all cases has been chosen according to this normal mode, the horizontal line represents the growth of wave 6 in the absence of nonlinear processes. The dash-dot line gives the growth rate for the nonlinear case with a horizontal truncation of N = 8 and without wave 12, that is, the solution shown in Fig. 12. The thin solid line and the dashed line represent the model including wave 12 for a truncation N = 8, and the model without wave 12 but for N = 11, respectively. These two curves tend to show a similar deviation from the first curve which indicates that a larger resolution in either zonal or meridional direction tends to reduce the nonlinear damping of the wave. The heavy solid line is for the case N = 11, with wave 12 included, and seems to combine the effects above for a number of days until after day 7 the growth rate is reduced. The curves shown in Fig. 18 will not vary significantly with the initial wave amplitude - except for a shift to the left - as long as the initial wave energy does not exceed $\overline{K}_1 = 1\ m^2/sec^2$. In the

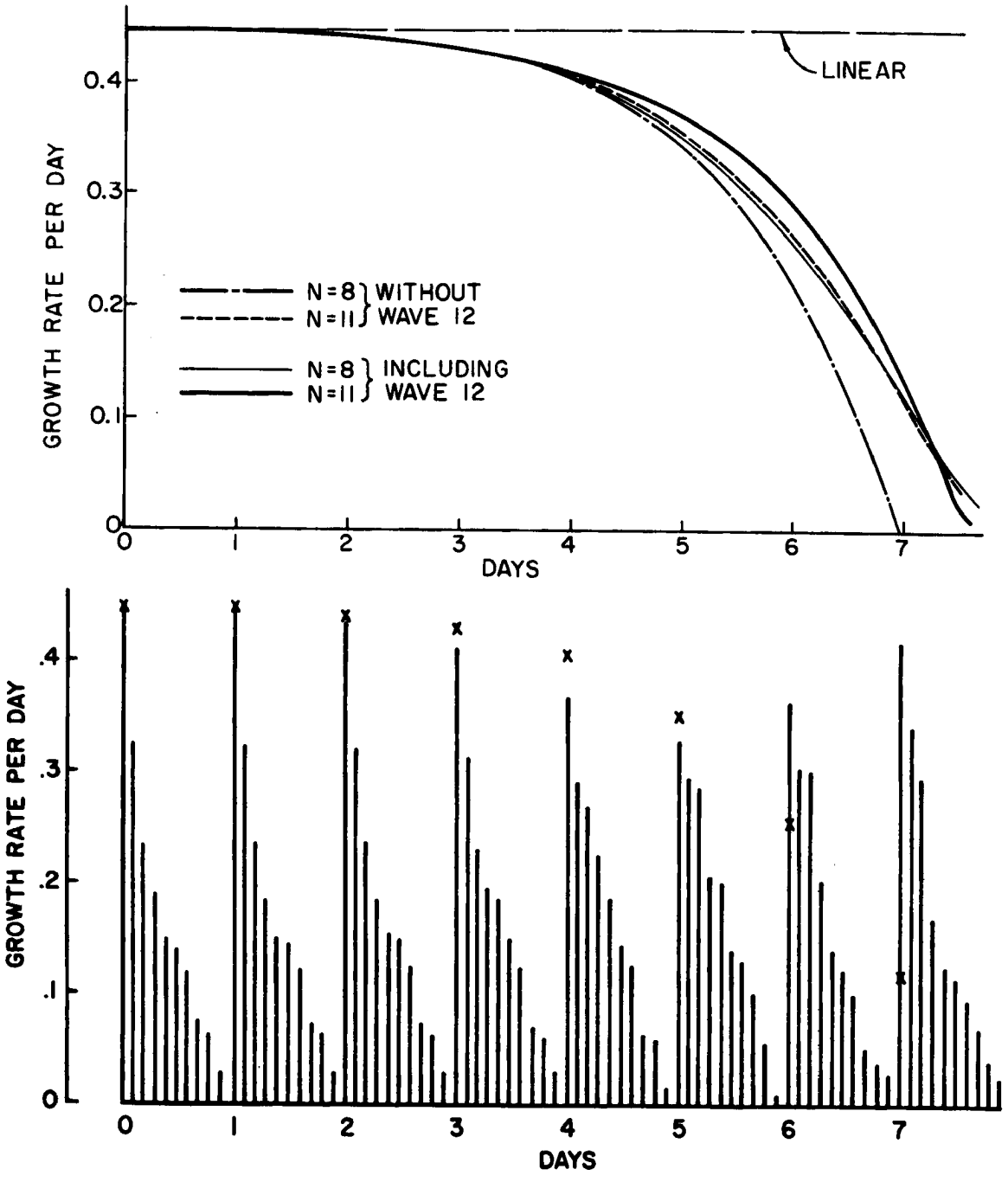

Fig. 18

Rate of growth, $\frac{1}{2}(d\overline{K}/dt)/\overline{K}$, of wave 6 as part of system of zonal and wave 6, with or without wave 12, and as a function of horizontal-spectral truncation (above). Instability of basic flow with respect to perturbations of wave number 6 as a function of time (below), represented by the growth rates of the ten most unstable modes.

present calculations this energy was reached after about 2 days at which time the nonlinear effects are still negligible as seen from Figs. 12 and 18.

One of the most interesting aspects of the nonlinear problem is the modification of the stability properties of the zonal flow as a result of the growth of the perturbation. It is to be expected that the instability of the basic current is in some way released as the wave extracts zonal energy for conversion into wave energy. In the purely baroclinic problem it is seen indeed that the vertical shear of the zonal current - and therefore the instability - decreases while zonal available potential energy is released to the wave. In the general barotropic-baroclinic case the relationship between zonal instability and wave growth is not necessarily so straight-forward. We have therefore computed the stability character of the zonal wind at various stages of the nonlinear integration by employing the methods of Chapter III. The lower part of Fig. 18 shows the results for the nonlinear system consisting of the zonal flow, wave 6, and wave 12, for a horizontal-spectral truncation of N = 8. Only the instability of the zonal flow with respect to wave 6 is shown, and the actual growth rate of wave 6 is denoted by the crosses corresponding to the thin solid line in the upper part of Fig. 18. Initially the instability of the basic current decreases faster than the actual decrease of the growth rate of the wave. After 5 days, however, the instability of the zonal flow starts to increase again. By tracking the various normal modes it can be established that the new mode of maximum instability is not the same as the originally most unstable mode. This then, in turn, is clearly related to the modification of

which exhibits a high degree of instability in a linear model. Again we may then assume that this perturbation - which was before the primary wave and which is now the second wave of the system - has been able to grow toward the structure of its most unstable normal mode before the onset of our integration. This assumption is supported by the observation that the first unstable mode of a wave of major instability shows a considerably larger growth rate than the remaining modes. This feature is not observed, however, for the longer waves in Fig. 5, and hence the initial structure of the first wave in the present system is not immediately obvious. One might even ask the question whether the linear behavior of the long waves is of any relevance in view of the continuous forcing effect of the earth's surface upon these quasi-permanent waves, which necessarily must be reflected in their structure. We have therefore considered various initial configurations for the long wave in the present study, including the structure obtained from the climatological-mean flow pattern for January from which we have derived our basic current.

The second problem associated with the initialization procedure lies in the initial amplitudes of the waves in the present system of a zonal flow and two waves. As before we take initial values of the wave kinetic energies such that the waves grow toward observed energy levels within the time period for which our results are meaningful, supposedly of the order of 5 days. The relative magnitude of the initial amplitudes of the waves seems to have a fairly consistent effect as illustrated in Fig. 19. This figure shows the kinetic energy and the growth rate as defined by (50) for each of the waves of the system consisting of the zonal flow, wave 3, and wave 6, for

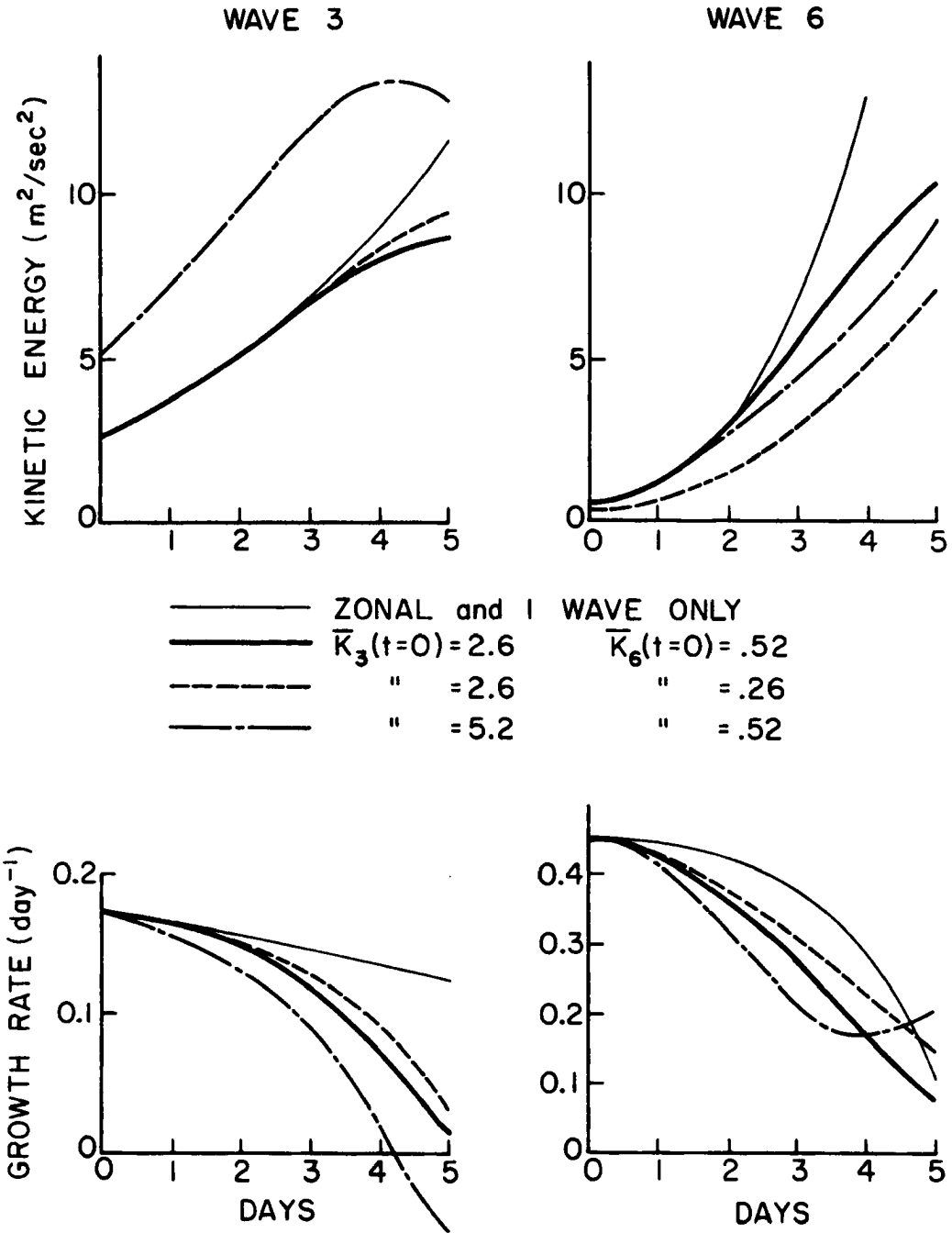

Fig. 19

Wave kinetic energies and growth rates for system of zonal, wave 3, and wave 6, for various values of initial wave kinetic energy. Initial wave structures corresponding to most unstable modes.

different values of the initial wave kinetic energies. The initial configuration of each wave corresponds to the structure of the most unstable mode of the wave. For comparison the thin solid line for wave 3 represents the system of the zonal flow and wave 3 only, and the thin solid line for wave 6 shows the results for the zonal flow plus wave 6 without wave 3. It follows therefore that the addition of the second wave reduces the growth rate of the first and vice versa. If the initial amplitude of the second wave is increased while the initial value of the first is kept constant we go from the dashed curves to the heavy solid curves and both growth rates are reduced. The same effect is observed if we increase the initial amplitude of the first wave, i.e., if we proceed from the solid curves to the dash-dot curves.

A great many numerical experiments have been performed concerning the present problem. Various initial amplitudes and initial configurations were tested for the system of wave 3 and wave 6. Furthermore, similar calculations were performed for a system containing wave 4 and wave 8. From these computations it would appear that the nonlinear effects illustrated in Fig. 19 are typical for the majority of the cases. Nevertheless, another effect seems to occur rather frequently, namely the long wave may derive additional growth from the cyclone wave. This is illustrated in Fig. 20 which differs from Fig. 19 only in that the initial configuration of the first wave corresponds to the second unstable mode. An analysis of the energy conversions shows that the difference between Fig. 19 and Fig. 20 is caused by a different sign of the energy conversion CK_{12} between the first and second wave, at least initially. In the first case the energy flows from the long wave to the cyclone wave and in the second case the direction of the energy

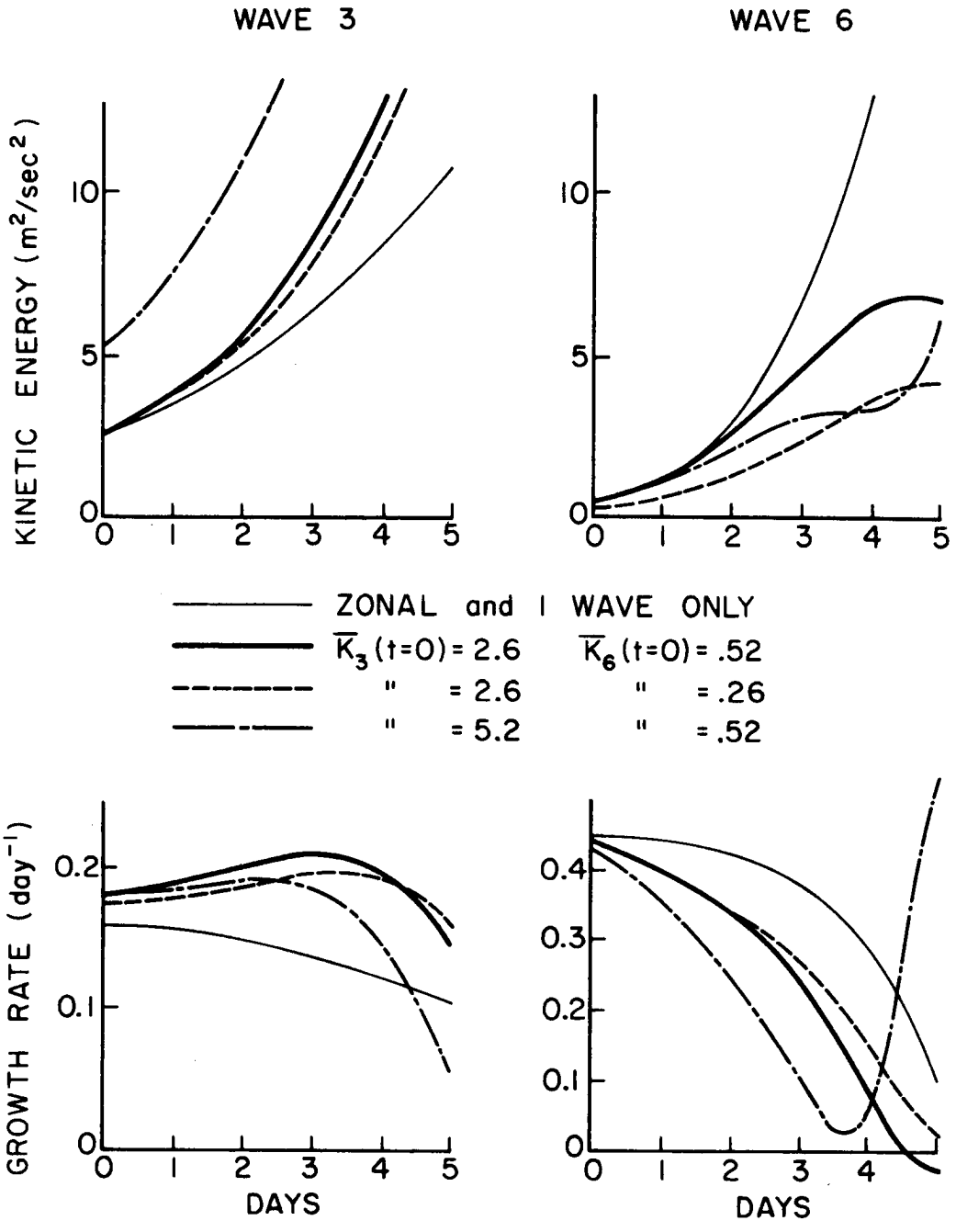

Fig. 20

Same as Fig. 19 but initial configuration of wave 3 corresponding to second unstable mode.

flow is reversed. The second case would therefore correspond to the atmospheric observations by Saltzman and Teweles (1964). In fact a flow of energy from wave 6 to wave 3 is also observed for the case of Fig. 19 after about two days. Furthermore, the exchange of kinetic energy with the zonal flow represented by CK_{10} and CK_{20} is always in the direction of the zonal flow for both waves in accordance with actual observations.

The results of all our calculations appear to be consistent with respect to the reduction of the initial growth of the cyclonic wave under the influence of the long wave. This does not imply however that the subsequent growth rate of the unstable wave is continuously below its value derived from linear theory. However, if we want to consider their later development we run again into the problem of the numerical truncation. Consider for instance again Fig. 19 and Fig. 20 which represent the results of numerical models with a horizontal-spectral truncation of N = 8. The same computations were repeated for truncations N = 9, 10, and 11, at least for the cases represented by the solid curves. The convergence was fair up to about 4 days but after 5 days the growth rates varied by 10 to 20 per cent which is the reason for showing only the results for the first 5 days in Figs. 19 and 20. In this context let us consider the interesting behavior of the dash-dot curves for wave 6, especially in Fig. 20. Such explosive growth is observed in many cases if the amplitude of the second wave becomes sufficiently large. For instance, the solid line for wave 6 in Fig. 20 shows a similar increase at day 6 which is not included in the figure. Such nonlinear wave growth might be suggestive for the development of a "short" wave interacting with a long wave in the atmosphere. However,

the convergence tests above tend to indicate that these large growth rates are reduced if the horizontal resolution increases. At any rate, the convergence of the solutions after 5 to 6 days is virtually non-existing and hence we must restrict ourselves to the initial nonlinear effects in the present study.

In summary, we may conclude that the results of the investigation above are consistent with respect to the nonlinear effects on the growth of a cyclone-scale wave resulting from the self-interaction of a long wave. At least during the first three or four days the growth rate of the second wave of the nonlinear system is considerably reduced as a result of the presence of the first. This damping effect increases with increasing initial amplitudes of the waves. If the initial amplitude of the second wave increases, the resulting reduction of the growth rate is simply the reflection of an increase of the nonlinear effects studied in the first part of this section. On the other hand, if the initial amplitude of the first wave becomes larger, the effect may be a direct result of an increased interaction of the two waves but it is probably more an indirect effect of the interaction of the first wave and the zonal flow. Again we should not conclude, however, that the growth rates are simply reduced as a result of the loss of zonal flow instability. Fig. 21 shows the stability properties of the zonal wind with respect to perturbations of wave numbers 3 and 6 for the two cases shown in Figs. 19 and 20. As before in Fig. 18 we observe again the remarkable lack of correlation between the actual growth rates of the waves and the potential growth rates represented by the normal modes.

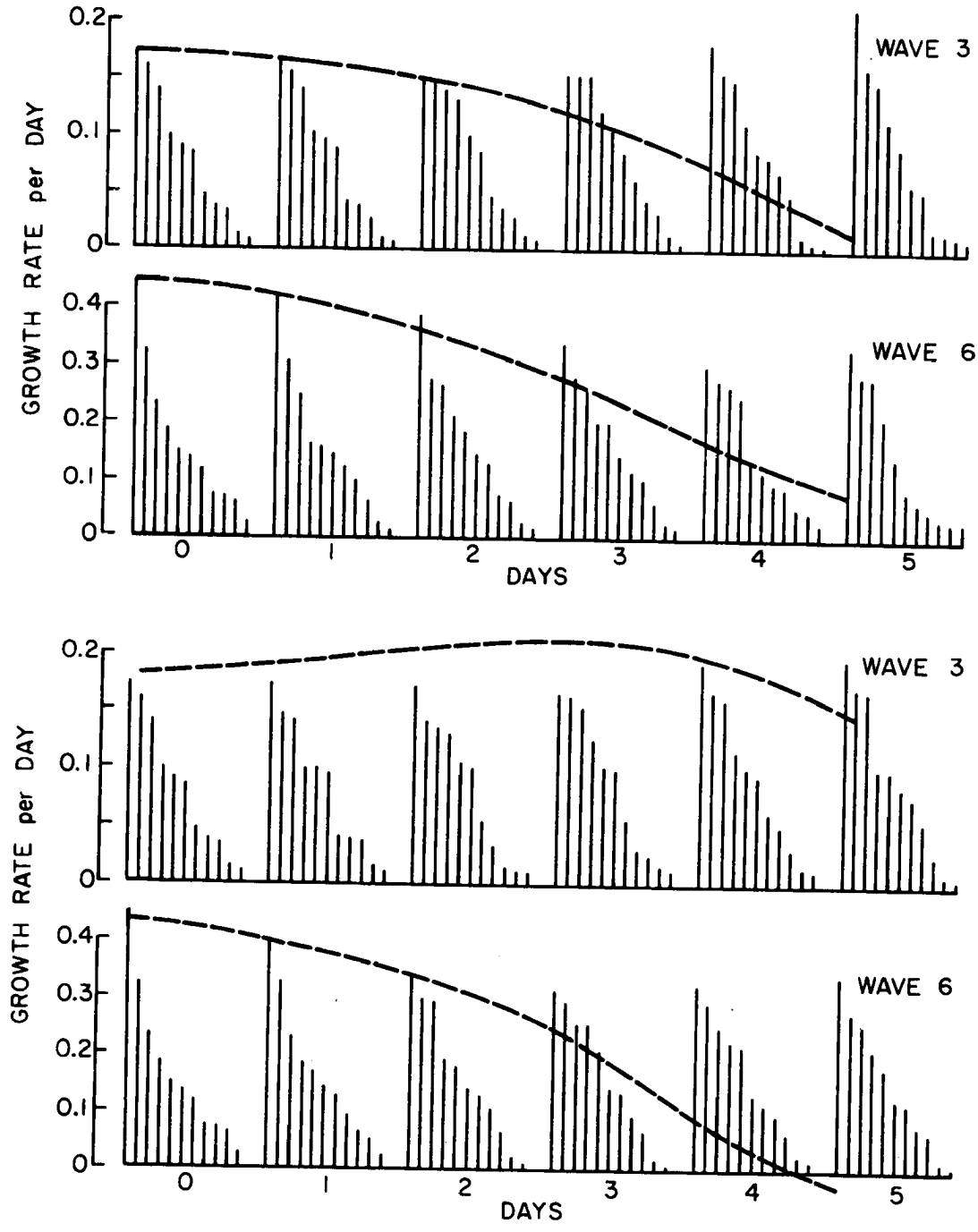

Fig. 21

Stability properties of basic current with respect to waves 3 and 6 as a function of time for nonlinear system of Fig. 19 (above) and system of Fig. 20 (below). Actual growth rate of perturbations denoted by dashed lines.

V. INITIAL STRUCTURE OF PERTURBATIONS

A. Outline of Initial-Value Study

One of the most significant aspects of a nonlinear study is the initial-value problem. If the study is concerned with the nonlinear effects on the growth of a dynamically unstable perturbation, the initial-value problem may be treated by invoking the results of linear instability theory. According to the latter, the unstable perturbation will grow toward one particular configuration corresponding to the most unstable normal mode. In the nonlinear extension of the instability problem this configuration can therefore be adopted for the initial wave, if the latter is sufficiently small for nonlinear effects to be negligible initially. This procedure was followed in the previous computations.

Two important assumptions enter into the above treatment of the initialization problem. The first one is that a given unstable perturbation possesses one normal mode which is distinctly more unstable than the remaining normal modes. As we have seen in the foregoing this is not always the case and there may be some ambiguity as to which unstable normal mode should be adopted for the initial wave. Recalling our discussion of Figs. 19 and 20 it is abundantly clear that such ambiguity can make it very difficult to establish the direction of certain nonlinear effects. The second assumption is that the time-scale of the quasi-linear development is such that the perturbation has an opportunity to adjust to its unstable normal mode structure. In the case of atmospheric development we are dealing with finite initial disturbances which might cause the nonlinear effects to become active

before this adjustment can take place. In such case the initial configuration of a disturbance may be more important than the normal mode behavior.

The foregoing illustrates the need for adequate information concerning the effects of the initial structure of a perturbation on its subsequent growth from the viewpoint of the initial-value aspect of a nonlinear study. The problem is also of somewhat more physical interest if it is considered that the atmosphere at any time displays an abundance of large-scale eddies of all scales and configurations. The question is then why certain eddies grow while others do not and part of the answer may well lie in that the structure--rather than the scale--of some of the perturbations is more favorable for development than others. Obviously we enter here into the realm of operational weather prediction which from the viewpoint of theoretical physics must be regarded as an initial-value problem (see e.g., Thompson, 1961; Shuman and Hovermale, 1968). Actually, the computational techniques and modeling procedures employed in a study of the present type have been mostly developed for the purpose of numerical weather prediction.

The purpose of the present part of this report, then, is to investigate the effects of various initial wave configurations on the subsequent growth rates of the perturbations. A general solution of this problem is difficult to obtain because of the large number of degrees of freedom in the initial structure of the wave. It is therefore advisable to follow a course outlined by previous studies of atmospheric instability, and deal first with purely barotropic or purely baroclinic models. The barotropic initial value problem has been discussed recently by Baer (1968) and King (1970). In the present paper

we consider the baroclinic problem in view of our earlier observation that the instabilities of the general barotropic-baroclinic model are rather well approximated by certain quasi-baroclinic models. Such models are quasi-baroclinic by virtue of the prescribed latitudinal configuration of the perturbation, although the zonal flow has an arbitrary variation with latitude. As shown in Section IIID the justification for such models lies more in a physical than a mathematical argument.

For this study we use a numerical model which is different from the previous one in that the layered representation in the vertical is replaced by a spectral expansion. This model enables us to select an initial wave structure which can be represented by only a few "parameters" of the vertical expansion, such that an inspection of the subsequent generation of smaller vertical scales gives a good indication of the effects of truncating the vertical expansion. A similar procedure was followed for the horizontal-spectral representation in the previous chapter (see e.g., Fig. 15).

The basic equation is again the quasi-geostrophic potential vorticity equation (20)of Chapter II. It will be recalled that the stability parameter, s, in that equation takes on a standard value depending upon z alone in order for the model to satisfy the consistency requirements with respect to energy. It has been shown by Simons (1968) that approximately

$$\frac{1}{s} = \frac{1}{s_o}(1-z) \tag{51}$$

where the subscript o denotes the value of s at the lower boundary, the reciprocal of which was determined to range from 1.2 to 1.5 10^{-12} m^{-2}.

In order to arrive at the linear relationship (51) it was assumed that the effects of the stratosphere on the tropospheric motions could be simulated by a relatively thin mathematical upper layer in which the static stability approaches an infinitely large value. The latter assumption was justified to a satisfactory degree in a normal mode study of baroclinic instability by Simons (1969). As an example, the dash-dot lines in Fig. 1 represent the static stability variation and the upper boundary for a model of this type. For the present computations we have adopted the numerical value $1/s_o = 1.5\ 10^{-12}\ m^{-2}$ which may be interpreted to correspond to a troposphere with a lapse rate of about 6.5 ^{o}C/km and a tropopause level of 225 mb. A detailed description of the relationship between the numerical value of s and the physical model parameters may be found in the paper by Simons (1968).

Before proceeding to the vertical representation let us first recall the horizontal-spectral equations. Further let us restrict ourselves to a quasi-baroclinic system as defined in Section IIID. Thus the zonal streamfunction ψ_o is represented by a series of Legendre functions but the perturbation streamfunction has a meridional variation corresponding to a single associated Legendre polynomial. Thus we have

$$\psi_o = \sum_{\alpha} \psi_\alpha(z,t)Y_\alpha(\mu) \qquad \psi_1 = \psi_\beta(z,t)Y_\beta(\mu) \tag{52}$$

These expansions and the resulting horizontal-spectral equations are discussed in Appendix A. It can be shown immediately that as a result of the simple horizontal wave configuration the nonlinear processes will not generate a wave of wave number 2ℓ as they did before. Thus we do not consider the secondary perturbation streamfunction ψ_2. The coefficients of the expansion (52) will be referred to as the horizontal-

spectral components or briefly "components". The components are functions of the time and the vertical coordinate and they were specified before at regular intervals in the vertical (layered model). In the present model, however, each of the components itself is represented by a series of orthogonal polynomials as follows

$$\psi_\alpha = \sum_m \psi_{\alpha,m}(t)\, Z_m(z) \qquad \psi_\beta = \sum_m \psi_{\beta,m}(t)\, Z_m(z) \tag{53}$$

where now the expansion coefficients are only time-dependent. The latter coefficients will be called "parameters" because of the similarity between the present model and the historical two-parameter models (e.g., Eliassen, 1952).

The vertical polynomials $Z_m(z)$ which are appropriate for the expansions (53) have been derived by Simons (1968). The choice of the functions depends upon the specified vertical variation of the static stability and for the particular variation given by (51) the polynomials are the well-known Bessel functions of the first kind of order zero. The properties of these functions are reviewed in Appendix B, and the spectral prediction equations for the expansion parameters are formulated. It will be helpful for the following discussion if we here reproduce the equations for the present simple case of a quasi-baroclinic model. From Appendix B we obtain immediately the following equations for the zonal parameters $\psi_{\alpha,m}$ ($\alpha = 1,2,3..,\ N_\alpha$; $m = 0,1,2,\ldots,\ M-1$) and the wave parameters $\psi_{\beta,m}$ ($m = 0,1,2\ldots,\ M-1$)

$$\left(c_\alpha + \frac{d_m}{s_o}\right) \frac{d\psi_{\alpha,m}}{dt} = K_{\beta\beta\alpha} \sum_k \sum_j J_{mkj} \frac{1}{s_o} (d_j - d_k)\ \mathrm{Im}\left(\psi_{\beta,j}\, \psi^*_{\beta,k}\right) \tag{54}$$

$$\left(c_\beta + \frac{d_m}{s_o}\right) \frac{d\psi_{\beta,m}}{dt} = 2i\ell\, \psi_{\beta,m} + \tag{55}$$

$$+ i \sum_\alpha K_{\beta\beta\alpha} \sum_k \sum_j J_{mkj} \left((c_\beta - c_\alpha) + \frac{1}{s_o}(d_j - d_k)\right)\left(\psi_{\alpha,k}\, \psi_{\beta,j}\right)$$

where c_α, c_β, d_m, d_j, d_k, and also $K_{\beta\beta\alpha}$ and J_{mkj}, are certain constants defined in Appendix A and Appendix B. The numerical values of these constants are irrelevant for the purpose of the following discussion except for the fact that $(d_j - d_k)\, J_{mkj} = 0$ for $m = 0$. It follows then from (54) that the first parameter of any zonal component $\psi_{\alpha,o}$ is a constant. Since the first polynomial $Z_o = 1$, this simply means that the vertical average of the zonal flow does not change, which is a basic property of the simple system (52).

B. Normal Mode Solutions

Before going to the initial value problem we must establish the linear stability characteristics of the spherical spectral model described in the previous section. It is then advantageous to consider certain zonal wind profiles which are reasonable in the light of observed winds but at the same time simple enough for a meaningful interpretation of the results of our study. Now the general expression for the zonal wind corresponding to (52) and (53) is

$$U(\phi,z,t) = -\,463. \sum_\alpha \sum_m \psi_{\alpha,m}\, Z_m \frac{dY_\alpha}{d\phi} \tag{56}$$

where the number 463 represents the equatorial speed of rotation of the earth's surface in m/sec and hence converts from the non-dimensional

units of velocity defined in Chapter II to units of m/sec. Fig. 22a shows a few latitudinal profiles. The points represent the observed mean zonal wind profile at 500 mb for December 1 through 5, 1960, on the same scale. Vertical zonal wind profiles are plotted in Fig. 22b against a linear height scale. The vertical mean wind can be assigned any value by adding the polynomial $Z_o = 1$ with its coefficient.

It will be seen from (56) that it would be difficult to compare the results of various experiments if we would vary all coefficients in an arbitrary manner. It seems advisable to select only a few coefficients as basic parameters of the flow and to let the remaining ones be specified with respect to these basic coefficients. The latitudinal profile should represent in some general way the belt of westerlies at middle latitudes. More detail is irrelevant for the purpose of the present baroclinic study and thus the curves II and III in Fig. 22a may be considered satisfactory. The variation of the coefficients is restricted by requiring that the latitudinal profiles are the same at all levels which again seems a reasonable convention in a study of baroclinic instability. Thus if we take curve III in Fig. 22a as an example then $\psi_{2,m} = \frac{1}{3}\,\psi_{1,m}$ and $\psi_{3,m} = \frac{1}{12}\,\psi_{1,m}$ for all values of m and hence the zonal wind is then specified completely by the coefficients $\psi_{1,m}$ for $m = 0,1,2,\ldots, M-1$. In turn we choose one of the latter coefficients as our **basic variable**. An appropriate choice is $\psi_{1,1}$ since it specifies the over-all vertical shear in our model. The corresponding polynomial Z_1 is represented by curve I in Fig. 22b. All other parameters except for $\psi_{\alpha,o}$ will then be known once the vertical profile has been specified, e.g., $\psi_{\alpha,2} = .2\ \psi_{\alpha,1}$ and $\psi_{\alpha,3} = -1.\ \psi_{\alpha,1}$ if profile II of Fig. 22b is adopted. The coefficient $\psi_{1,o}$ finally will be chosen such that the

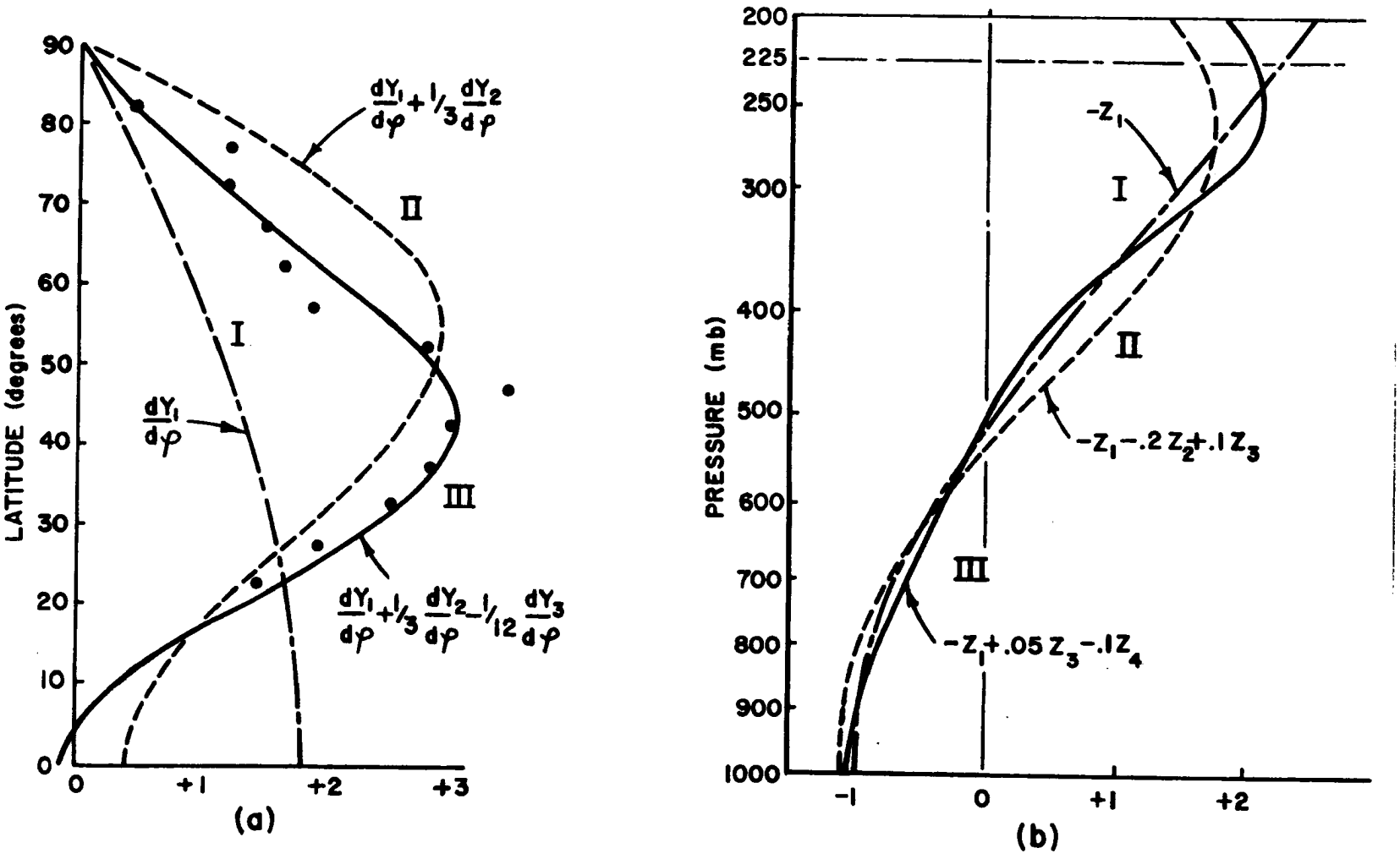

Fig. 22

Latitudinal and vertical profiles of basic current employed in this chapter.

vertical-mean winds assume reasonable atmospheric values, but it is well known that this mean wind is irrevelant for the stability characteristics of our model.

The zonal wind profiles have now been established for easy reference, and we can proceed to the actual stability computations. Since this section is concerned with linear normal mode studies, the first step is to linearize the equations by setting the zonal wind constant with respect to time. Let us briefly review the solution of the two-parameter model as an example. In the two-parameter model the series (53) are truncated after two terms, thus m = 0,1. The zonal equations (54) may be discarded and the wave equations (55) may be written

$$\frac{d\psi_{\beta,o}}{dt} = i\,(a_{oo}\,\psi_{\beta,o} + a_{o1}\psi_{\beta,1})$$

$$\frac{d\psi_{\beta,1}}{dt} = i\,(a_{10}\,\psi_{\beta,o} + a_{11}\psi_{\beta,1}) \qquad (57)$$

where the matrix elements a_{jk} are real constants which follow immediately from (55) for m = 0,1. For the present discussion it is only important to realize that these matrix elements depend upon the static stability and the shear parameters $\psi_{\alpha,1}$ of the basic flow.

The solution of (57) is of the form exp $(-i\nu t)$. After substitution into (57) we obtain two homogeneous equations, the solution of which can only exist if the determinant equals zero. This condition is satisfied for

$$\nu_{a,b} = -\tfrac{1}{2}(a_{oo}+a_{11}) \pm \sqrt{\tfrac{1}{4}(a_{oo} - a_{11})^2 + a_{01}\,a_{10}} \qquad (58)$$

The solution will grow exponentially if the wave speeds become complex, thus the condition for instability is

$$- a_{01}\, a_{10} > \tfrac{1}{4}(a_{00} - a_{11})^2 \tag{59}$$

in which case we can write

$$\nu_r = - \tfrac{1}{2}(a_{00} + a_{11})$$

$$\nu_{a,b} = \nu_r \pm i\nu_i \qquad \nu_i = \sqrt{-a_{01}a_{10} - \tfrac{1}{4}(a_{00}-a_{11})^2} \tag{60}$$

The solution above may be compared with baroclinic instability studies presented by Eliassen (1952) for a two-parameter model and by Phillips (1954) for a two-layer model.

The wave perturbation involves two wave numbers: the zonal wave number ℓ occurring in (21) and a latitudinal wave number associated with the particular associated Legendre function $Y_\beta(\mu)$ in (52). Following the usual notation we denote the degree of the polynomial by n, and we recall that the difference $n-\ell$ gives the number of zeros between the poles (see also Appendix B). Clearly both wave numbers will occur in the solution, together with basic state parameters such as the static stability and the zonal shear. Since the effects of the latter parameters are sufficiently well known, we will here consider the results only as a function of both wave numbers. Fig. 23 shows the growth rates per day, ν_i, of the unstable wave components in the two-parameter model for $1/s_o = 62.9$ and $\psi_{1,1} = .00919$ (non-dimensional units defined in Chapter II). The points in the figures represent the wave components here considered, i.e., $n-\ell$ is odd since we are dealing with Legendre functions of odd parity as explained in Appendix A. The lower right parts of the

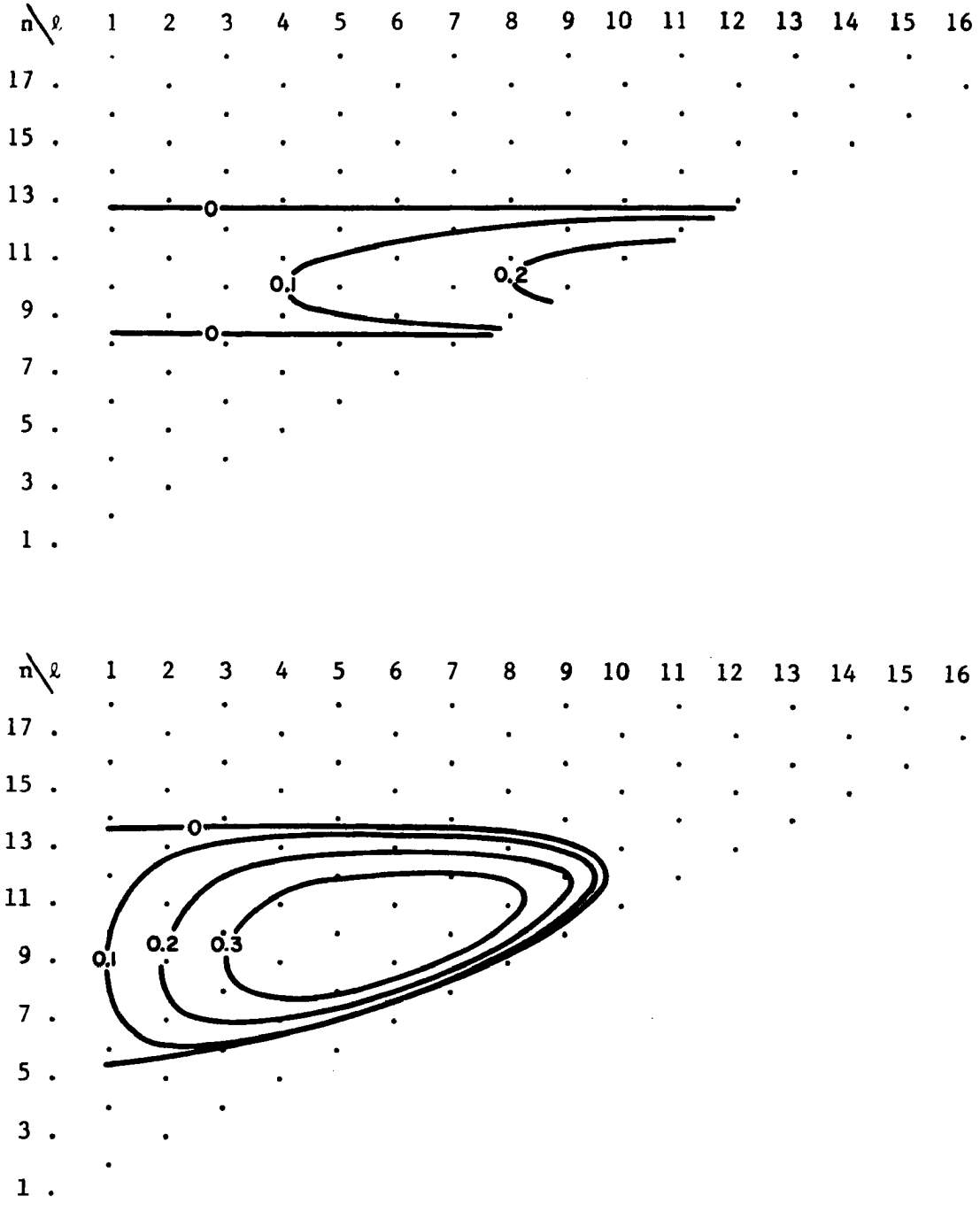

Fig. 23

Growth rates (per day) of perturbations in two-parameter model for zonal profiles corresponding to curve I of Fig. 22a (above) and curve II of Fig. 22a (below)

figures are empty because $n>\ell$ by definition of the associated Legendre polynomials. The upper part of Fig. 23 represents the case where the zonal wind is a linear function of μ, that is the purely baroclinic model. Note that the instability criterion is independent of the zonal wave number ℓ, but the growth rate is proportional to ℓ for given n. The lower part of Fig. 23 shows the effect of introducing a second zonal polynomial into the same model such that we go from curve I to curve II in Fig. 22a. The growth rates look now far more reasonable in view of atmospheric observations. This feature was noted also in Chpater IIID and constitutes the main argument for defining the quasi-baroclinic model in the present manner.

Having discussed the two-parameter model in great detail, we will now briefly review the effects of increased vertical resolution. Since the solutions of the present stability problem for a continuous atmosphere (Charney, 1947; Kuo, 1952) do not show the short wave cut-off of the two-level model, one might expect that the instability of the short waves increases if the number of layers or the number of vertical parameters is increased. This feature was indeed observed by Kuo (1953) and recently has been shown in much detail by Brown (1968). The upper and lower parts of Fig. 24 show the growth rates of the unstable waves for the present three-parameter and four-parameter models, respectively. The zonal wind and the static stability are the same as those considered in the lower part of Fig. 23. Indeed there is a tendency for the smaller scales (larger n and ℓ) to become more unstable with increasing vertical resolution.

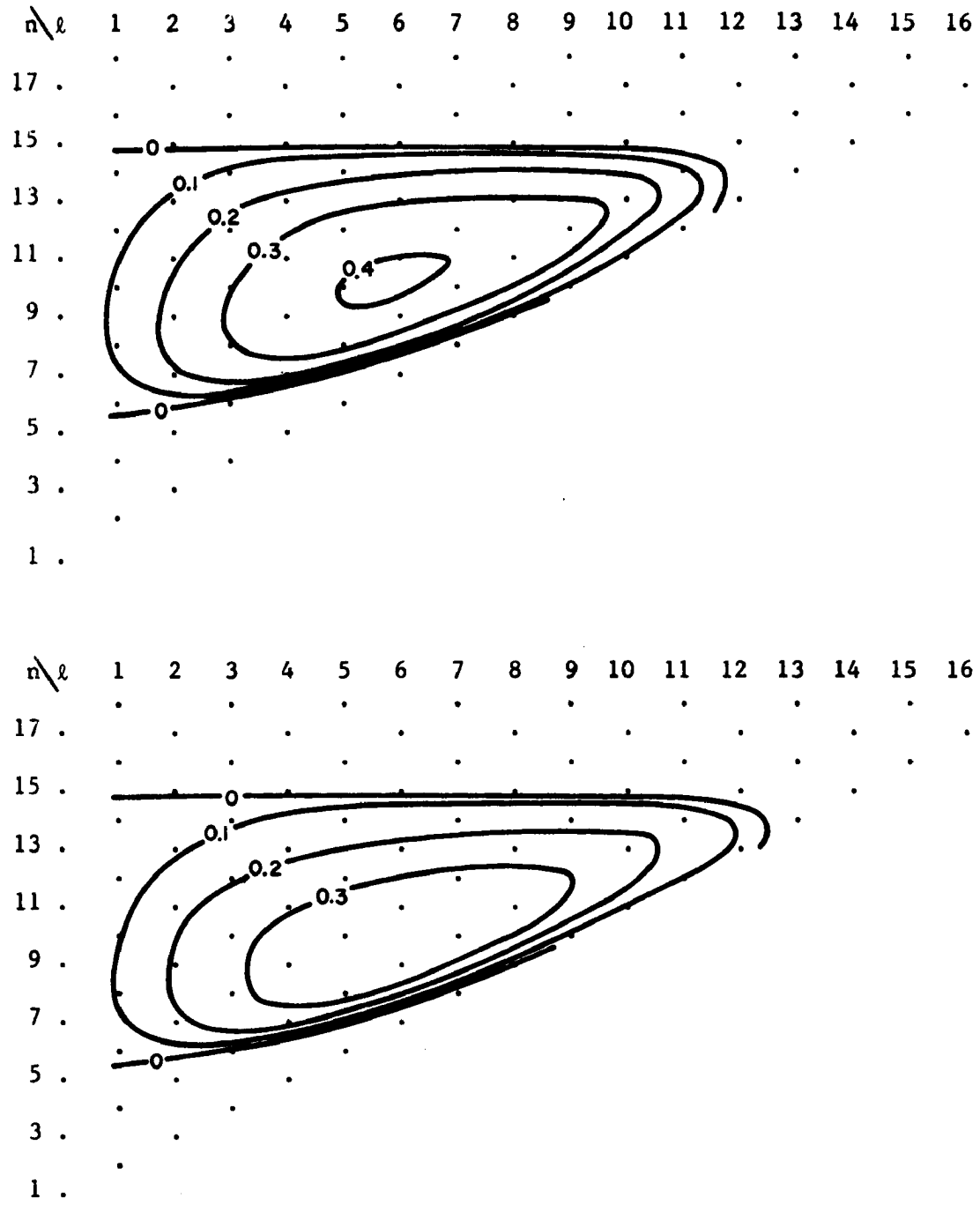

Fig. 24

Growth rates (per day) of perturbations in three-parameter (above) and four-parameter model (below). Zonal profile corresponding to curve II of Fig. 22a.

C. Linear Initial Value Problem

The normal mode instabilities of the previous section may be interpreted as the behavior of certain wave perturbations in the atmosphere under the condition that nonlinear effects may be neglected. The basic assumption is then that such perturbations can approach the normal mode structure corresponding to the unstable mode, before the nonlinear effects will drastically alter the development of the wave. This was the assumption made in the nonlinear study of Chapter IV, where the initial perturbation was made to fit the configuration of the most unstable normal mode. If we are dealing with atmospheric cyclone development we note, however, that the atmosphere is a turbulent fluid in which we may find an abundance of relatively large perturbations at any moment. The emphasis is therefore on the development of such perturbations during the relatively short time scales associated with cyclone developments. The asymptotically different behavior of neutral and unstable waves is irrelevant and it may be of more importance to determine what initial wave configurations are most suitable for development. To gain a first insight into this problem we consider here the solution of the linear initial value problem. Again the two-parameter model will be considered in detail to serve as an example.

The solutions for the linearized two-parameter model (57) may be written

$$\psi_{\beta,o} = Ae^{-i\nu_a t} + BC_o e^{-i\nu_b t} \qquad \psi_{\beta,1} = AC_1 e^{-i\nu_a t} + Be^{-i\nu_b t} \tag{61}$$

where ν_a and ν_b are given by (58) and the constants C_o and C_1 are obtained by substituting (61) into (57), thus

$$C_o = \frac{\nu_b + a_{11}}{-a_{10}} \qquad C_1 = \frac{\nu_a + a_{oo}}{-a_{01}} \tag{62}$$

The constants A and B are determined by the initial conditions for the wave, since from (61) we have

$$A = \frac{(\psi_{\beta,o} - C_o\psi_{\beta,1})_{t=0}}{1-C_oC_1} \qquad B = \frac{(\psi_{\beta,1} - C_1\psi_{\beta,o})_{t=0}}{1-C_oC_1} \tag{63}$$

For an unstable wave, the wave speeds are of the form (60) and thus all constants are complex numbers. Moreover, the first parts of the solutions (61) will grow indefinitely while the second part will soon damp out. Thus with increasing time, the ratio between the shear parameter and the mean parameter of the wave becomes equal to C_1. Let us interpret this in terms of the perturbation at the earth's surface and the perturbation at upper levels. The polynomial Z_o is a constant equal to unity, while the function Z_1 equals 1 at the surface and -1 at the 350 mb level . Taking the latter as the upper level denoted by subscript u and denoting the surface by subscript s we obtain from (53)

$$\psi_{\beta,s} = \psi_{\beta,o} + \psi_{\beta,1} \qquad \psi_{\beta,u} = \psi_{\beta,o} - \psi_{\beta,1} \tag{64}$$

for the present two-parameter model. The ratio between upper and lower wave for the unstable perturbation approaches then

$$\frac{\psi_{\beta,u}}{\psi_{\beta,s}} \rightarrow \frac{1-C_1}{1+C_1} \equiv r_1 e^{i\theta_1} \tag{65}$$

It follows then from (21) of Chapter II and from (52) that the upper wave stays behind if θ_1 is positive. Actual evaluation of (65) shows

that $r_1>1$ and $0<\theta_1<90^o$ for all unstable waves. Therefore the upper wave perturbation is larger than the lower one and is behind by $0-90^o$ if there is sufficient time for the perturbation to attain the structure of the unstable mode. This result was derived by Phillips (1954) for a two-layer model on a beta-plane.

An interesting feature of (63) is that the constant A becomes zero if $\psi_{\beta,o}/\psi_{\beta,1} = C_o$ at the initial time, which means that the wave energy will go to zero even though the wave is unstable. Clearly then the vertical distribution of the initial wave energy is of major importance for the subsequent growth of the perturbation and an interesting question is at what level a given wave perturbation should be introduced in the atmosphere in order to cause a maximum conversion of potential into kinetic energy. This problem can be solved readily for the case of the present linearized two-parameter model. We have here the freedom to introduce a perturbation either at the surface or in the upper layer, or we may distribute the given initial perturbation energy over lower and upper levels. In the latter case we have an additional freedom in the form of the phase difference between initial upper and lower waves.

The surface perturbation and the upper level perturbation have been defined by (64) in terms of the vertical-mean and shear parameters of the two-parameter model. Since we are dealing with only the difference of the initial phases of the upper and lower perturbations, we may choose one phase angle equal to zero. We define thus initially

$$\psi_{\beta,s}\ (t=0) \equiv x \qquad\qquad \psi_{\beta,u}\ (t=0) \equiv y\ e^{i\theta} \tag{66}$$

Now the kinetic energy in the wave component has been derived in Appendix D. For a two-parameter model we obtain

$$\overline{K}_1 = c_\beta \left(\psi_{\beta,o} \, \psi^*_{\beta,o} + \psi_{\beta,1} \, \psi^*_{\beta,1} \right) \tag{67}$$

Thus from (64) and (66) we have for the initial time

$$\frac{2}{c_\beta} \overline{K}_1 \ (t=0) = x^2 + y^2 \equiv k \tag{68}$$

The problem is to find the values of x, y, and θ, for which $\overline{K}_1$ becomes a maximum after a given time for a given value of k defined by (68).

Consider first an unstable wave with complex wave speeds. Then according to (60) the second part of the solutions (61) will decrease with time and after a few days this part becomes negligible. We have already noted that only the constants A and B are dependent upon the initial energy distribution within the wave. We then conclude from (61) and (67) that $\overline{K}_1$ attains its largest value with increasing time if $|A|$ assumes a maximum. Consequently from (63), (64), and (66) it follows that we must determine the maximum value of

$$a^2 \equiv x^2 + y^2 r^2 - 2 \, xyr \cos (\theta + \theta_o) \tag{69}$$

where we have defined

$$\frac{C_o + 1}{C_1 - 1} \equiv r \, e^{i\theta_o} \tag{70}$$

since x, y, and r are by definition positive, the maximum value of a^2 is obtained for given x and y if $\theta = \pi - \theta_o$ in which case $a^2 = (x + ry)^2$. For this value of θ we find the maximum of a^2 by setting $\partial a^2 / \partial x = 0$ after substituting (68). For positive x, y, and r, the only solution is $y = rx$ and thus we find from (68) the following initial conditions which

are most favorable for the growth of the wave kinetic energy

$$\theta = \pi - \theta_o \qquad x^2 = \frac{k}{1+r^2} \qquad y = rx; \qquad a^2 = k(1+r^2) \tag{71}$$

If the solutions (60) and (62) are substituted into (70)it can be shown that for all unstable waves $r<1$ and $0<\theta_o<90^o$ and therefore the increase of the perturbation energy is a maximum if the initial amplitude of the surface wave exceeds that of the upper level wave, and if the initial upper wave is behind by 90^o-180^o. We may recall here that according to (65) the unstable upper level wave will eventually become larger than the lower wave and that the upper wave will be behind by 0-90^o. This implies that even an initial surface disturbance will ultimately propagate to upper levels.

So far we have discussed the growth of unstable wave perturbations. Since such waves grow without bounds in a linear model, there is a sharp distinction between their asymptotic behavior and the long-term behavior of neutral perturbations. On the other hand, if we are interested in the initial development of a perturbation for a period of a few days, we do not notice a sudden transition from a set of unstable waves to a set of neutral waves. Just as unstable waves may decay due to their initial vertical distribution, so a neutral wave can grow over a given period of time. This may be seen immediately by considering the sum of two complex number z_1 and z_2. From the triangle rule in the theory of complex numbers we have

$$(|z_1| - |z_2|)^2 \leq |z_1 + z_2|^2 \leq (|z_1| + |z_2|)^2 \tag{72}$$

Thus although we have solutions of the type (61) where each individual

exponential solution has a constant amplitude for the case of neutral waves, the amplitude of their sum can vary with time between the two limits given by (72). Considering the neutral solutions for our two-parameter model we may write (58) in the form $\nu_{a,b} = \nu_1 \pm \nu_2$ where ν_1 and ν_2 are real numbers, while also C_o and C_1 are real according to (62). Depending on the initial conditions A and B may be complex, thus we write the general expressions $A = |A| \exp(i\alpha)$, $B = |B| \exp(i\beta)$ and obtain from (61) and (67)

$$\overline{K}_1 = c_\beta \left((1+C_1^2)|A|^2 + (1+C_o^2)|B|^2 + 2(C_o+C_1)|A||B| \cos(\beta-\alpha+2\nu_2 t)\right) \quad (73)$$

Similar to the case of the unstable waves we may again determine the conditions under which $\overline{K}_1$ reaches a maximum growth for a given time.

The typical dependence of the initial rate of growth of the perturbation amplitude upon the initial vertical configuration of the wave is illustrated in Fig. 25 for an arbitrary wave component in a two-parameter model. The figure shows the ratio of the kinetic energy after 5 days over the initial wave kinetic energy as a function of the amplitude ratio and the phase difference of the initial upper and lower wave, i.e., as a function of y/x and θ defined by (66). We may for a given day and for each wave perturbation, neutral and unstable alike, construct a figure like Fig. 25 and pick off the maximum value of the kinetic energy. These maxima are shown in Fig. 26 for all wave components and for two different days. The zonal wind is the same as the one used in the lower part of Fig. 23. By comparing the latter with Fig. 26 it is seen that the normal mode study tends to underestimate the instability of the shorter waves. We may also determine the amplitude ratio and the phase difference of the initial upper and

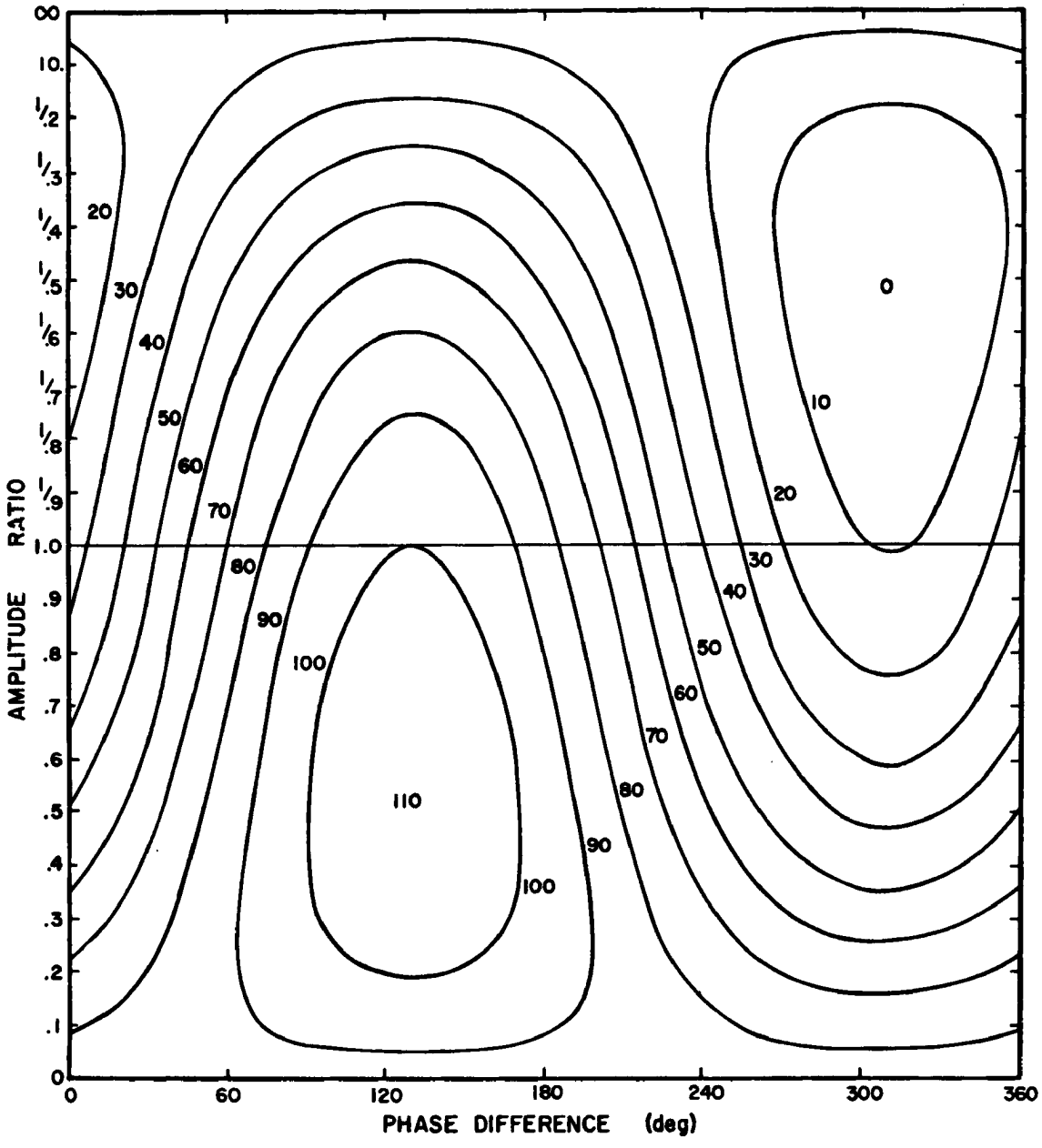

Fig. 25

Perturbation kinetic energy after 5 days in terms of its initial value in a two-parameter model as a function of the amplitude ratio and phase difference of initial upper and lower waves.

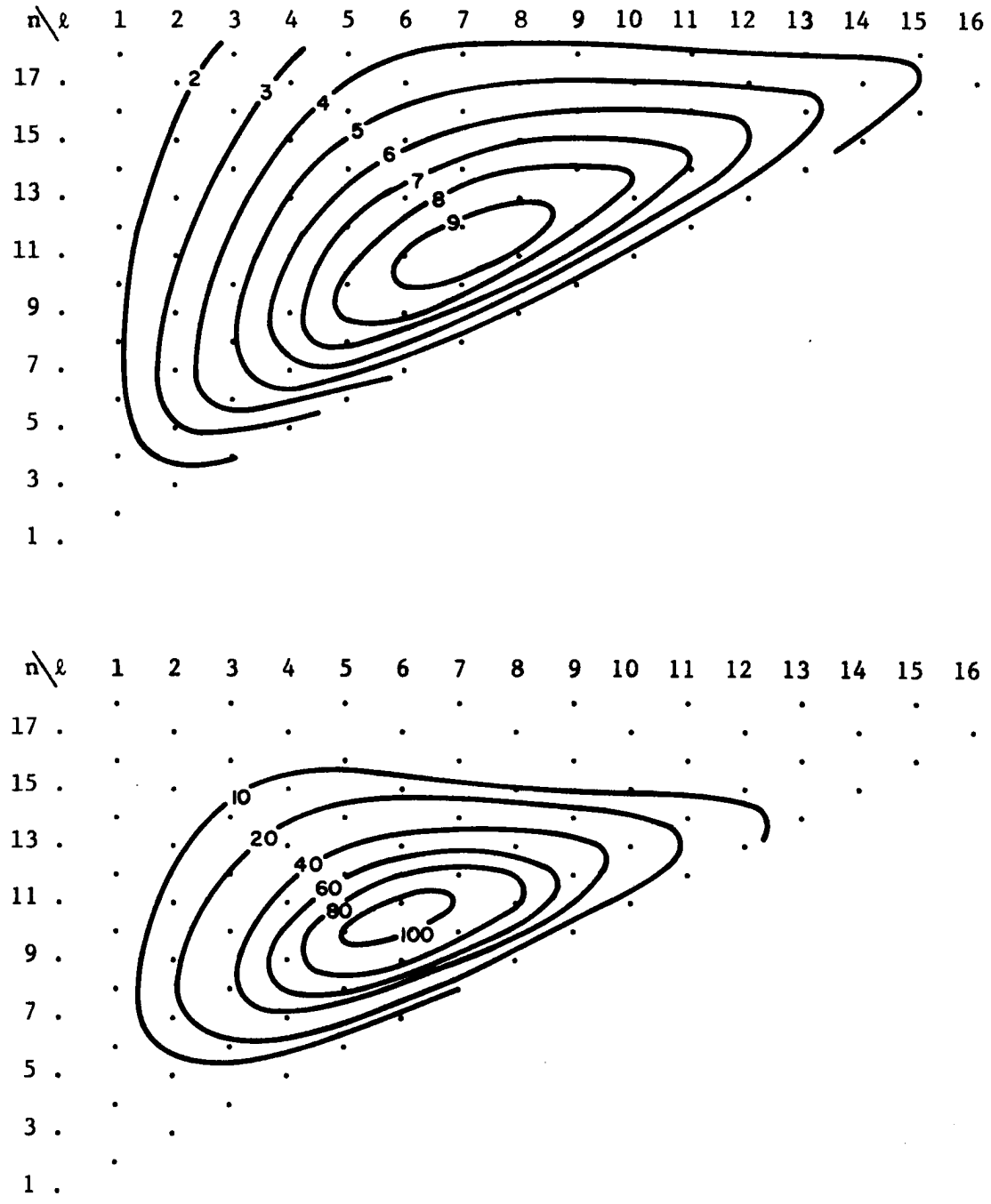

Fig. 26

Maximum kinetic energy of perturbations in a two-parameter model after 2 days (above) and 5 days (below) in terms of initial kinetic energy.

The chosen initial wave configurations and the relatively short periods of integration allow only very little energy to flow into the highest parameter and the series expansion along the vertical is therefore effectively not truncated. We will consider initial disturbances which are more or less concentrated at certain levels in the vertical. A study of the development of such perturbations will indicate at which level a perturbation should be introduced in order for the generation of kinetic energy to reach a maximum. We adopt three basic perturbations, the maxima of which occur at upper, middle, and lower levels, respectively. The phases will be assumed to be uniform with respect to height, which is reasonable for shallow disturbances. In addition, we consider a few disturbances which represent smooth transitions from one basic profile to the next. Fig. 27 shows the initial wave profiles normalized such that all profiles represent the same perturbation kinetic energy.

The basic zonal flow varies with latitude according to profile II of Fig. 22a. The three vertical profiles of Fig. 22b are considered in turn. The second profile causes always much larger growth rates than the first and the third. This is probably due to a larger effective shear between the surface and jet-stream levels. Therefore, the shear parameter for this profile has been reduced by 15 per cent as compared to the other zonal profiles. Otherwise the value assigned to the basic vertical shear is the same as before. Furthermore, all wind profiles have been made to contain the same kinetic energy by varying the vertical-mean zonal wind. The influence of the latter on the stability properties of the flow is found to be negligible. The advantage of this normalization is that the total kinetic energy is the same for all experiments and hence can be used as the unit of energy. The

kinetic energy of the basic flow and the perturbation at any time will be expressed in per cent of this unit.

For all subsequent experiments the relevant parameters will be given in the following manner. The vertical zonal wind profile used in a particular experiment will be denoted by ZP1, ZP2, or ZP3, according to the numbers of the curves in Fig. 22b, but where the average shear of profile III has been reduced by 15 per cent. The initial vertical wave profiles will be denoted by WP1 to WP9 according to Fig. 27. The initial wave kinetic energy is always 1 per cent of the initial total kinetic energy. Owing to this small initial amplitude of the perturbation, the nonlinear effects are relatively small for the few days over which the present integrations extend.

Let us now consider the development of a wave perturbation as a function of the initial vertical wave profiles shown in Fig. 27. Computations were carried out for all components of waves 3, 6, 9, and 12, and for all three vertical zonal wind profiles. Since the effects of the initial perturbation structure are very similar for the various zonal profiles we will restrict ourselves to a discussion of the first zonal profile, ZP1. Fig. 28 shows the kinetic energy of the perturbation after 5 days (abscissa) as a function of the initial wave profile (ordinate). The point values obtained for the 9 initial wave profiles, WP1 through WP9, have been connected by straight lines for easier interpretation of the diagrams. The energy is again expressed in per cent of the initial total kinetic energy such that the initial wave kinetic energy equals unity. The spectral wave components have been numbered according to their order of appearance in the series for ψ_1 given by (52) such that the first component represents the

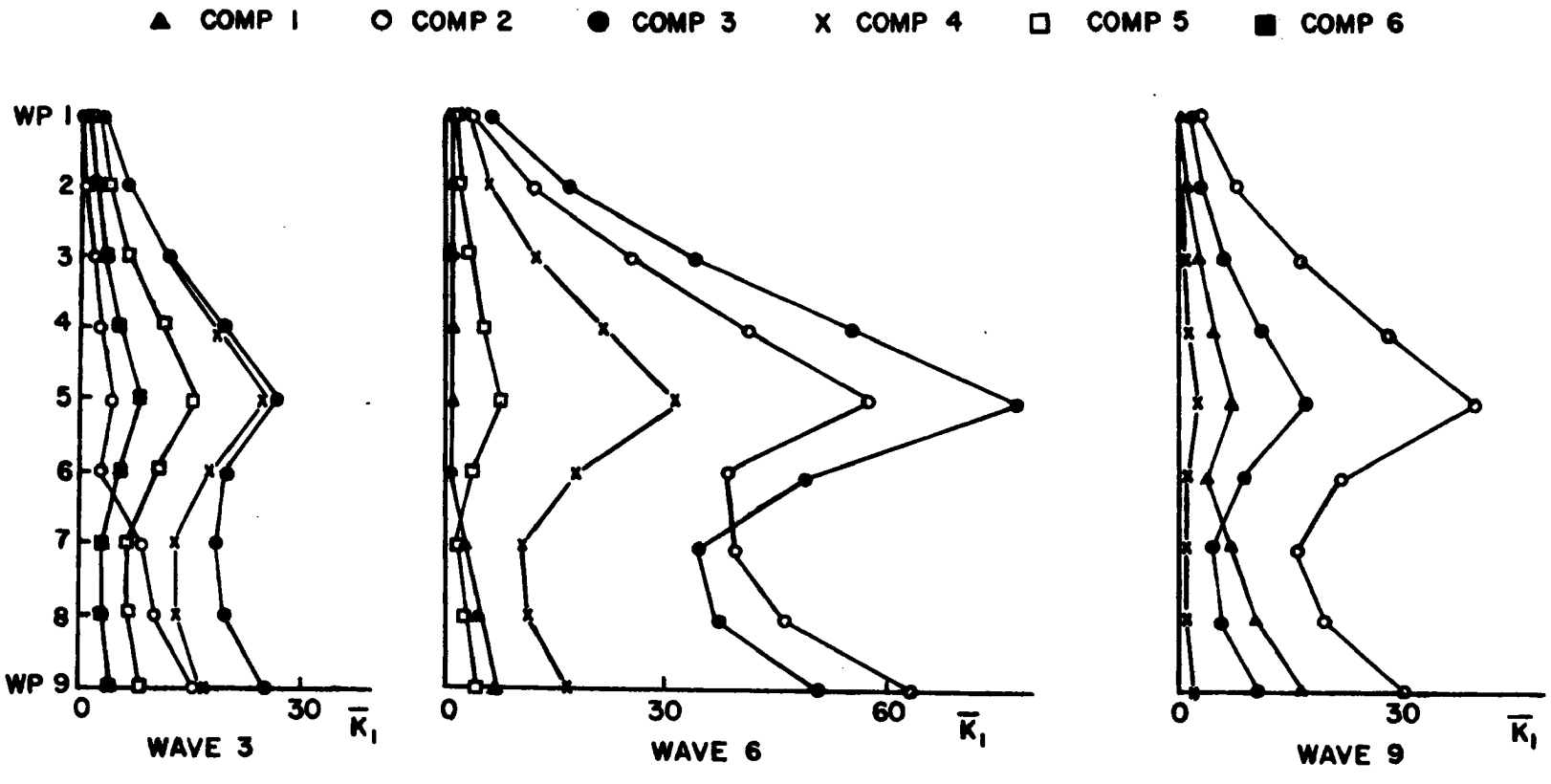

Fig. 28

Increase of wave kinetic energy after 5 days for 9 initial wave profiles shown in Fig. 27 and for various waves and components of horizontal-spectral expansion.

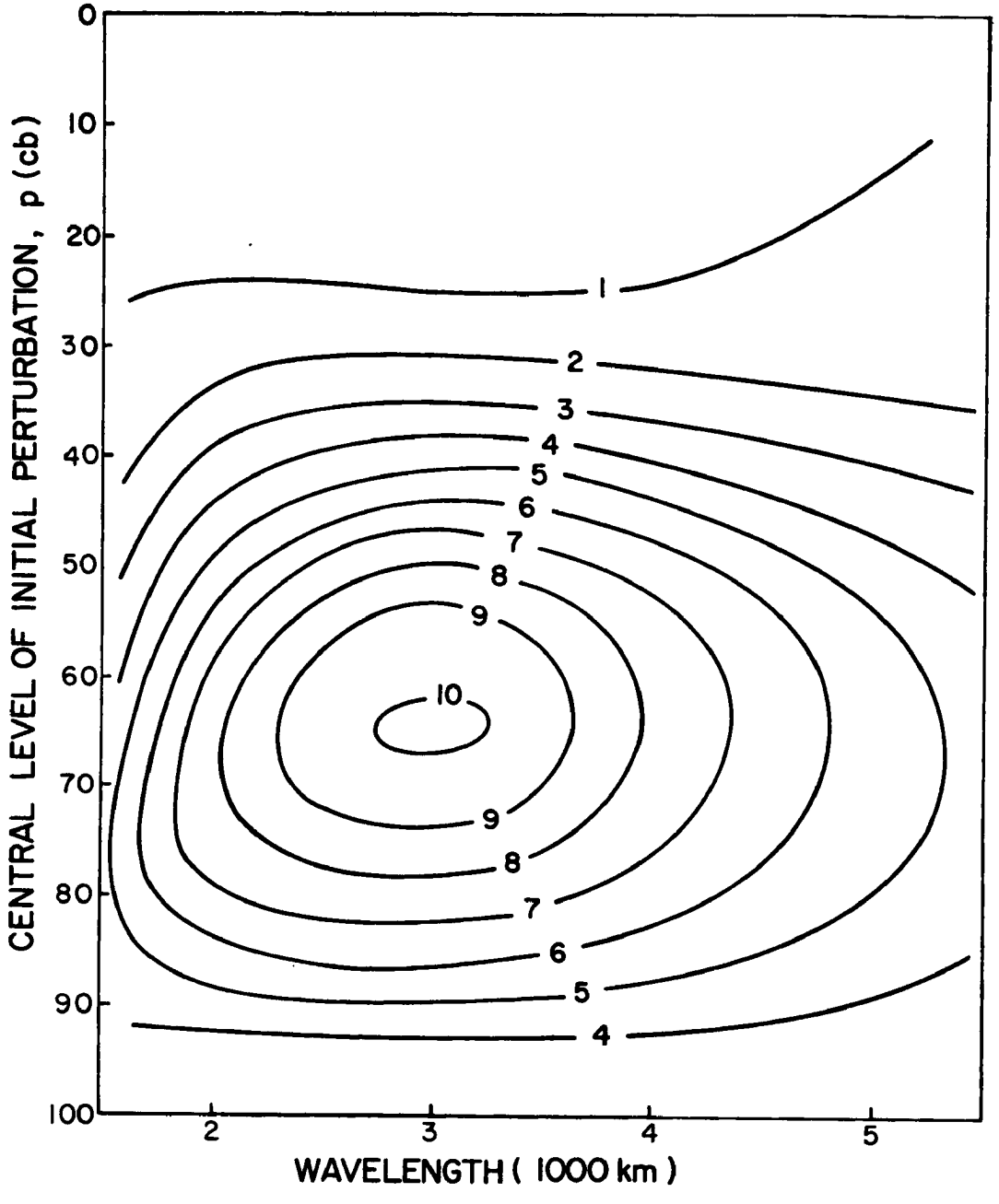

Growth of wave perturbations (measured by $\sqrt{K_3/K_o}$ where K_n is the wave kinetic energy after n days) as a function of wavelength and level of initial perturbation. Beta-plane model, perturbations independent of lateral coordinate, initial perturbation depths 300 mb. (Simons, 1969)

A final point of interest is the history of the development of the perturbations from the initial profiles shown in Fig. 27 to the final vertical profiles of the steadily growing waves. As noted before, the initial amplitude is sufficiently small for the wave to behave quasi-linear for a number of days and hence the wave tends to its unstable normal mode structure. Fig. 30 represents the vertical profile of the amplitude of the third component of wave 6 after 3.5 days for a few different initial wave profiles and for the three zonal wind profiles ZP1, ZP2, and ZP3. The unit of horizontal scale is the vertical average of the amplitude of the initial wave. Indeed, the final wave profile of this highly unstable wave is nearly independent of the initial profile after these few days. On the other hand the vertical zonal wind profile tends to force its profile upon the wave profile. The same is observed for all other wave components and all initial vertical wave profiles. As indicated by Fig. 20 the actual increase of wave kinetic energy is fairly independent of the vertical zonal wind profiles here considered. This suggests that the instability is mainly determined by the over-all vertical shear (which is about the same for the three zonal profiles) rather than the curvature of the profile. It has been found, however, that the growth rates associated with profile ZP2 are in general smaller for the perturbations of larger scales and larger for the smaller scales.

The position of the wave as a function of time is strongly dependent upon the initial wave profile. This is of course related to the well-known tilt of the unstable wave such that the surface perturbation is well ahead of the upper level wave. Thus during the

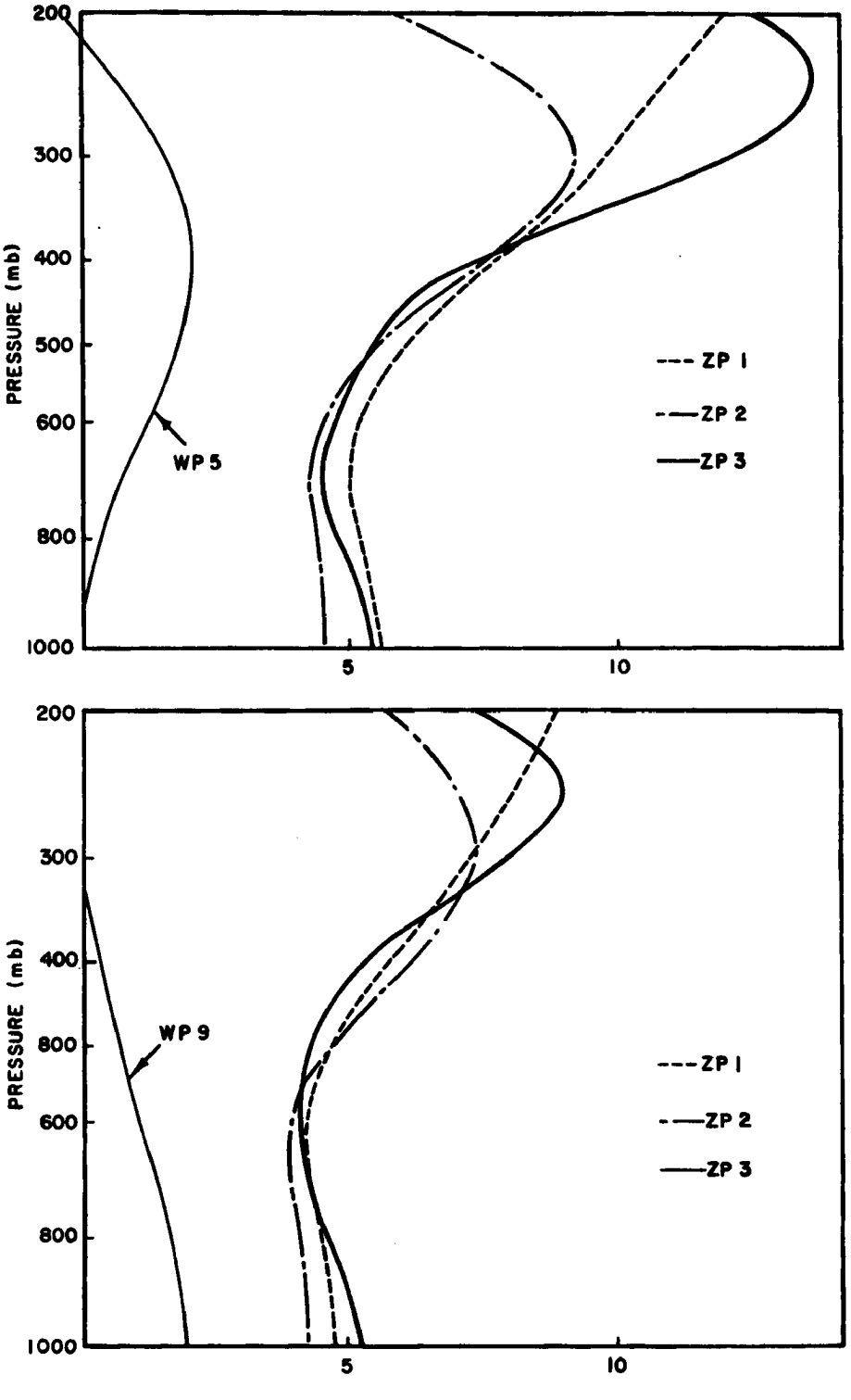

Fig. 30

Amplitude of wave perturbation after 3.5 days, in terms of initial vertical-mean, as a function of zonal profiles and initial wave profiles (shown by thin solid lines).

first three days or so, the wave moves about twice as far for the case WP1 (tropopause disturbance) than for the case WP9 (surface perturbation). These differences in wave position are largely due to the initial development of the wave. The upper level perturbation starts moving immediately - or so it appears - because it tends to establish a surface perturbation ahead of the upper level wave. The initial surface disturbance on the other hand must first generate the upper level wave behind and stays at the same place for about a day.

VI. SUMMARY AND CONCLUSIONS

In this paper we have investigated the development of atmospheric cyclones from the viewpoint of the instability of large scale wave perturbations superimposed on a basic zonal current. The stability properties of an observed atmospheric mean zonal flow were evaluated and the linear results have been extended to include the nonlinear effects resulting from the self-interaction of the wave perturbation. Furthermore, the initial value problem associated with the present study has been considered in some detail. The model employed in this investigation is quasi-geostrophic, adiabatic, inviscid, and hemispheric. The numerical methods used are the spectral technique in the horizontal and either a spectral or a layered representation in the vertical.

In the linear part of this study we have considered a basic current corresponding to the zonal average of the climatological-mean flow for January. The current is found to be unstable with respect to perturbations of all wave numbers 1 through 16 here considered. The cyclone-scale waves show a maximum growth rate and furthermore these waves exhibit one normal mode which is distinctly more unstable than the others. By considering the energy conversion processes it is established that the instabilities are almost completely of a baroclinic nature with barotropic stabilizing effects, in accordance with general atmospheric observations. The linear investigation shows also that the stability properties of the January zonal flow vary strongly with longitude which might affect the development of cyclones as a function of geographical location. Finally it is shown that the dynamic

instability of the general barotropic-baroclinic current can be studied rather well with the help of a special quasi-baroclinic model.

The investigation of the effects of nonlinear processes on the growth of an unstable wave perturbation is based on a system consisting of the zonal flow and two planetary waves, the second of which is the higher harmonic of the first. The first problem concerns the development of a highly-unstable cyclone-scale wave interacting with the zonal flow and producing a secondary wave as a result of the self-interaction of the primary wave. Owing to the nonlinear interactions with the zonal flow the growth rate of the unstable perturbation is reduced to a very small value or it may become negative when the wave kinetic energy reaches the order of magnitude of observed atmospheric wave energies. It is found that at this time the conversion of potential to kinetic energy in the wave (baroclinic growth) starts decreasing while at the same time the release of wave kinetic energy to the zonal flow (barotropic damping) increases tremendously. This combination of energy conversion processes causes the wave growth to come to a halt while building up the zonal kinetic energy by an amount up to 20 percent of the initial zonal kinetic energy. This process will maintain the zonal flow against frictional dissipation as also indicated by the energy conversions within the zonal flow which tend to transport the kinetic energy downwards after receiving it from the wave. The general effect of the secondary wave is found to be a slight increase of the growth rates above the values obtained in the absence of this wave. A similar effect is observed when the horizontal resolution of the numerical model is increased.

The second problem investigated in the nonlinear extension of the atmospheric stability studies is concerned with the effects on a cyclone-scale unstable perturbation resulting from the self-interaction of a long quasi-permanent wave. It is found that the initial growth rate of the cyclone wave is considerably reduced as a result of the presence of the long wave. This damping effect increases with increasing initial amplitude of either wave. An investigation of the linear stability properties of the zonal current at various stages during the nonlinear integrations indicates that the nonlinear damping effects on the growth rates of the perturbations are not directly related to a loss of dynamic instability of the zonal flow. Actually it is found that the degree of instability of the zonal flow is comparable to the initial instability by the time the growth rate of the unstable wave reaches a minimum.

The final part of the present investigation is devoted to the initialization problem associated with the theory of atmospheric development. A baroclinic two-layer model is discussed in detail in order to demonstrate the effect of the initial wave structure on the subsequent growth of a perturbation. It is shown that for cyclone waves of major instability the perturbation energy will exhibit a maximum growth if the initial amplitude of the lower wave exceeds that of the upper wave by a factor of about 2 and if the lower wave lags behind initially. This is just opposite to the structure of the unstable normal mode. Models with higher vertical resolution indicate that an initial perturbation centered around the 600-mb level is most favorable for development.

REFERENCES

Arnason, G., 1963: The stability of nongeostrophic perturbations in a baroclinic zonal flow. Tellus, 15, 205-229.

Baer, F., 1968: Studies in low-order spectral systems. Dept. of Atmos. Sci., Colorado State Univ., Atmos. Sci. Paper No. 129, 77 pp.

Baer, F., and G. W. Platzman, 1960: A procedure for numerical integration of the spectral vorticity equation. J. Meteor., 18, 393-401.

Baer, F., and T. J. Simons, 1968: Computational stability and time truncation of coupled nonlinear equations with exact solutions. Dept. of Atmos. Sci., Colorado State Univ., Atmos. Sci. Paper No. 131, 43 pp.

Blumen, W., 1968: On the stability of quasi-geostrophic flow. J. Atmos. Sci., 25, 929-931.

Brown, J. A., 1969a: A numerical investigation of hydrodynamic instability and energy conversions in the quasi-geostrophic atmosphere, Part I. J. Atmos. Sci., 26, 352-365.

Brown, J. A., 1969b: A numerical investigation of hydrodynamic instability and energy conversions in the quasi-geostrophic atmosphere, Part II. J. Atmos. Sci., 26, 366-375.

Burger, A. P., 1962: On the non-existence of critical wavelengths in a continuous baroclinic stability problem. J. Atmos. Sci., 19, 31-38.

Case, K. M., 1960: Stability of inviscid plane Couette flow. Physics of Fluids, 3, 143-148.

Case, K. M., 1962: Hydrodynamic stability and the initial value problem. Proc. Symp. Appl. Math., 13, 25-33.

Charney, J. G., 1947: The dynamics of long waves in a baroclinic westerly current. J. Meteor., 4, 135-163.

Charney, J. G., and M. E. Stern, 1962: On the stability of internal baroclinic jets in a rotating atmosphere. J. Atmos. Sci., 19, 159-172.

Derome, J. F., and A. Wiin-Nielsen, 1966: On the baroclinic stability of zonal flow in simple model atmospheres. Dept. of Meteor. and Oceanography, Univ. of Michigan, NSF Grant No. GP-2561, Tech. Report No. 2, 93 pp.

Eady, E. T., 1949: Long waves and cyclone waves. Tellus, 1, 33-52.

Eady, E. T., 1952: Note on weather computing and the so-called 2½ - dimensional model. Tellus, 4, 157-167.

Eliasen, E., 1954: Numerical solutions of the perturbation equation for linear flow. Tellus, 6, 183-191.

Eliasen, E., and B. Machenhauer, 1965: A study of the fluctuations of the atmospheric planetary flow patterns represented by spherical harmonics. Tellus, 17, 220-238.

Eliassen, A., 1952: Simplified dynamic models of the atmosphere, designed for the purpose of numerical weather prediction. Tellus, 4, 145-156.

Fjørtoft, R., 1953: On the changes in the spectral distribution of kinetic energy for two-dimensional, nondivergent flow. Tellus, 5, 225-231.

Gary, J., 1965: A computer survey of linear atmospheric instability. National Center for Atmospheric Research, Manuscript PM-13, 45 pp.

Gates, W. L., 1961a: Static stability measures in the atmosphere. J. Meteor., 18, 526-533.

Green, J. S. A., 1960: A problem in baroclinic stability. Quart. J. R. Meteor. Soc., 86, 237-251.

Haltiner, G. J., 1963: Finite difference approximations for the determination of dynamic instability. Tellus, 15, 231-240.

Haltiner, G. J., and R. T. Song, 1962: Dynamic instability in barotropic flow. Tellus, 14, 383-393.

Hirota, I., 1968: On the dynamics of long and ultra-long waves in a baroclinic zonal current. J. Meteor. Soc. Japan, Ser. II, 46, 234-249.

Hollmann, G., 1956: Ueber prinzipielle Mängel der geostrophichen Approximation und die Einfuhrung ageostrophischer Windkomponenten. Meteor. Rundschau, 9, 73-78,

Howard, L. N., and P. G. Drazin, 1964: On instability of parallel flow of inviscid fluid in a rotating system with variable Coriolis parameter. J. Math. Phys., 43, 83-99.

Jacobs, S. J., and A. Wiin-Nielsen, 1966: On the stability of a barotropic basic flow in a stratified atmosphere. J. Atmos. Sci., 23, 682-687.

King, R. L., 1970: On atmospheric kinetic energy transfer. (To be published).

Kung, E. C., 1970: On the meridional distribution of source and sink terms of the kinetic energy balance. Dept. Atmos. Sci., Univ. of Missouri, Tech. Report, 31 pp.

Kuo, H. L., 1949: Dynamic instability of two-dimensional non-divergent flow in a barotropic atmosphere. J. Meteor., 6, 105-122.

Kuo, H. L., 1951: A note on the kinetic energy balance of the zonal wind systems. Tellus, 3, 82-88.

Kuo, H. L., 1952: Three-dimensional disturbances in a baroclinic zonal current. J. Meteor., 9, 260-278.

Kuo, H. L., 1953: The stability properties and structure of disturbances in a baroclinic atmosphere. J. Meteor., 10, 235-243.

Lipps, F. B., 1962: The barotropic stability of the mean winds in the atmosphere. J. Fluid Mech., 12, 397-407.

Lipps, F. B., 1963: Stability of jets in a divergent barotropic fluid. J. Atmos. Sci., 20, 120-129.

Lipps, F. B., 1965: The stability of an asymmetric zonal current in the atmosphere. J. Fluid Mech., 21, 225-239.

Lorenz, E. N., 1960a: Maximum simplification of the dynamic equations. Tellus, 12, 243-254.

Lorenz, E. N., 1960b: Energy and numerical weather prediction. Tellus, 12, 364-373.

Magata, M., 1964: On the baroclinic instability and the Rossby number. J. Meteor. Soc. Japan, 42, 109-118.

Miles, J. W., 1964a: Baroclinic instability of the zonal wind. Reviews of Geophys., 2, 155-176.

Miles, J. W., 1964b: Baroclinic instability of the zonal wind, Part II. J. Atmos. Sci., 21, 500-506.

Miles, J. W., 1964c: Baroclinic instability of the zonal wind, Part III. J. Atmos. Sci., 21, 603-609.

Pedlosky, J., 1963: Baroclinic instability in two layer systems. Tellus, 15, 20-25.

Pedlosky, J., 1964a: The stability of currents in the atmosphere and the ocean, Part I. J. Atmos. Sci., 21, 201-219.

Pedlosky, J., 1964b: The stability of currents in the atmosphere and the ocean, Part II, J. Atmos. Sci., 21, 342-353.

Pedlosky, J., 1964c: An initial value problem in the theory of baroclinic instability. Tellus, 16, 12-17.

Pedlosky, J., 1970: Finite-Amplitude Baroclinic Waves. J. Atmos. Sci., 27, 15-30.

Phillips, N. A., 1954: Energy transformations and meridional circulations associated with simple baroclinic waves in a two-level quasi-geostrophic model. Tellus, 6, 273-286.

Phillips, N. A., 1959: An example of non-linear computational instability. The Atmosphere and Sea in Motion, ed. B. Bolin, New York, Rockefeller Institute Press, 501-504.

Phillips, N. A., 1963: Geostrophic motion. Reviews of Geophysics, 1, 123-176.

Phillips, N. A., 1964: An overlooked aspect of the baroclinic stability problem. Tellus, 16, 268-270.

Platzman, G. W., 1960: The spectral form of the vorticity equation. J. Meteor., 17, 635-644.

Rao, D. B., and T. J. Simons, 1969: Stability of a sloping interface in a rotating two-fluid system. Dept. of Atmos. Sci., Colorado State Univ., Atmos. Sci. Paper No. 151, 31 pp.

Rosenthal, S. L., 1964: Comparison of analytical and numerical solutions to an initial value problem defined by a linearized, quasi-geostrophic model. Mon. Wea. Rev., 92, 579-587.

Saltzman, B., and S. Teweles, 1964: Further statistics on the exchange of kinetic energy between harmonic components of the atmospheric flow. Tellus, 16, 432-435.

Sela, J., and S. J. Jacobs, 1968: On baroclinic and barotropic ageostrophic stability. Dept. of Meteor. and Oceanography, Univ. of Michigan, ORA Project 07344, Tech. Report, 98 pp.

Shuman, F. G., and J. B. Hovermale, 1968: An operational six-layer primitive equation model. J. Appl. Meteor, 7, 525-547.

Silberman, I., 1954: Planetary waves in the atmosphere. J. Meteor., 11, 27-34.

Simons, T. J., 1968: A three-dimensional spectral prediction equation. Dept. of Atmos. Sci., Colorado State Univ., Atmos. Sci. Paper No. 127, 27 pp.

Simons, T. J., 1969: Baroclinic instability and atmospheric development Dept. of Atmos. Sci., Colorado State Univ., Atmos. Sci. Paper No. 150, 36 pp.

Simons, T. J., 1970: Non-geostrophic baroclinic instability. Dept. of Atmos. Sci., Colorado State Univ., Tech. Report, 29 pp.

Simons, T. J., and D. B. Rao, 1970: Instability of rotational and gravitational modes of oscillation. Dept. of Atmos. Sci., Colorado State Univ., Atmos. Sci. Paper No. 155, 21 pp.

Stone, P., 1966: On non-geostrophic baroclinic stability. J. Atmos. Sci., 23, 390-400.

Thompson, P. D., 1961: Numerical weather analysis and prediction. New York, The Macmillan Co., 170 pp.

Wiin-Nielsen, A., 1959: On certain integral restraints for the time-integration of baroclinic models. Tellus, 11, 45-59.

Wiin-Nielsen, A., 1961: On short-and long-term variations in quasi-barotropic flow. Mon. Wea. Rev., 89, 461-476.

Wiin-Nielsen, A., 1962: On truncation errors due to vertical differences in various numerical prediction models. Tellus, 14, 261-280.

Wiin-Nielsen, A. 1963: On baroclinic instability in filtered and non-filtered numerical prediction models. Tellus 15, 1-19.

Yanai, M., and T. Nitta, 1968: Finite difference approximations for the barotropic instability problem. J. Meteor. Soc. Japan, 46, 389-403.

and the functions of odd parity are orthogonal over one hemisphere, thus

$$\int_0^1 Y_\varepsilon Y_\delta \, d\mu = \begin{cases} 1 & \varepsilon = \delta \\ 0 & \varepsilon \neq \delta \end{cases} \tag{A6}$$

where $\varepsilon = \delta$ implies that both $\ell_\varepsilon = \ell_\delta$ and $n_\varepsilon = n_\delta$.

Each of the three streamfunctions ψ_0, ψ_1 and ψ_2, defined by (21) may now be expanded in a series of these orthonormal polynomials. To distinguish the three streamfunctions from one another let us identify any zonal spectral component by a subscript α, and the components of the first and second wave by subscripts β and γ, respectively. We may write then (24) in the form

$$\ell_\alpha = 0 \qquad \ell_\beta = \ell \qquad \ell_\gamma = 2\ell \tag{A7}$$

and the expansions for the streamfunctions become

$$\psi_0 = \sum_\alpha \psi_\alpha Y_\alpha \qquad \psi_1 = \sum_\beta \psi_\beta Y_\beta \qquad \psi_2 = \sum_\gamma \psi_\gamma Y_\gamma \tag{A8}$$

where the expansion coefficients ψ_α, ψ_β, and ψ_γ are functions of z and t only, and will be referred to in the sequel as the horizontal-spectral components. In exactly the same way we will expand the vertical motion parameters w_j, the linear functions Λ_j, and the nonlinear functions G_j, H_j, P_j and Q_j, in terms of the polynomials Y_α, Y_β, and Y_γ for $j = 1,2$, and 3, respectively. From (23) and (A5) we obtain then immediately

$$\Lambda_\alpha = - c_\alpha \psi_\alpha \qquad \Lambda_\beta = - c_\beta \psi_\beta \qquad \Lambda_\gamma = - c_\gamma \psi_\gamma \tag{A9}$$

After substituting the horizontal expansions of the type (A8) into the model equations (26-28) and applying the orthogonality relationship (A6) we obtain the following set of spectral equations

$$c_\varepsilon \frac{\partial \psi_\varepsilon}{\partial t} = 2i\ell_\varepsilon \psi_\varepsilon + G_\varepsilon + H_\varepsilon + \frac{\partial w_\varepsilon}{\partial z} \tag{A10}$$

$$\frac{\partial}{\partial z} \frac{\partial \psi_\varepsilon}{\partial t} = - s(P_\varepsilon + Q_\varepsilon - w_\varepsilon) \tag{A11}$$

$$\left(c_\varepsilon - \frac{\partial}{\partial z}\left(\frac{1}{s}\frac{\partial}{\partial z}\right)\right) \frac{\partial \psi_\varepsilon}{\partial t} = 2i\ell_\varepsilon \psi_\varepsilon + G_\varepsilon + H_\varepsilon + \frac{\partial}{\partial z}(P_\varepsilon + Q_\varepsilon) \tag{A12}$$

where $\varepsilon = \alpha$, β, or γ and therefore ε stands for any component of the horizontal-spectral expansion, whether the spectral component is an element of the zonal flow (α), the first wave (β), or the second wave (γ). Thus if N is the total number of horizontal-spectral components, then $\varepsilon = 1, 2, 3, \ldots, N$. Note, that all the dependent variables in (A10-12) are functions of z and t only, and that they are real numbers for $\varepsilon = \alpha$ (zonal components) but complex quantities for $\varepsilon = \beta$ or $\varepsilon = \gamma$ (wave components).

The derivation of the spectral expressions for the nonlinear functions (29) has been discussed in detail by Platzman (1960), and will be omitted here. Using the series expansions for ψ_j, Λ_j, G_j, and H_j, ($j = 1, 2, 3$) and applying the orthogonality relationship (A6) one obtains from (29)

$$\begin{aligned}
G_\alpha &= \mathrm{Im} \sum_\beta \sum_{\beta'} K_{\beta\beta'\alpha} \left(\psi_\beta \Lambda^*_{\beta'} - \psi^*_{\beta'} \Lambda_\beta\right) \\
H_\alpha &= \mathrm{Im} \sum_\gamma \sum_{\gamma'} K_{\gamma\gamma'\alpha} \left(\psi_\gamma \Lambda^*_{\gamma'} - \psi^*_{\gamma'} \Lambda_\gamma\right) \\
G_\beta &= i \sum_\alpha \sum_{\beta'} K_{\beta\beta'\alpha} \left(\psi_{\beta'} \Lambda_\alpha - \psi_\alpha \Lambda_{\beta'}\right) \\
H_\beta &= i \sum_{\beta'} \sum_\gamma K_{\gamma\beta\beta'} \left(\psi_\gamma \Lambda^*_{\beta'} - \psi^*_{\beta'} \Lambda_\gamma\right)
\end{aligned} \tag{A13}$$

$$G_\gamma = i \sum_\alpha \sum_{\gamma'} K_{\gamma\gamma'\alpha} \left(\psi_{\gamma'}\Lambda_\alpha - \psi_\alpha\Lambda_{\gamma'}\right)$$

$$H_\gamma = \frac{i}{2} \sum_\beta \sum_{\beta'} K_{\gamma\beta\beta'} \left(\psi_\beta \Lambda_{\beta'} - \psi_{\beta'}\Lambda_\beta\right)$$

where by partial integration we have reduced all interaction coefficient to the following three types.

$$K_{\beta\beta'\alpha} = \ell \int_0^1 Y_\beta Y_{\beta'} \frac{dY_\alpha}{d\mu} d\mu \qquad K_{\gamma\gamma'\alpha} = 2\ell \int_0^1 Y_\gamma Y_{\gamma'} \frac{dY_\alpha}{d\mu} d\mu$$

$$K_{\gamma\beta\beta'} = \ell \int_0^1 Y_\gamma \left(Y_\beta \frac{dY_{\beta'}}{d\mu} - Y_{\beta'} \frac{dY_\beta}{d\mu}\right) d\mu \tag{A14}$$

The expressions for P_ε may be obtained from G_ε, and Q_ε can be obtained from H_ε by replacing Λ_ε by $(1/s)\ \partial\psi_\varepsilon/\partial z$ for ε ranging over all α, β, and γ. In (A 13-14) the prime attached to a symbol denotes a dummy component of the wave indicated by that symbol. Thus the two summations in the double sum G_α extend over the same components such that each pair of components occurs twice, except for the diagonal terms $\beta = \beta'$. It is seen however that the pair renders twice the same contribution and therefore the double sum for G_α may be written as a single non-redundant summation over all combinations (rather than permutations) of β and β'. The same if true for H_α, H_γ, P_α, Q_α, and Q_γ. Further details concerning the computations of the nonlinear functions (A13) and the interaction coefficients (A14) may be found in Baer and Platzman (1960).

APPENDIX B: Spectral Representation in the Vertical

We seek the eigen functions of the vertical operator in (28)

$$L \equiv \frac{\partial}{\partial z}\left(\frac{1}{s(z)}\frac{\partial}{\partial z}\right) \tag{B1}$$

which satisfy the boundary condition (19) at the top and the bottom of the model atmosphere. By virtue of (27) the vertical boundary conditions to be imposed on the eigenfunctions for the streamfield may be stated

$$\frac{1}{s(z)}\frac{\partial \psi}{\partial z} = 0 \qquad \text{for} \quad z = 0,\ 1 \tag{B2}$$

Once the eigensolutions of (B1) and (B2) have been determined, the appropriate polynomials for the vertical representation of the vertical motion field follow from (26) and (27). Alternatively, one may first derive the omega equation by eliminating $\partial\psi/\partial t$ between (26) and (27) and then determine the characteristic functions for the vertical operator occurring in that equation with boundary conditions $w = 0$ for $z = 0,\ 1$. In that case that polynomials for the streamfunction follow from (26) and (27) and the results are, of course, the same.

Clearly, the eigenfunctions are dependent upon the vertical variation of s. The author has shown previously (Simons, 1968) that the inverse static stability 1/s may be represented by a linear function of pressure if one is mainly concerned with the troposphere and if the effects of the stratosphere are simulated by a mathematical upper layer. Thus we write (see also equation (51) of Chapter V)

$$\frac{1}{s} = \frac{1}{s_0}(1-z) \tag{B3}$$

In that case the eigenvalue problem allows for a simple solution and the vertical polynomials for the expansion of the streamfunction have been determined to be

$$Z_m(z) = \frac{J_0\left(2\sqrt{d_m(1-z)}\right)}{J_0\left(2\sqrt{d_m}\right)} \tag{B4}$$

where J_0 is Bessel's function of the first kind of order zero and $d_m = x_m^2/4$, where x_m, m = 0, 1, 2, ..., are the zeros of the Bessel function of order one, J_1. These functions are defined, respectively,

$$J_0(x) = \sum_{n=0}^{\infty} \frac{(-)^n}{(n!)^2} \left(\frac{x}{2}\right)^{2n} \qquad J_1(x) = -\frac{dJ_0}{dx} \tag{B5}$$

For linear variation of 1/s with pressure, the polynomials (B4) are the characteristic functions of the operator (B1) which satisfy the boundary conditions (B2), while d_m, m = 0, 1, 2, ..., are the characteristic numbers, thus

$$\frac{d}{dz}(1-z)\frac{dZ_m}{dz} = -d_m Z_m \tag{B6}$$

The polynomials are orthogonal and have been normalized such that

$$\int_0^1 Z_m Z_n \, dz = \begin{cases} 1 & m=n \\ 0 & m\neq n \end{cases} \tag{B7}$$

The orthogonal functions for the representation of the vertical motion field are related to Bessel's function of order one as follows

$$X_m(z) = -\sqrt{1-z}\ \frac{J_1\left(2\sqrt{d_m(1-z)}\right)}{J_0\left(2\sqrt{d_m}\right)} \tag{B8}$$

The functions X_m are zero for z=0 and z=1 and therefore satisfy the vertical boundary condition (19). By virtue of the relationships between

the Bessel functions of order zero and of order one, the functions Z_m and X_m are related as follows

$$\frac{dX_m}{dz} = \sqrt{d_m}\, Z_m \qquad (1-z)\frac{dZ_m}{dz} = -\sqrt{d_m}\, X_m \tag{B9}$$

By inspection of (26) and (27) one may verify immediately that an expansion of the streamfield in terms of Z_m is indeed consistent with an expansion of the vertical motion in terms of X_m. It follows further that the functions Z_m are also the required eigenfunctions for the nonlinear functions G_j and H_j, while the polynomials X_m are to be used for an expansion of P_j or Q_j.

Let us apply the present spectral representation to the horizontal-spectral equations (A 10-13). Each of the horizontal-spectral components defined by (A8) may then be expanded in a series of polynomials (B4). If again the subscript ε denotes any spectral component of the horizontal expansion, then

$$\psi_\varepsilon(z,t) = \sum_m \psi_{\varepsilon,m}(t)\, Z_m(z) \tag{B10}$$

and a similar expansion holds for G_ε and H_ε. On the other hand, the vertical motion components w_ε, and the components P_ε and Q_ε are to be expanded in terms of the polynomials (B8), thus for instance

$$w_\varepsilon(z,t) = \sum_m w_{\varepsilon,m}(t)\, X_m(z) \tag{B11}$$

Upon substituting these expansions into (A 10-12) and applying the orthogonality relationship (B7) we obtain the system of spectral equations

$$c_\varepsilon \frac{d\psi_{\varepsilon,m}}{dt} = 2i\ell_\varepsilon \psi_{\varepsilon,m} + G_{\varepsilon,m} + H_{\varepsilon,m} + \sqrt{d_m}\, w_{\varepsilon,m} \tag{B12}$$

$$\frac{\sqrt{d_m}}{s_0}\ \frac{d\psi_{\varepsilon,m}}{dt} = P_{\varepsilon,m} + Q_{\varepsilon,m} - w_{\varepsilon,m} \tag{B13}$$

$$\left(c_\varepsilon + \frac{d_m}{s_0}\right) \frac{d\psi_{\varepsilon,m}}{dt} = 2i\ell_\varepsilon \psi_{\varepsilon,m} + G_{\varepsilon,m} + H_{\varepsilon,m} + \sqrt{d_m}\left(P_{\varepsilon,m} + Q_{\varepsilon,m}\right) \tag{B14}$$

where ε ranges over all horizontal-spectral components, $\varepsilon = 1,2,3,\ldots,N$, and m extends over all vertical-spectral parameters, $m = 0,1,2,\ldots,M-1$, and therefore each of the equations above represents of system of N x M equations. Note, however, that the space-dependence has been removed completely from the equations, which is, of course the prime target of the spectral technique.

The spectral expressions for the nonlinear functions are also obtained by substituting the expansions (B10) and applying the orthogonality conditions. Since the nonlinear functions in (A13) are all of the same form there is no need to reproduce the expansion coefficients for all of them. Therefore we will restrict ourselves to the system of a zonal flow and one wave, which is considered in Chapter 4 of this report, and which only involves the functions G_α, G_β, P_α, and P_β. The spectral components for these functions are

$$G_{\alpha,m} = \mathrm{Im} \sum_\beta \sum_{\beta'} K_{\beta\beta'\alpha} (c_\beta - c_{\beta'}) \sum_k \sum_j \psi^*_{\beta',k}\, \psi_{\beta,j}\, J_{mkj}$$

$$G_{\beta,m} = i \sum_\alpha \sum_{\beta'} K_{\beta\beta'\alpha} (c_{\beta'} - c_\alpha) \sum_k \sum_j \psi_{\alpha,k}\, \psi_{\beta',j}\, J_{mkj} \tag{B15}$$

$$\sqrt{d_m}\, P_{\alpha,m} = \mathrm{Im} \frac{1}{s_0} \sum_\beta \sum_{\beta'} K_{\beta\beta'\alpha} \sum_k \sum_j (d_j - d_k)\, \psi^*_{\beta',k}\, \psi_{\beta,j}\, J_{mkj}$$

$$\sqrt{d_m}\, P_{\beta,m} = \frac{i}{s_0} \sum_\alpha \sum_{\beta'} K_{\beta\beta'\alpha} \sum_k \sum_j (d_j - d_k)\, \psi_{\alpha,k}\, \psi_{\beta',j}\, J_{mkj}$$

where the interaction coefficients are defined

$$J_{mkj} = \int_0^1 Z_m\, Z_k\, Z_j\, dz \tag{B16}$$

A more detailed treatment of the nonlinear functions and the interaction coefficients with regard to the vertical spectral expansion may be found in the paper by Simons (1968).

APPENDIX C: Layered Representation in the Vertical

Following the usual procedure in numerical modeling we divide the model atmosphere into M layers of depth $\Delta z = 1/M$ each, and define the streamfunction at the midpoints of the layers and the vertical motion between two successive layers. Applying this technique to the horizontal-spectral equations (A 10-13) we define a set of time-dependent functions

$$\psi_{\varepsilon,m}(t) = \psi_{\varepsilon}\left(t, z = (m+\tfrac{1}{2})\Delta z\right) \qquad m = 1,2,3,\ldots,M, \tag{C1}$$

and similarly

$$w_{\varepsilon,m+\frac{1}{2}}(t) = w_{\varepsilon}\left(t, z = m\Delta z\right) \qquad m = 0,1,2,\ldots,M, \tag{C2}$$

where again ε denotes any horizontal-spectral component as defined in Appendix A. In accordance with (A 10-11) we represent the nonlinear functions G_{ε} and H_{ε} at the ψ-levels and the functions P_{ε} and Q_{ε} at the w-levels. The vertical boundary conditions (19) are satisfied by requiring

$$w_{\varepsilon,\frac{1}{2}} = w_{\varepsilon,M+\frac{1}{2}} = 0 \tag{C3}$$

Applying the vorticity equation (A10) at the ψ-levels and the thermodynamic equation (A11) at the w-levels, we obtain

$$c_{\varepsilon}\frac{d\psi_{\varepsilon,m}}{dt} = 2i\ell_{\varepsilon}\psi_{\varepsilon,m} + G_{\varepsilon,m} + H_{\varepsilon,m} + M\left(w_{\varepsilon,m+\frac{1}{2}} - w_{\varepsilon,m-\frac{1}{2}}\right) \tag{C4}$$

$$\frac{M}{s_{m+\frac{1}{2}}}\frac{d}{dt}\left(\psi_{\varepsilon,m} - \psi_{\varepsilon,m+1}\right) = P_{\varepsilon,m+\frac{1}{2}} + Q_{\varepsilon,m+\frac{1}{2}} - w_{\varepsilon,m+\frac{1}{2}} \tag{C5}$$

Eliminating the vertical motion components and using the boundary conditions (C3) we arrive at

$$\left(c_{\varepsilon} + S_{1\frac{1}{2}}\right)\frac{d\psi_{\varepsilon,1}}{dt} - S_{1\frac{1}{2}}\frac{d\psi_{\varepsilon,2}}{dt} = R_{\varepsilon,1} \tag{C6}$$

$$-S_{m-\frac{1}{2}} \frac{d\psi_{\varepsilon,m-1}}{dt} + \left(c_\varepsilon + S_{m-\frac{1}{2}} + S_{m+\frac{1}{2}}\right) \frac{d\psi_{\varepsilon,m}}{dt} - S_{m+\frac{1}{2}} \frac{d\psi_{\varepsilon,m+\frac{1}{2}}}{dt} = R_{\varepsilon,m}$$

$$-S_{M-\frac{1}{2}} \frac{d\psi_{\varepsilon,M-1}}{dt} + \left(c_\varepsilon + S_{M-\frac{1}{2}}\right) \frac{d\psi_{\varepsilon,M}}{dt} = R_{\varepsilon,M} \qquad m = 2,3..,M-1,$$

where we have defined

$$S_{m+\frac{1}{2}} = M^2/s\,(z = m\Delta z) \qquad m = 1,2,\ldots, M-1, \tag{C7}$$

and the R.H.S. of (C6) are obviously

$$\begin{aligned}
R_{\varepsilon,1} &= 2i\ell_\varepsilon \psi_{\varepsilon,1} + G_{\varepsilon,1} + H_{\varepsilon,1} + M\left(P_{\varepsilon,1\frac{1}{2}} + Q_{\varepsilon,1\frac{1}{2}}\right) \\
R_{\varepsilon,m} &= 2i\ell_\varepsilon \psi_{\varepsilon,m} + G_{\varepsilon,m} + H_{\varepsilon,m} + M\left(P_{\varepsilon,m+\frac{1}{2}} + Q_{\varepsilon,m+\frac{1}{2}} - P_{\varepsilon,m-\frac{1}{2}} - Q_{\varepsilon,m-\frac{1}{2}}\right) \\
&\qquad\qquad m = 2,3,.., M-1, \\
R_{\varepsilon,M} &= 2i\ell_\varepsilon \psi_{\varepsilon,M} + G_{\varepsilon,M} + H_{\varepsilon,M} - M\left(P_{\varepsilon,M-\frac{1}{2}} + Q_{\varepsilon,M-\frac{1}{2}}\right)
\end{aligned} \tag{C8}$$

The nonlinear time-dependent functions $G_{\varepsilon,m}$ and $H_{\varepsilon,m}$ are obtained by applying (A13) at the ψ-levels, and $P_{\varepsilon,m+\frac{1}{2}}$ and $Q_{\varepsilon,m+\frac{1}{2}}$ are derived by applying the equations for P_ε and Q_ε at the w-levels. We will only write down the expressions for G_β and P_β which are used in the linear analysis of Chapter 3.

$$\begin{aligned}
G_{\beta,m} &= i \sum_\alpha \sum_{\beta'} K_{\beta\beta'\alpha}\left(c_{\beta'}-c_\alpha\right) \psi_{\alpha,m}\, \psi_{\beta',m} \\
M\, P_{\beta,m+\frac{1}{2}} &= i\, S_{m+\frac{1}{2}} \sum_\alpha \sum_{\beta'} K_{\beta\beta'\alpha}\left(\psi_{\alpha,m+1}\, \psi_{\beta',m} - \psi_{\alpha,m}\, \psi_{\beta',m+1}\right)
\end{aligned} \tag{C9}$$

The system of equations (C4-6) is equivalent to the spectral system (B 12-14). However, the latter can be solved immediately for the time-derivatives of the streamfunction components, while the system (C6) requires a matrix inversion. In order to solve for the unknown

$d\psi_{\varepsilon,m}/dt$, m = 1,2..., M, from the M equations (C6) we define for every component ε the following constants

$$C_{\varepsilon,1} \equiv \left(c_\varepsilon + S_{1\frac{1}{2}}\right)^{-1}$$

$$C_{\varepsilon,m} \equiv \left(c_\varepsilon + S_{m-\frac{1}{2}} + S_{m+\frac{1}{2}} - S^2_{m-\frac{1}{2}}\ C_{\varepsilon,m-1}\right)^{-1} \qquad m = 2,3,..,M-1$$

$$C_{\varepsilon,M} \equiv \left(c_\varepsilon + S_{M-\frac{1}{2}} - S^2_{M-\frac{1}{2}}\ C_{\varepsilon,M-1}\right)^{-1} \qquad \text{(C10)}$$

and the following time-dependent variables

$$B_{\varepsilon,1} \equiv C_{\varepsilon,1}\ R_{\varepsilon,1}$$

$$B_{\varepsilon,m} \equiv C_{\varepsilon,m}\left(R_{\varepsilon,m} + S_{m-\frac{1}{2}}\ B_{\varepsilon,m-1}\right) \qquad m = 2,3,\ldots,\ M \qquad \text{(C11)}$$

The solution is then

$$\frac{d\psi_{\varepsilon,M}}{dt} = B_{\varepsilon,M}$$

$$\frac{d\psi_{\varepsilon,m}}{dt} = S_{m+\frac{1}{2}}\ C_{\varepsilon,m}\ \frac{d\psi_{\varepsilon,m+1}}{dt} + B_{\varepsilon,m} \qquad m = M-1,\ M-2,\ldots,2,1 \qquad \text{(C12)}$$

APPENDIX D: Energy Conversions in the Spectral Domain

The kinetic energy, given by (32), the available potential energy (34), and the various energy conversions (39-40), will be written here in a form suitable for numerical computation. First we substitute the horizontal-spectral expansions of the type (A8-9) and apply the orthogonality relationships (A6) to obtain

$$K_o = \sum_\alpha \tfrac{1}{2} c_\alpha \psi_\alpha \psi_\alpha \qquad K_1 = \sum_\beta c_\beta \psi_\beta \psi_\beta^* \qquad K_2 = \sum_\gamma c_\gamma \psi_\gamma \psi_\gamma^* \tag{D1}$$

$$A_o = \sum_\alpha \frac{1}{2s} \frac{\partial \psi_\alpha}{\partial z} \frac{\partial \psi_\alpha}{\partial z} \qquad A_1 = \sum_\beta \frac{1}{s} \frac{\partial \psi_\beta}{\partial z} \frac{\partial \psi_\beta^*}{\partial z} \qquad A_2 = \sum_\gamma \frac{1}{s} \frac{\partial \psi_\gamma}{\partial z} \frac{\partial \psi_\gamma^*}{\partial z} \tag{D2}$$

$$CK_{10} = \sum_\alpha \psi_\alpha G_\alpha \qquad CK_{20} = \sum_\alpha \psi_\alpha H_\alpha \qquad CAK_o = \sum_\alpha \psi_\alpha \frac{\partial w_\alpha}{\partial z}$$

$$CK_{01} = 2\mathrm{Re} \sum_\beta \psi_\beta G_\beta^* \qquad CK_{02} = 2\mathrm{Re} \sum_\gamma \psi_\gamma G_\gamma^*$$

$$CK_{21} = 2\mathrm{Re} \sum_\beta \psi_\beta H_\beta^* \qquad CK_{12} = 2\mathrm{Re} \sum_\gamma \psi_\gamma H_\gamma^* \tag{D3}$$

$$CAK_1 = 2\mathrm{Re} \sum_\beta \psi_\beta \frac{\partial w_\beta^*}{\partial z} \qquad CAK_2 = 2\mathrm{Re} \sum_\gamma \psi_\gamma \frac{\partial w_\gamma^*}{\partial z}$$

$$CA_{10} = -\sum_\alpha \frac{\partial \psi_\alpha}{\partial z} P_\alpha \qquad CA_{20} = -\sum_\alpha \frac{\partial \psi_\alpha}{\partial z} Q_\alpha \qquad CKA_o = \sum_\alpha \frac{\partial \psi_\alpha}{\partial z} w_\alpha$$

$$CA_{01} = -2\mathrm{Re} \sum_\beta \frac{\partial \psi_\beta}{\partial z} P_\beta^* \qquad CA_{02} = -2\mathrm{Re} \sum_\gamma \frac{\partial \psi_\gamma}{\partial t} P_\gamma^*$$

$$CA_{21} = -2\mathrm{Re} \sum_\beta \frac{\partial \psi_\beta}{\partial z} Q_\beta^* \qquad CA_{12} = -2\mathrm{Re} \sum_\gamma \frac{\partial \psi_\gamma}{\partial z} Q_\gamma^* \tag{D4}$$

$$CKA_1 = 2\mathrm{Re} \sum_\beta \frac{\partial \psi_\beta}{\partial z} w_\beta^* \qquad CKA_2 = 2\mathrm{Re} \sum_\gamma \frac{\partial \psi_\gamma}{\partial z} w_\gamma^*$$

It can be shown that $CK_{10} = -CK_{01}$, $CA_{10} = -CA_{01}$, etc., for any horizontal-spectral truncation, and hence the spectral equations conserve the quantity $\overline{K} + \overline{A}$ just as the original equations (26-28) do.

The computations of the energy quantities at various heights in the layered model is straight forward if we recall the procedure outlined in Appendix C. Similarly, if the spectral representation in the vertical is employed, the energy in the vertical-spectral components is obtained by substituting (B10-11) into (D1-2) and applying the orthogonality condition (B7). For example, the results for $\overline{K}_1$ and $\overline{A}_1$ are

$$\overline{K}_1 = \sum_{\beta} c_\beta \sum_{m} \psi_{\beta,m} \psi^*_{\beta,m} \qquad \overline{A}_1 = \frac{1}{s_o} \sum_{\beta} \sum_{m} d_m \psi_{\beta,m} \psi^*_{\beta,m} \tag{D5}$$

where we have used (B3) and (B6) after an integration by parts with respect to the vertical coordinate.

APPENDIX E: Spectral Equations for the Linear Model

The equations for a combination of the horizontal-spectral and the vertically-layered representations have been derived in Appendix C. Again we will identify a zonal spectral component by the subscript α and a wave component by the subscript β. The second wave (denoted before by subscript γ) is not considered in the linear model and the zonal flow is not allowed to vary with time. The wave equations are then obtained from (C 6-8) by replacing ε by β and by discarding the nonlinear terms H_β and Q_β which represent the interaction with the second wave. To simplify matters somewhat, we will however first define a "static stability" at the lower and upper model boundaries as follows

$$S_{\frac{1}{2}} = S_{M+\frac{1}{2}} \equiv 0 \tag{E1}$$

These constants have been only introduced for notational purposes and no physical interpretation should be attached to them. An obvious advantage of the definitions (E1) is that the wave equations may now be simply written as follows

$$-S_{m-\frac{1}{2}} \frac{d\psi_{\beta,m-1}}{dt} + \left(c_\beta + S_{m-\frac{1}{2}} + S_{m+\frac{1}{2}}\right) \frac{d\psi_{\beta,m}}{dt} - S_{m+\frac{1}{2}} \frac{d\psi_{\beta,m+1}}{dt} = R_{\beta,m} \tag{E2}$$

$$R_{\beta,m} = 2i\ell_\beta \psi_{\beta,m} + G_{\beta,m} + M\left(P_{\beta,m+\frac{1}{2}} - P_{\beta,m-\frac{1}{2}}\right) \tag{E3}$$

where now m extends over all layers m = 1,2,3,..., M.

Substituting the expressions for the nonlinear functions (C9) and rearranging terms we obtain from (E3)

$$\begin{aligned} R_{\beta,m} = 2i\ell_\beta \psi_{\beta,m} + i \sum_{\beta'} \Big(& \psi_{\beta',m-1} \sum_\alpha K_{\beta\beta'\alpha} \left(-S_{m-\frac{1}{2}}\, \psi_{\alpha,m}\right) + \\ & + \psi_{\beta',m} \sum_\alpha K_{\beta\beta'\alpha} \left(S_{m-\frac{1}{2}}\, \psi_{\alpha,m-1} + (c_{\beta'} - c_\alpha)\psi_{\alpha,m} + S_{m+\frac{1}{2}}\, \psi_{\alpha,m+1}\right) + \\ & + \psi_{\beta',m+1} \sum_\alpha K_{\beta\beta'\alpha} \left(-S_{m+\frac{1}{2}}\, \psi_{\alpha,m}\right) \Big) \end{aligned} \tag{E4}$$

where β' represents a wave component and therefore both β and β' range over the same array of component. If N is the number of spectral wave components and M is the number of layers in the vertical, then $\beta = 1,2,\ldots,N$, and $m = 1,2,\ldots, M$, and we are dealing with NxM time-dependent variables $\psi_{\beta,m}$. After substituting (E4) into (E2) we will obtain a system of NxM coupled equations which are linear since $\psi_{\alpha,m}$ are constant, and this system can therefore be solved without difficulty.

The variables $\psi_{\beta,m}$ are to be arranged in a specified order. It is convenient to define a new index as follows

$$k = M(\beta-1) + m \qquad k' = M(\beta'-1) + m \tag{E5}$$

The array of variables $\psi_{\beta,m}$ may then be written ψ_k, $k = 1,2,\ldots,K$ where $K = NxM$, and the system of equations may be written in the following form

$$-S_{m-\frac{1}{2}} \frac{d\psi_{k-1}}{dt} + \left(c_\beta + S_{m-\frac{1}{2}} + S_{m+\frac{1}{2}}\right) \frac{d\psi_k}{dt} - S_{m+\frac{1}{2}} \frac{d\psi_{k+1}}{dt} = R_k$$

$$R_k = 2i\ell_\beta \psi_k + i \sum_{\beta'} \left(a_{k,k'-1}\, \psi_{k'-1} + a_{k,k'}\, \psi_{k'} + a_{k,k'+1} \psi_{k'+1}\right) \tag{E6}$$

where we have defined the constants

$$\begin{aligned} a_{k,k'-1} &\equiv \sum_\alpha K_{\beta\beta'\alpha} \left(-S_{m-\frac{1}{2}}\, \psi_{\alpha,m}\right) \\ a_{k,k'} &\equiv \sum_\alpha K_{\beta\beta'\alpha} \left(S_{m-\frac{1}{2}}\, \psi_{\alpha,m-1} + (c_{\beta'} - c_\alpha)\, \psi_{\alpha,m} + S_{m+\frac{1}{2}}\, \psi_{\alpha,m+1}\right) \\ a_{k,k'+1} &\equiv \sum_\alpha K_{\beta\beta'\alpha} \left(-S_{m+\frac{1}{2}}\, \psi_{\alpha,m}\right) \end{aligned} \tag{E7}$$

where it is understood that with every k we have associated one β and one m, and this index m together with the index β' determine k' according to (E5).

The system of equations may be written in matrix notation as follows

$$\frac{d}{dt} \left(\mathbb{A}\, \vec{\Psi}\right) = i\, \mathbb{B}\, \vec{\Psi} \tag{E8}$$

where $\mathbb{A}$ and $\mathbb{B}$ are matrices with constant elements, and $\vec{\Psi}$ is the array of time-dependent variables ψ_k, k = 1,2,..., K. By inversion of matrix $\mathbb{A}$ one obtains finally

$$\frac{d}{dt}\vec{\Psi} = i\left(\mathbb{A}^{-1}\,\mathbb{B}\right)\vec{\Psi} \equiv i\;\mathbb{D}\,\vec{\Psi} \tag{E9}$$

which is the equation referred to in Chapter 3. Owing to the form of the maxtrix $\mathbb{A}$, the latter may be inverted for every component β individually such that we may apply again the inversion technique outlined by (C10-12).

The system of equations given by (E9) allows for solutions of the form exp (-iνt). Upon substituting such a solution, (E9) reduces to

$$-\nu\,\vec{\Psi} = \mathbb{D}\,\vec{\Psi} \qquad \text{or} \qquad \left|\mathbb{D} + \nu\,\mathbb{I}\right| = 0 \tag{E10}$$

where $\mathbb{I}$ is the unit matrix. Therefore the ν's are equal to the eigenvalues of the matrix D with reversed sign. The complete solution for the vector $\vec{\Psi}$ is then obtained in the following form

$$\psi_k = \sum_{j=1}^{K} b_{k,j}\; e^{-i\nu_j t} \qquad k = 1,2,\ldots, K \tag{E11}$$

where $b_{k,j}$ (k = 1,2,...., K) is the eigenvector associated with the eigenvalue ν_j and in physical terms represents the structure of the normal mode ν_j.

Since $\mathbb{D}$ is a coefficient matrix of order K there will be a total of K eigenvalues. Most of these will be real numbers, but one may find a number of complex eigenvalues. Due to the character of the coefficient matrix the complex values will occur in conjugate pairs and the eigenvalue with positive imaginary part corresponds to an exponentially growing solution.